uOttawa

L'Université canadienne
Canada's university

**FACULTÉ DES ÉTUDES SUPÉRIEURES ET POSTOCTORALES**

uOttawa

L'Université canadienne
Canada's university

**FACULTY OF GRADUATE AND POSDOCTORAL STUDIES**

Susan Thurston
AUTEUR DE LA THÈSE / AUTHOR OF THESIS

M.Sc. (Cellular and Molecular Medicine)
GRADE / DEGREE

Department of Cellular and Molecular Medicine
FACULTÉ, ÉCOLE, DÉPARTEMENT / FACULTY, SCHOOL, DEPARTMENT

INFI is a Novel Microtubule and Actin Cytoskeleton Cross-linking Protein
TITRE DE LA THÈSE / TITLE OF THESIS

John Copeland
DIRECTEUR (DIRECTRICE) DE LA THÈSE / THESIS SUPERVISOR

CO-DIRECTEUR (CO-DIRECTRICE) DE LA THÈSE / THESIS CO-SUPERVISOR

Jonathan Lee

Laura Trinkle-Mulcahy

Gary W. Slater
Le Doyen de la Faculté des études supérieures et postdoctorales / Dean of the Faculty of Graduate and Postdoctoral Studies

# INF1 is a Novel Microtubule and Actin Cytoskeleton Cross-linking Protein

**Susan Frances Thurston**

Thesis submitted to the Faculty of Graduate and Postdoctoral Studies in partial fulfillment of the requirements for the M.Sc. program in Cellular and Molecular Medicine

Cellular and Molecular Medicine
Faculty of Medicine
University of Ottawa

*Your file Votre référence*
*ISBN:* 978-0-494-61301-6
*Our file Notre référence*
*ISBN:* 978-0-494-61301-6

## Abstract

Formin proteins, characterized by two conserved formin homology (FH) domains, play an important role in cytoskeletal regulation and dynamics. The FH domains are most commonly implicated with the polymerization of F-actin and more recently with the stabilization of microtubules. Inverted formin 1 (INF1) is an atypical formin that has its FH1 and FH2 domains in its N-terminus. The C-terminus of INF1 contains five conserved regions unlike any other sequence found in the database. In this study, we demonstrate that INF1 discreetly associates with microtubules via a unique bipartite microtubule-binding domain (MTBD) in the C-terminus. Additionally, similar to the diaphanous related formin mDia, INF1 induces microtubule stabilization and acetylation. Expression of the MTBD alone, and not the FH2 domain, is sufficient to induce microtubule stabilization. However, in the absence of the MTBD, the N-terminus induces microtubule stabilization dependent on the presence of both the FH1 and the FH2 domains. In addition, knockdown of INF1 protein in NIH 3T3 fibroblasts results in a dramatic loss of acetylated microtubules suggesting INF1 is required for MT acetylation in these cells. Furthermore, we show that INF1 is not regulated by auto-inhibition, but is constitutively active both *in vivo* and *in vitro*. Our overexpression results suggest the INF1 C-terminus contains a putative regulatory domain targeted by an unknown inhibitory factor. Finally, we show that INF1 is capable of bundling both microtubules and F-actin simultaneously, implying that INF1 is a cytoskeletal cross-linking protein that could play an important role in cell polarity, cell migration and other cytoskeletal dependent processes.

# Table of Contents

# List of Figures

## Chapter 1



## Chapter 2



## Chapter 3



## Chapter 4

## List of Abbreviations

ATP: Adenosine Triphosphate
APC: Adenomatous polyposis coli
ARP 2/3: Actin Related Proteins 2 and 3
CA: Constitutively Active
CC: Coiled Coil
CoIP: Co-Immunuprecipitation
DAAM: disheveled-associated activators of morphogenesis
DAD: Diaphanous autoregulatory domain
DAPI: 4',6-diamidino-2-phenylindole
DD: Dimerization domain
Dia: Diaphanous
DID: Diaphanous Inhibitory Domain
DRF: Diaphanous Related Formin
EB1: End binding protein 1
EGTA: Ethyleneglycol-*bis*(β-aminoethyl)-N,N,N′,N′-tetraacetic Acid
ER: Endoplasmic reticulum
F-actin: Filamentous actin
FBS: Fetal Bovine Serum
FH1: Formin homology domain one
FH2: Formin homology domain two
FHDC: Formin homology domain containing
FHOD: Formin Homology Domain-Containing Protein
FRL: formin-related proteins identified in leucocytes
G-actin: Globular actin
GDP: Guanosine Diphosphate
GFP: Green Fluorescent Protein
GSK-3β: Glycogen Synthase Kinase 3β
GTP: Guanosine Triphosphate
INF: Inverted formin
LPA: Lysophosphatidic acid
MAPs: Microtubule associated proteins
MARK2: MAP/microtubule affinity-regulating kinase 2
MRTF: Myocardin Related Transcription Factor
MT: Microtubules
MTBD: Microtubule Binding Domain
MTOC: Microtubule Organizing Center
PBS: Phosphate Buffered Saline

RBD: Rho-GTPase binding domain
ROCK: Rho-Associated Kinase
siRNA: Small Interfering Ribonucleic Acid
SRE: Serum Response Element
SRF: Serum Response Factor
WASP: Wiskott-Aldrich syndrome protein
WH2: WASP Homology two
YFP: Yellow fluorescent protein

## Acknowledgements

I would like to thank everyone who helped and supported me throughout my Masters. First, I would like to thank Dr. John Copeland for his mentorship and advice. His dedication and enthusiasm always kept me motivated and thirsting for more. I would also like to thank the members of my advisory committee, Dr. Heidi McBride and Dr. Rashmi Kothary for their advice and suggestions for my project.

I also need to acknowledge those I worked side-by-side with everyday. I would like to thank my friends Fatima and Kevin for being always ready to give a lending hand. My appreciation also goes to Sarah; without her expertise I am certain I would still be trying to get my preps to work. I would be remiss to forget our summer students, Chelsea, Thea and Karine, who managed to always keep me on my toes with their inquisitive minds. Thank you.

I would not have survived graduate studies without a group of friends who were always willing to listen and give advice. The Lohnes lab was always accepting and has been a great home to me in times of need. In particular, thanks Beta for always listening when I needed a colleague, a peer or, more importantly, a friend.

Finally I would like to thank my family for their endless support. Thanks to my mom and my sister Madelaine who always remind me to relax when life gets stressful, and my brother Alex who always encourages me to do my best. I would like to thank my dad who read, and re-read, through all my reports to "remind" me of my grammatical flaws. One day I will remember the difference between 'bring' and 'take'. I also would like to thank Matt, who has helped and supported me in every way.

# Chapter 1: Introduction

Cell morphology is uniquely tailored to perform specific physiological functions. Changes in these morphologies represent changes in the underlying cytoskeleton in response to a variety of internal and external signals. The dynamic response of the cytoskeleton plays a major role not only in controlling cell shape, but also in providing cell structure and rigidity.

The cytoskeleton is made up of three different networks: microtubules (MTs), actin filaments and intermediate filaments. The actin cytoskeleton regulates cellular processes such as cell migration, cell division, cell adhesion, polarity and organelle trafficking (Faix and Grosse, 2006, Goode and Eck, 2007). For example, in migrating cells, actin filaments shape the cell by pushing the plasma membrane outward toward the direction of migration. The essential and ubiquitous nature of cytoskeletal function requires numerous proteins to regulate localization, nucleation and polymerization of cytoskeletal networks. These small-scale molecular events can lead to large-scale morphological changes.

Cells use a vast array of proteins to bind cytoskeletal polymers and organize them into larger force generating structures. Much effort has been directed at determining how actin and MT network dynamics are individually regulated. More recently, it has become apparent that the coordination of the function of actin filaments and MTs is equally important. Several proteins have been demonstrated to affect actin dynamics directly. The formins, for example, were identified as the first factors capable of directly nucleating *de novo* actin polymerization. Recent work demonstrates that some formins are also capable of directly inducing the re-orientation and stabilization of MTs (Gasteier et al., 2005, Bartolini et al., 2008). Thus, formins may represent a unique class of cytoskeletal cross-

linking proteins that connect the F-actin and MT networks (Bartolini et al., 2009). Given that integrity of the cytoskeleton underlies essentially all cellular functions, it is not surprising that defects in formin function have been associated with a variety of human diseases such as colorectal cancer, prostate cancer, limb deformity and sterility (Ryley et al., 2005, Zhu et al., 2008, Sarmiento et al., 2008, Di Vizio et al., 2009, Zhou et al., 2009). The work presented here provides the first description of the function of Inverted Formin 1 (INF1), a novel MT-associated member of the formin family of cytoskeletal remodelling proteins.

### 1.1. The Actin Cytoskeleton and Formins

Actin filaments (F-actin) are composed of monomeric globular actin subunits (G-actin). Actin filaments have a fast-growing "barbed end" and a slow-growing "pointed end" giving the filaments an inherent polarity (Pollard and Earnshaw, 2004). These dynamic filaments use other proteins to nucleate and direct their polymerization. Following nucleation, the rate of polymerization is directly proportional to the concentration of available actin monomers.

The nucleation of new filaments is the rate-limiting step in polymerization and serves as a major regulatory target of pathways that govern actin dynamics (Goode and Eck, 2007). Nucleation initiates with the formation of an actin dimer. Actin dimers and trimers are highly unstable; nucleation factors act to stabilize these intermediates to allow the addition of more actin monomers (Alberts, 2004). Once past this rate-limiting step, ATP bound G-actin preferentially associates with the barbed end of the filaments and dissociates from the pointed ends of the actin filaments (Zigmond, 2004).

Actin filaments can be organized to form different structures such as stress fibres, filopodia, lamelliopodia, actin cables, and cytokinetic actin rings. Stress fibres are long, thick, unbranched actin filaments responsible for generating contractile forces and providing structural integrity to a cell (Russell et al., 2009).

Three nucleation promoting factors have been described to date. These three factors nucleate filament assembly by distinct mechanisms. The Arp2/3 complex nucleates actin polymerization from the sides of previously assembled filaments to create branches projecting out at a 70 degree angle (Soderling, 2009). This branching creates a dendritic network similar to those found in the leading edge of migrating cells. Spire nucleates the polymerization of unbranched actin filaments using four short WASP homology two (WH2) repeats. The four Spire WH2 domains each bind an actin monomer to promote actin assembly. Similar to Arp2/3, Spire remains associated with the pointed-end of the growing filament. In contrast, formins nucleate polymerization through the action of the formin homology two (FH2) domain which binds and stabilizes actin dimers. Unlike Spire and Arp2/3, formins remain associated with the barbed-end of long-growing, unbranched actin filaments and are thus termed "leaky" barbed end capping proteins or "leaky cappers".

### 1.2. Formin Homology Proteins

Formins are a family of widely-expressed, highly-conserved, cytoskeleton remodelling proteins that commonly act downstream of Rho GTPase signalling (Faix and Grosse, 2006, Goode and Eck, 2007). Formins are large multi-domain proteins (120-220kDa) that have numerous regions that associate with other proteins to mediate their localization and regulation. Formin activity is thought to play a major role in a variety of

actin- and MT-dependent processes, such as the regulation of mitotic spindle assembly, cytokinesis, stress fibre formation, filopodia formation, MT organization and stabilization, cell polarity, cell motility and invasion, phagocytosis, endosome motility, and adherens junction formation (Faix and Grosse, 2006, Goode and Eck, 2007).

The name formin originates from the original description of a mouse mutation that resulted in limb deformity (Woychik et al., 1990). There has been some controversy as to whether or not this original mutation was responsible for the observed deformity (Zuniga et al., 2004). However, recently it was demonstrated that knockout mice devoid of Formin1 activity lack digits and have deformed posterior limbs (Zhou et al., 2009). Formin homologues in *Drosophila melanogaster, Saccharomyces cerevisiae* and *Schizosaccharomyces pombe* have since been characterized and shown to play an important role in a variety of developmental processes (Castrillon and Wasserman 1994, Chang et al., 1997, Evangelista et al., 1997). In mammals, fifteen formin genes have been identified. All 15 mammalian formins are characterized by their highly conserved formin homology domains (FH1 and FH2) (Castrillon and Wasserman, 1994). Formins can be further divided into seven sub-families, based on the presence of regulatory domains and the similarities between their FH2 domains (Figure 1.1) (Higgs and Peterson, 2005).

The best characterized and understood function of formins is the *de novo* nucleation of actin filaments from the cytosolic pool of G-actin. This function is carried out by the FH1 and FH2 domains and allows for temporal and spatial remodelling of actin (Copeland and Treisman, 2002, Pruyne et al., 2002, Li and Higgs, 2003, Copeland et al., 2004). The FH2 domain is approximately 400 amino acids long and flanked N-terminally by the shorter proline-rich FH1 domain.

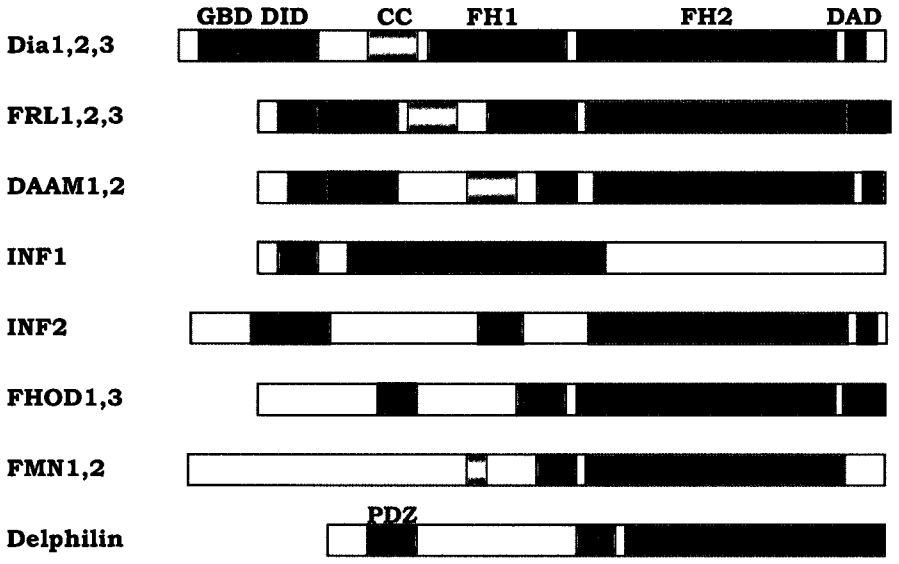


**Figure 1.1: Schematics of the fifteen mammalian formin protein.**

Formins are characterized by their highly conserved Formin Homology domains (FH1 and FH2). Formins are grouped into seven sub-families based on sequence homology. Diaphanous Related Formins (DRFs) include the sub-families Dia, DAAM and FRL and are distinguished by their GTPase binding domain (GBD), Diaphanous Inhibitory Domain (DID) and Diaphanous Autoregulatory Domain (DAD) domains. CC is the Coiled Coil domain which mediates N-terminal dimerization. PDZ domain mediates an interaction with membrane proteins. INF1 and INF2 are grouped in the same sub-family because of sequence homology, but it was later discovered that INF2 has an upstream ORF which contains the regulatory domains DID.

In models of formin activity, the FH2 domain forms a head-to-tail dimer that nucleates actin polymerization by stabilizing the initial actin dimer. FH2 dimers function as barbed end 'leaky' caps which accommodate barbed-end growth while also antagonizing the function of barbed-end capping proteins (Pruyne et al., 2002, Zigmond et al., 2003, Li and Higgs, 2003).

Adjacent to the FH2 domain is the short proline-rich FH1 domain that helps polymerise actin filaments. FH1 is required to recruit and use profilin–bound G-actin from the cytoplasm (Watanabe et al., 1997, Li and Higgs, 2003, Ezezika et al., 2009). The FH1-profilin interaction increases the rate of filament elongation by overcoming limitations imposed by monomer diffusion. The higher concentration of profilin-actin complexes results in a higher local concentration of actin and therefore more effective and faster polymerization.

Actin exists in a dynamic relationship between filamentous actin (F-actin) and globular actin (G-actin). G-actin associates with profilin, a small protein (15kDa) which contains two binding regions. One region binds to actin monomers and the other region binds to poly-proline sequences (Witke, 2004). It is thought that profilin binding to G-actin regulates microfilament assembly by inhibiting spontaneous nucleation (Krebs et al., 2001). Point mutations in FH1, which disrupt the FH1-profilin interaction, greatly reduces the efficiency of actin polymerization suggesting that profilin-actin complexes bind to the FH1 domain to increase the rate of polymerization by delivering G-actin to the growing barbed end (Sagot et al., 2002, Kovar et al., 2003, Li and Higgs, 2003, Pring et al., 2003, Moseley et al., 2004).

### 1.2.1. Auto-inhibition model of Diaphanous Related Formin Regulation

The Diaphanous-Related Formins (DRFs) are the best characterized formin family members. In mammals this group includes Dia1, 2 & 3, DAAM1 & 2 and FRL1, 2 & 3 and in budding yeast Bni1p, and Bnr1p. DRFs contain three regulatory and two functional domains (Figure 1.1). The C-terminus of the molecule contains the two functional domains, FH1 and FH2. The Diaphanous Autoregulatory Domain (DAD) is also found at the extreme C-terminal end of the protein. The N-terminal half of the protein contains the remaining regulatory domains, the GTPase Binding Domain (GBD), Diaphanous Inhibitory Domain (DID), dimerization domain (DD) as well as the coiled-coil region (CC) (Figure 1.1) (Watanabe et al., 1999, Alberts, 2001, Li and Higgs, 2005, Copeland et al., 2007). The DD and CC regions both mediate dimerization of the N-terminal region of the DRFs and are required for the Rho-independent membrane targeting of the N-terminus of Dia (Copeland et al., 2007).

A simplified model of auto-inhibition suggests that DID binds directly to DAD to block the activity of the FH2 domain (Figure 1.2). GTP-bound Rho activates mDia by associating with the GTPase binding domain. The GBD overlaps slightly with DID and therefore, Rho-GTP association with GBD disrupts the DID/DAD interaction. Release of the DID/DAD interaction activates the protein by unmasking the FH2 domain (Figure 1.2). Deletion of either the DID, DAD or GBD domains renders the protein constitutively active. Recent data suggest this model is not completely accurate and that the DID/DAD interaction likely induces an inhibitory conformational change in the FH2 domain. For example, activity of the FH2 domain of FRL2 is not inhibited by the DID/DAD interaction (Vaillant et al., 2008); the crystal structure of the Daam1 FH2 dimer is also

thought to represent an autoinhibited conformation of the isolated FH2 domain (Lu et al., 2007). Revised models of DRF auto-regulation will also have to incorporate heteroligomerization of the full-length proteins. For example, full-length mDia1 can bind to full-length mDia2, apparently through a DID/DAD interaction (Copeland et al., 2007). Heteroligomerization is suggested to permit differential targeting and activation of specific DRF pairs to unique sites of action within the cell (Copeland et al., 2007).

### 1.2.2. Structural analysis of formins

Crystallographic studies of the FH2 domain of yeast Bni1p and mouse Dia1 show that these proteins form head-to-tail dimers (Xu et al., 2004). Each segment of the dimer serves as a functional actin-binding sub-unit. This structure is shared by all FH2 domains and serves an important function in actin assembly. It is probable that all formins have the ability to nucleate actin assembly at different levels.

Each of the FH2 subunits has a N-terminal linker sequence which mediates the dimerization to the other subunit. Analysis of the three-dimensional structure of Bni1p FH2 reveals that two elongated actin binding subunits are connected on either side by a flexible linker sequence to form a doughnut-shaped structure (Xu et al., 2004). The link at either end of the FH2 domain is composed of a closed loop, the 'lasso', that encircles a protrusion on the other subunit, so that they are organized in a head-to-tail fashion (Goode and Eck, 2007). The crystal structure of mDia1 is essentially identical to that of yeast Bni1p, suggesting that this is a conserved functional structure (Shimada et al., 2004).

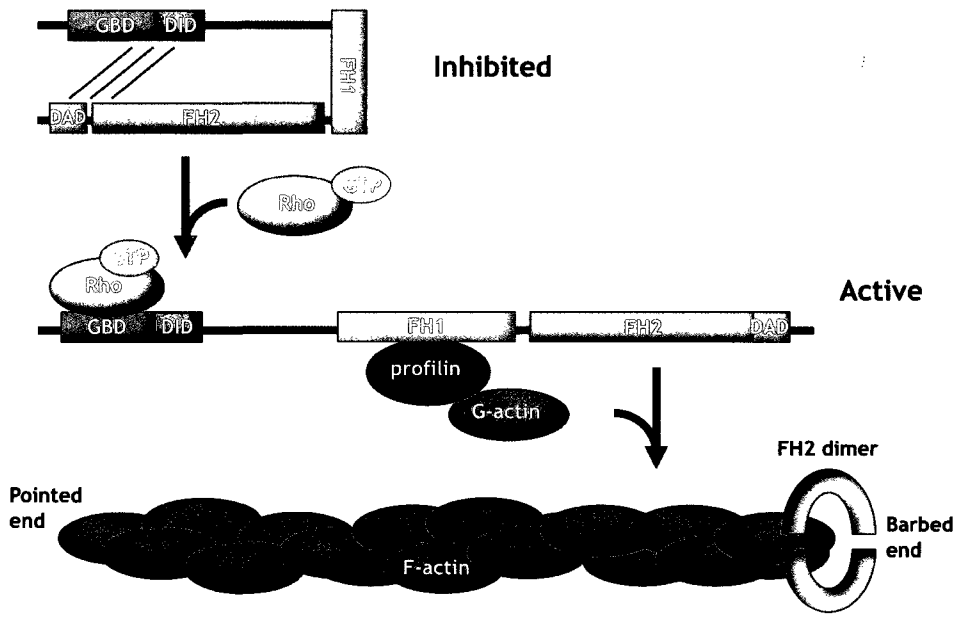


**Figure 1.2: Autoregulation model of Diaphanous-Related Formins.**

GTP-bound Rho binds the GTPase Binding Domain (GBD) relieving the inhibitory DID-DAD interaction. The open active conformation allows the FH2 domain to form a dimer (here drawn as a monomer for simplicity) and nucleate actin polymerization. The FH1 is a proline-rich domain that recruits actin-bound profilin for more efficient filament elongation. Following nucleation, the FH2 dimer remains associated with barbed end of growing filaments, adding new actin monomers in a stair-stepping manner. The FH2 dimer also forms a processive leaky cap at the barbed-end of filaments antagonizing capping proteins.

The FH2 structure suggests a 'stair-stepping' model for processive capping of growing actin filaments (Otomo et al., 2005). The head-to-tail dimer allows formins to rapidly nucleate and processively move along the barbed end of growing actin filaments. The two independent FH2 subunits associate with either the growing actin filament or an incoming actin monomer. The flexible linker segment allows repositioning, so that the subunits alternate binding between the growing actin filament and the incoming monomer. In this model the flexible FH1 domain feeds profilin-bound actin monomers to the barbed end for rapid polymerization of actin filaments.

FH2 domains of different formins vary considerably in their efficacy in nucleating actin polymerization (Goode and Eck, 2007). FH2 domains with higher affinities for actin dimers and trimers will nucleate a greater number of filaments and increase their rate of elongation in comparison to FH2 domains with a lower affinity. After filament nucleation, most FH2 domains retain a high affinity for binding to the growing barbed end of the actin filament acting as processive capping proteins that also permit the rapid addition of actin subunits (Moseley et al., 2004). This processive capping is sometimes referred to as 'leaky' capping, because formins protect the ends of the filaments from the capping proteins, such as gelsolin and heterodimeric capping protein in the cytoplasm, allowing filaments to continue to grow (Goode and Eck, 2007).

### 1.3. The Actin/MAL/SRF Pathway

Formins also induce the expression of cytoskeletal proteins through activation of the actin/MAL/SRF transcriptional response. Formin induced polymerization of F-actin

depletes the cytosolic pool of G-actin causing the shuttling of myocardin-related SRF cofactor, MAL (a.k.a MRTF/ MKL1), to the nucleus. In the nucleus, MAL binds SRF on target promoters and activates the transcription of downstream target genes (Figure 1.3) (Sotiropoulos et al., 1999, Copeland and Treisman, 2002, Miralles et al., 2003).

### 1.4. Microtubules and Formins

Microtubules (MTs) are polarized polymers of α and β-tubulin dimers. The head-to-tail addition of the α-β dimers gives an intrinsically polarized molecule with α-tubulin exposed at the minus end and β-tubulin exposed at the plus end (Downing and Nogales, 1998, 1999, Nogales et al., 1999). In order for α and β-tubulin dimers to attach to growing MTs, they must be GTP bound. The addition of GTP bound sub-units gives stability to the growing filaments. A GTP cap is maintained at the plus end of the microtubules to allow additional α-β tubulin dimers to bind. However, shortly after their addition, β-tubulin subunits hydrolyze GTP to GDP resulting in unstable microtubules which are prone to depolymerization. If this GTP cap is lost, MTs go into a state of rapid shrinkage called 'catastrophe'. Rescue occurs when a GTP cap is re-established and growth continues. MT dynamics are also dependent upon MT associated proteins (MAPs) and kinesin molecular motors. Some MAPs, such as tau and MAP2, contribute to stability by bundling adjacent filaments (Cassimeris and Spittle, 2001). Other MAPs are plus-end tracking proteins (+TIPS). Common +TIP proteins are EB1 and adenomatous polyposis coli (APC) which associate with the growing plus end and mediate MT attachment to various intracellular sites (Akhmanova and Steinmetz, 2008).

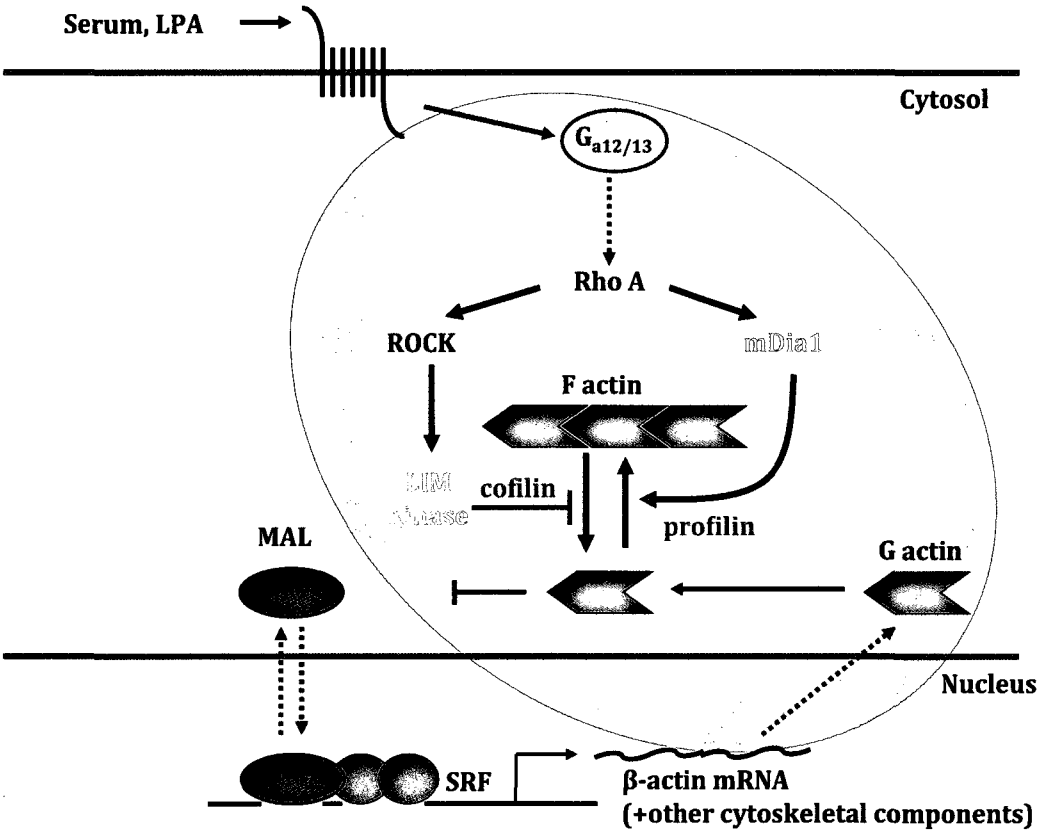


**Figure 1.3: The actin/MAL/SRF signalling pathway.**

Active Rho-GTP can stimulate F-actin accumulation through two pathways. The activation of ROCK/LIM kinase by phosphorylation prompts filament stabilization by inactivating cofilin an actin filament severing protein. Rho also stimulates actin filament polymerization through the formin mDia1. The resulting depletion of G-actin pool following polymerization leads to the release of the myocardin related co-factor MAL. Free MAL is then shuttled to the nuclear to act as a co-factor for the serum response factor (SRF). The transcription factor SRF can then activate the transcription of target genes such as actin.

Microtubules are nucleated at microtubule-organizing centers (MTOC) such as the centrioles and the basal bodies. Within the MTOC, γ-tubulin and many other proteins combine to form the γ-tubulin ring complex which acts as a scaffold for microtubule assembly. The MTOC caps the minus end of the filament while dimers polymerize at the growing plus end.

There are two sub-types of MTs inside a cell, dynamic and stable. The dynamic instability of MTs provides a mechanism that allows the plus end to probe the cellular environment in search of a specific target or organelle (Kirschner and Mitchison, 1986). Stable microtubules are preferentially used as a railway track for motor proteins allowing organelles and other proteins to move along MTs. Stable MT arrays are also assembled into larger structures such as the mitotic spindle or cilia and flagellae.

### 1.4.1. Post-translational modifications of stable microtubules

MTs are subject to a variety of unique post-translational modifications. Stable cytoplasmic MTs tend to be either detyrosinated or acetylated. Detyrosination refers to the removal of a tyrosine residue from the C-terminal end of α-tubulin exposing a penultimate glutamate residue. These newly formed detyrosinated microtubules, or Glu-MTs, are stable and resistant to depolymerization (Gundersen et al., 1987). It is not clear whether detyrosination is a cause or effect of stabilization, although a recent study has suggested that detyrosination induces MT stability by interfering with the action of depolymerising MT motor proteins (Peris et al., 2009). In the sub-group of stable acetylated MTs the α-tubulin subunit is acetylated on Lys-40 (Gaertig et al., 1995).

Stable MTs are found in all cells, but not all stable MTs are marked by both acetylation and detyrosination. What distinguishes between these two modification is still not known.

### 1.4.2. How Formins Regulate MT Dynamics

In migrating cells, formins are required for microtubule alignment with stress fibres and microtubule stabilization. It is unclear if the role of formins in MT organization can be separated from their effects on actin polymerization. Initially, it was found that the expression of mDia1(ΔN3), a constitutively active mDia1 mutant in HeLa cells, induces the formation of elongated cells (Ishizaki et al., 2001). Cells expressing mDia (ΔN3) were polarized and MTs co-aligned to F-actin bundles (Ishizaki et al., 2001). Overexpression of mutant mDia1 FH2 protein in HeLa cells and induced disorganized F-actin fibres without cell elongation and MT alignment (Ishizaki et al., 2001). This indicates that the organization of MTs by mDia1 is dependent on a functional FH2 region.

Later, it was established that constitutively active mDia induces stable MT formation oriented towards the leading edge of wounded cells downstream of LPA and Rho GTPase (Palazzo et al., 2001). Activated endogenous mDia2 also induces the formation and orientation of stable Glu-MTs (Palazzo et al., 2001). In this same study it was also shown that mDia2 associated with MTs *in vitro* and a sub-population of MTs *in vivo*. The ability of mDia to induce the formation and orientation of Glu-MTs is independent of its ability to co-align the microtubule and actin cytoskeleton (Palazzo et al., 2001).

Observations from recent publications hypothesized that mDia acts as a scaffolding protein for the microtubule plus end binding proteins EB1 and APC (Wen et al., 2004). EB1 is necessary for the formation of stable MTs downstream of Rho and mDia activation (Wen et al., 2004). Dia, APC and EB1 may stabilize microtubules by binding to MT tips and forming a capping complex in migrating cells. This complex is stabilized by multiple interactions; the basic region in APC associates with the FH1 region of mDia, while the C-terminus of APC associates with the C-terminus of EB1, the N-terminus of EB1 then associates with the FH2 region of mDia.

Formins may also play an indirect role in microtubule stabilization through the negative regulation of APC by GSK-3β (Eng et al., 2006). It has previously been shown that the Rho-mDia1 pathway regulates cell polarity and focal adhesion turnover in migrating cells through the mobilization of APC and c-Src (Yamana et al., 2006). Active mDia induces activation of novel PKCs that phosphorylates and inactivates GSK3β (Eng et al., 2006).

More recently, it has been demonstrated that mDia2 stabilizes microtubules independent of its actin nucleation activity. Three separate mutations in the mDia2 FH2 domain were identified that abrogate mDia-induced actin polymerization. FH1FH2 mDia2 directly binds MTs *in vitro* and stabilizes against cold- and dilution-induced MT disassembly. Three mutant versions of mDia2 (K853A, I704A and W630A) all induced the formation of stable microtubules, but were unable to induce F-actin accumulation, showing that FH2 functionality is not required for MT stabilization (Bartolini et al., 2008).

The overexpression of constitutively active FHOD1 has also been shown to induce the parallel alignment of MTs with actin stress fibres (Gasteier et al., 2005). It was not shown whether or not FHOD1 associates directly with MTs. However, based on immunofluorescence, it appears that MT coordination is mediated by the FH1 domain via an indirect mechanisms and not by physical contact. Although FHOD1 and mDia resemble each other in their overall effects on MT alignment with actin in elongated cells, they may mediate MT coordination by different mechanisms.

*Drosophila melanogaster* proteins Spire and Cappuccino have also been shown to have MT and microfilament cross-linking activity. One of the spire isoforms, SpireD, was shown to nucleate actin, but did not have cross-linking capabilities, however, SpireC was shown to be a cross-linker. Spire is a WH2 (WASP homology domain 2) containing protein which binds to Capu and inhibits F-actin/MT cross-linking (Rosales-Nieves et al., 2006).

### 1.5. Inverted formins (INF)

Inverted formins are an exclusively metazoan innovation. INF1 and INF2 were initially described as inverted formins with the typically C-terminal FH domains localized in the N-terminus. The FH2 domains of INF1 and INF2 have a higher degree of similarity to each other than to any other formin family member. Subsequent database searches revealed an extended N-terminal open reading frame in INF2 containing an obvious DID domain and a C-terminal DAD domain (Chhabra and Higgs, 2006). Thus INF2 is more similar to other DRFs and is most likely autoregulated by a DID/DAD

interaction. However, no extended ORF has been found for INF1, therefore it remains a true inverted formin.

INF1 was originally identified from a brain cDNA library (Nagase et al., 2000). In 2004, Katoh and Katoh, described Inverted formin 1 (INF1) (aka FHDC1) and noted the presence of 5 highly conserved C-terminal regions (labelled FHDC 1-5). These conserved C-terminal regions are unlike any other sequence in the database and INF1 lacks any previously described formin regulatory domains. No alternative regulatory domains exist and full-length INF1 is apparently constitutively active. In initial experiments we noted that INF1 is obviously recruited to the MT network. The experiments described in this thesis are aimed at furthering our understanding of the role played by INF1 in the coordinated regulation of actin and MT dynamics.

# Chapter 2:

# INF1 is a novel microtubule-associated formin

Kevin G. Young, Susan F. Thurston, Sarah Copeland, Chelsea Smallwood
and John W. Copeland

A similar report was published in Kevin G. Young, Susan F. Thurston, Sarah Copeland, Chelsea Smallwood and John W. Copeland. 2008. Mol. Biol. Cell **19:**5168-5180.

*Kevin Young performed the phylogeny analysis, expressional analysis and made the observations about microtubule acetylation. Sarah J. Copeland completed protein purification and antibody production. I made the initial observations and characterized INF1 overexpression activity. I also perform all *in vitro* and *in vivo* experiments to confirm that INF1 is a microtubule associating formin dependent on microtubule integrity show in figures 2.2, 2.4, and 2.7.

## 2.1 Abstract

Formin proteins, characterized by the presence of conserved formin homology (FH) domains, play important roles in cytoskeletal regulation via their abilities to nucleate actin filament formation and to interact with multiple other proteins involved in cytoskeletal regulation. The C-terminal FH2 domain of formins is key for actin filament interactions, and has been implicated in playing a role in interactions with microtubules. Inverted formin 1 (INF1) is unusual among the formin family in having the conserved FH1 and FH2 domains in its N-terminal half, with its C-terminal half being composed of a unique polypeptide sequence. In this study, we have examined a potential role for INF1 in regulating microtubule structure. INF1 associates discretely with microtubules, and this association is dependent upon a novel C-terminal microtubule binding domain. INF1 expressed in fibroblast cells induced actin stress fiber formation, co-alignment of microtubules with actin filaments, and the formation of bundled, acetylated microtubules. Endogenous INF1 showed an association with acetylated microtubules, and knockdown of INF1 resulted in decreased levels of acetylated microtubules. Our data suggests a role for INF1 in microtubule modification, and potentially in coordinating microtubule and F-actin structure.

## 2.2 Introduction

Formins are a family of effector proteins that commonly act downstream of small Rho GTPase activation (reviewed in Faix and Grosse, 2006; Goode and Eck, 2007). They have been primarily associated with regulating actin filament formation, and do so within various structures of most cell types in eukaryotic organisms. The formin homology 1 and 2 (FH1 and FH2) domains are largely responsible for the regulation of actin filament nucleation and elongation by formins. The FH1 domain associates with the monomeric actin binding protein, profilin, and the FH2 domain associates with nascent or mature actin filaments. Dimers of FH2 domains can nucleate actin filaments, aid in the addition of actin to the growing ends of filaments, protect the ends of actin filaments from associating with capping proteins, sever actin filaments, or cause actin filament depolymerization (Goode and Eck, 2007). The FH2 domain also regulates the expression of cytoskeletal proteins through the activation of MAL (MKL1/myocardin-related transcription factor A), which translocates to the nucleus to activate serum response factor (SRF) (Sotiropoulos et al., 1999; Copeland and Treisman, 2002; Miralles et al., 2003; Copeland et al., 2004). Formin activation of MAL is dependent on actin monomer depletion caused by the FH2 domain. The subsequent SRF activation is an additional mechanism by which stress fiber formation can be stimulated by formins (Schratt et al., 2002 and Morita et al., 2007)

Along with actin filament regulation, various studies have suggested that formins can directly regulate microtubule organization and stability (Palazzo et al., 2001; Wen et al., 2004; Rosales-Nieves et al., 2006; Bartolini et al., 2008). The FH2 domain of the Drosophila formin Cappuccino has been demonstrated to interact directly with

microtubules *in vitro* (Rosales-Nieves et al., 2006), with similar results being recently reported for the FH1/FH2 region of mDia2 (Bartolini et al., 2008). If generalized to other formin proteins, this would make the FH2 domain unique in being a single domain able to interact directly with two different types of cytoskeletal filaments.

Outside of the characteristic FH1/FH2 region, formin proteins can vary considerably (Higgs, 2005). While several contain a diaphanous-related region of homology (FH3 domain) and a GTPase binding domain in the N-terminal end, domains such as PDZ and WH2 are unique to particular formins (Miyagi et al., 2002; Chhabra and Higgs, 2006). These confer distinct localizations and functions upon these formins. For instance, the PDZ domain of delphilin mediates an interaction with a membrane protein, the glutamate receptor δ2, in neurons (Miyagi et al., 2002). This may provide a link between a post-synaptic density complex and the actin cytoskeleton. In mDia1, a dimerization motif/coiled coil region in its N-terminal half confers membrane localization on the protein (Seth et al., 2006; Copeland et al., 2007). While formin family members have been demonstrated to be essential regulators of cytoskeletal structure (Peng et al., 2007; Sakata et al., 2007; Ji et al., 2008) little is known about the diversity of functions performed by the individual family members.

In this study, we have assessed the potential function of a uniquely structured formin, INF1 (inverted formin 1; also known as FHDC1). INF1, originally identified in part from a brain cDNA library (Nagase et al., 2000), contains FH1 and FH2 domains that define it as a member of the formin family (Katoh and Katoh, 2004; Higgs and Peterson, 2005). Unlike other formins, however, the FH1 and FH2 domains of INF1 are at the N-terminus while the C-terminal end consists of a unique polypeptide sequence.

INF1 does not possess any other obvious region of homology with any other protein and lacks conserved regulatory domains. The high degree of conservation of several motifs within the C-terminal sequence of INF1 orthologues suggests that it may contain novel regulatory or functional domains. We have analyzed the expression and localization of INF1 protein in various cell lines and mouse tissues. We focus on a possible role for INF1 in regulating the structuring of microtubules. Our results demonstrate that INF1 is unique in being a primarily microtubule-associated formin, and may be involved in regulating structures where microtubule organization plays a prominent role.

## 2.3 Materials and Methods

*Analysis of INF1 evolutionary relationships*

The FH2 domains of INF1, INF2, nematode inft-1, and invertebrate FH2 sequences that were found to be most similar to the FH2 domains of INF1 and INF2 were compared to the FH2 domains of several other animal formins. The invertebrate formin proteins similar to INF1 and INF2 (named INFX in this study) were initially retrieved from GenBank using TBLASTN (http://www.ncbi.nlm.nih.gov/blast/Blast.cgi) with either the INF1 zebrafish or INF2 pufferfish sequence. The same invertebrate sequences were found when searching with either the INF1 or INF2 sequence. Specific sequences used are listed in Figure 1. The FH2 regions used from each formin were determined with SMART analysis (http://smart.embl-heidelberg.de/). A phylogenetic comparison was performed with ClustalX 2.0 run locally. We used a bootstrap analysis with 1000 replicates following initial alignment of the sequences. An unrooted tree based on this

analysis was generated with NJplot, and redrawn in Adobe Illustrator. The overall domain structure of these proteins was then compared using SMART analysis.

*Plasmid constructs*

INF1 expression plasmids were generated using the pEYFPN1, pEGFPC3 (Clontech), pGex6p2 (Amersham Pharmacia Biotech), and EFplink vectors with either myc or Flag epitope tags (Sotiropoulos et al., 1999). The full-length human INF1 open reading frame was generated using DNA from the KIAA1727 cDNA clone (obtained from the Kazusa DNA Research Institute), with missing 5' sequence being added on using oligonucleotides encoding amino acids 1-25. C-terminal truncated INF1 fusions were made in pEYFP by removing sequence coding for the region downstream from amino acid 1055 (INF1ΔC1-YFP) or amino acid 959 (INF1ΔC2-YFP) using internal *BglII* or *SacII* sites, respectively. The INF1 C-terminal fusion, GFP-INF1C (codons 958 – 1143), was made by removing a *SacII* fragment from the full-length INF1FL-YFP plasmid to insert into the pEGFPC3 vector. This same *SacII* fragment was also used to generate a GST-INF1C fusion in pGex6p2. GFP-ΔMTB1 and GFP-ΔMTB2 plasmids were generated by removing codons 958 – 1001 or 1033 – 1042, respectively. Myc-NT plasmid encoded amino acids 1 – 485, myc-FH2 encoded amino acids 85 – 485, and myc-CT encoded amino acids 486 – 1143. Codon numbering is given for the human INF1 protein in GenBank accession number NP_203751. For mouse INF1, the full open reading frame was cloned using overlapping fragments generated with RT-PCR, shown in Supplemental Figure 1. The full insert was cloned as a *BglII – SalI* insert into pEGFPC1 (GFP-mINF1) using standard cloning techniques. Constructs used for SRF

activation assays, 3DA.Luc and MLV-LacZ, have been described previously (Geneste et al., 2002 and Sotiropoulos et al., 1999, respectively). The inserts of all newly-generated plasmids were sequenced to ensure their accuracy, and appropriate expression of the fusion proteins was confirmed by immunoblotting.

*Cell culture and animals*

The Cos-1 monkey kidney cell line, N2A mouse neuroblastoma cells, F11 rat/mouse sensory neuron cell line, H9C2 rat cardiomyocyte line, and HeLa human carcinoma line were each maintained in DMEM containing 10% FBS and 1% pen/strep in a 37°C incubator with 5% $CO_2$. Sub-confluent cells were passaged in 10 cm plastic dishes. For differentiation of the N2A cells, serum-containing DMEM was replaced with DMEM containing 0.5 mM dibutyryl cAMP (Calbiochem) and 1% penicillin/streptomycin for 24 – 48 hours. Mouse NIH 3T3 fibroblast cells were maintained in DMEM containing 10% FBS and 1% pen/strep in a 37°C incubator with 10% $CO_2$. Sub-confluent cells were passaged in 10 cm plastic dishes for up to 13 passages.

Cos-1 cells were transfected with PEI (Polyethyleneimine; Polysciences Inc., Warrington, PA). This was done by mixing 5 µl of a 1 µg/µL PEI solution with 1.5 µg of plasmid DNA in 50 µl of OptiMEM (Invitrogen) for 15 – 30 minutes. This was then added to one well of cells in a six well plate in 1 mL of OptiMEM. Following a five to eight hour incubation, the transfection medium was replaced with normal growth medium. NIH 3T3 cells were transfected with either PEI, or in the case of the SRF activation assays, Lipofectamine (Invitrogen). Drug treatments with nocodazole (Sigma)

or latrunculin A (Sigma) were performed as indicated in the Results section. Both nocodazole and latrunculin A stock solutions were prepared in DMSO (Sigma); DMSO alone was used for control samples. For microscopy, all cells were plated on sterile glass coverslips.

Mouse tissues were collected from five day-old and two month-old C57BL/6 mice. Tissues use for immunohistology were immersed in OCT compound (Sakura) in plastic molds, frozen using liquid nitrogen, and stored at -80°C. Frozen sections were cut in a cryostat at an 8 μm thickness and placed on gelatin-coated Superfrost Plus slides (Fisher). The sections were air dried and either stained immediately or stored at -20°C. Tissue used for immunoblotting were collected in lysis buffer containing 50 mM Tris (pH 7.5), 100 mM NaCl, 5% glycerol, 1mM EDTA, and 1% Triton X-100. The protein content was determined by Bradford analysis, and samples were diluted in a standard SDS buffer for SDS-PAGE analysis.

*INF1 antibody generation*

INF1 antibody was generated against a protein corresponding to the human INF1 FH2 domain (amino acids 85 – 541). Briefly, protein expressed in BL21 bacteria was purified by Prescission Protease cleavage of GST-INF1 FH2 protein bound to glutathione sepharose 4B beads. The purified FH2 protein was dialyzed against phosphate buffered saline, and used for injection into New Zealand White rabbits (Cedarlane Laboratories, Burlington, ON). Antibody from the immune serum was affinity-purified against protein A, followed by purification against GST-INF1 FH2, using standard techniques. Antibody

was eluted with a glycine buffer (pH 2.8), then buffered with pH 9.0 Tris prior to dialysis into PBS.

*Immunoblotting*

Protein lysates were collected from cells grown in culture by two methods. Initially, equal numbers of cells were washed twice in PBS, scraped in Laemmli buffer and boiled for five minutes prior to cooling on ice. As a second method, cells were washed twice in PBS, then scraped in a high salt lysis buffer (50 mM Hepes pH7.5, 4% SDS, 300 mM NaCl, 1 mM EDTA) supplemented with a protease inhibitor cocktail (Roche) and dithiothreitol (5 mM) added directly prior to use. These samples were immediately boiled for five minutes, then cooled in room temperature water for one minute, prior to adding 50 µl of 300 mM iodoacetamide per 500 µl of sample. The samples were centrifuged and sheared through a 27 gauge needle. To load these samples on a gel, they were added to an equal volume of gel loading buffer containing 100 mM Tris pH 6.8, 4 % SDS, 20% glycerol, 5% β-mercaptoethanol, 1 M NaCl, 4 M Urea, and 0.1% bromophenol blue. Lysates were run on standard SDS-PAGE gels, and transferred onto PVDF membrane (Millipore). The blots were blocked with 5% non-fat dairy milk (NFDM) in Tris buffered saline (TBS). Primary and secondary antibody incubations were performed in TBS containing 0.5% Tween 20 (TBST). All washings were performed using TBST. HRP-labeled secondary antibodies were detected with chemiluminescence reagent (Perkin Elmer) prior to blots being exposed to autoradiography film. Affinity-purified anti-INF1 antibody was incubated at 1:500 overnight at 4°C, anti-α-tubulin

antibody was incubated at 1:5000 and anti-lamin B at 1:200 at room temperature for one hour.

*INF1 siRNA*

INF1 was knocked-down in NIH 3T3 cells using an RNA oligonucleotide duplex (Integrated DNA Technologies) with the following sequences: 5'-GCUAUAGCACCAAAGAGAAAUUCCT-3' and 5'-AGGAAUUUCUCUUUGGUGCUAUAGCAU-3'. This duplex was found to reliably reduce GFP-mINF1 levels when co-transfected in Cos-1 cells (Supplemental Figure 2). NIH 3T3 cells were transfected with the siRNA duplex using Dharmafect 1 (Dharmacon) following the manufacturer's instructions. We examined INF1 levels in cell lysates collected at two, three, five, seven and ten days post-transfection by immunoblotting. Lysates were collected in high salt lysis buffer as described above. Antibodies to detect acetylated tubulin (Sigma), α-tubulin (Sigma), and lamin B (Santa Cruz) were used to probe the blots following stripping in a pH 2.5 glycine (0.1 M) and 0.5% SDS buffer between each probing.

*Serum response factor activation assay*

SRF activation assays were performed as described previously (Copeland et al., 2002). Briefly, NIH 3T3 cells were transfected with 50 ng of the reporter construct 3DA.Luc, along with 250 ng of the reference plasmid, MLV-LacZ, and the expression plasmid encoding the fusion protein to be tested. Empty pEF Flag was co-transfected to a total of 1.5 μg of DNA per well in 6 well plates. Following the transfection, cells were

maintained in 0.5% FBS in DMEM with 1% penicillin/streptomycin. After 24 hours, cells were harvested for a standard luciferase assay. Transfection efficiency was standardized by a β-galactosidase assay. Data is shown relative to reporter activation by the constitutively active SRF derivative, SRFVP16 (50 ng).

In vitro *microtubule association and bundling assays*

GST-INF1C fusion protein was purified from BL21 bacteria induced with 0.2 mM IPTG at 37°C. Purified protein incubated on glutathione sepharose 4B beads (GE Healthcare) was recovered by PreScission Protease (GE Healthcare) cleavage of the GST moiety, followed by dialysis into PEM buffer (20 mM PIPES pH 7, 20 mM KCl, 1 mM DTT and 5% glycerol). Microtubule spin-down assays were performed using a microtubule spin-down kit (Cytoskeleton). Microtubules were assembled for 20 minutes at 35°C in a general tubulin buffer (80 mM PIPES pH 7.0, 2 mM $MgCl_2$, 0.5 mM EGTA) in the presence of GTP and taxol. INF1C or control protein was incubated with 0.83 μM tubulin dimers for 30 minutes. Microtubules and associated proteins were then pelleted at 100,000 x *g* through a 50% glycerol cushion buffer. Supernatant and pellet were combined with Laemmli loading buffer and equal amounts of sample were run on a 10% SDS-PAGE gel for analysis by Coomassie blue staining.

To examine microtubule bundling by immunofluorescence, INF1C or control protein was incubated with stabilized microtubules at room temperature for 30 minutes. Samples were then placed on gelatin-coated Superfrost Plus slides (Fisher) and incubated for 10 minutes before fixing with 4% paraformaldehyde. Microtubules were visualized with anti-α-tubulin antibody and an Alexa Fluor 594 labeled secondary antibody

(Invitrogen). The preparations were photographed on an AxioImager microscope (Zeiss) with a 63X Plan Apochromat objective.

*Immunofluorescence*

Tissue culture cells and mouse brain sections were stained using a basic immunofluorescence protocol. Briefly, cells or tissue sections were washed twice in PBS, then fixed with 4% paraformaldehyde in PBS for 10 minutes. The cells or tissue sections were washed 3 X 5 minutes in PBS, and permeabilized and blocked with PBS containing 0.4% Triton X-100 and 10% FBS. Primary antibody diluted in PBS containing 0.04% Triton X-100 and 5% FBS was then incubated on the samples either overnight at 4°C or for 1 hour at room temperature. The samples were washed 3 X 5 minutes, then incubated for 1 hour at room temperature with the appropriate secondary antibody. Following a final wash of 3 X 5 minutes in PBS, the samples were mounted using Vectashield with DAPI (Vector Laboratories). Primary antibodies used included affinity purified anti-INF1 polyclonal at 1:50, anti-α-tubulin monoclonal at 1:1000, anti-acetylated tubulin monoclonal at 1:1000 (Sigma), anti-detryrosinated tubulin at 1:250 (Chemicon), and anti-β III tubulin (tuj1) at 1:1000 (Covance). Phalloidin-rhodamine or phalloidin-Alexa Fluor 488 (1:20) (Invitrogen), incubated with the secondary antibody, were used to detect F-actin.

Cells and tissues were imaged primarily with a Zeiss AxioImager equipped with an apotome. Apotome optical sections were imaged with a 63X Plan Apochromat objective producing sections of 0.7 μm. Confocal imaging was done with a LSM 5 Pascal confocal system attached to an Axiovert 200M inverted microscope (Zeiss). Confocal

sections of 1 μm were produced using a 63X Plan Apochromat objective with 488 and 543 nm laser lines being used for excitation. A band pass 505 – 530 nm emission filter was used to collect the green emission and exclude non-specific emission from the red fluorophore, and a long pass 560 filter was used for the red emission.

## 2.4 Results

*INF1 is a unique microtubule-associated formin that affects F-actin organization*

To understand the origin of the unique INF1 domain structure, we analyzed the phylogenetic relationship between INF1 and other animal formins. The INF1 and INF2 proteins diverged in the early chordates from an ancestral form containing both a diaphanous-related region upstream from the FH1 and FH2 domains, and an extensive C-terminal end downstream. Related sequences for previously un-described Animalia formins with this type of structure are found in various insect species, as well as the sea urchin, *S. pupuratus* (Figure 2.1). We have named these the INFX proteins. These proteins resemble the INF2 protein (Higgs and Peterson, 2005), but have longer C-terminal regions downstream from the FH2 domain. The INFX FH2 domains are intermediate to INF1 and INF2 in their primary sequences. Regions coding for N-terminal diaphanous-related formin domains are absent 5' to the FH1/FH2 coding region in the INF1 gene from human, mouse and zebrafish (as assessed with MIT Genscan). Sequences resembling the diaphanous autoregulatory domain (DAD) and diaphanous inhibitory domain (DID) do not appear to be present in INF1. INF1 does contain several regions within its C-terminal end that are conserved between vertebrate orthologues (Katoh and Katoh, 2004), including regions we have labeled as MTB1 and MTB2

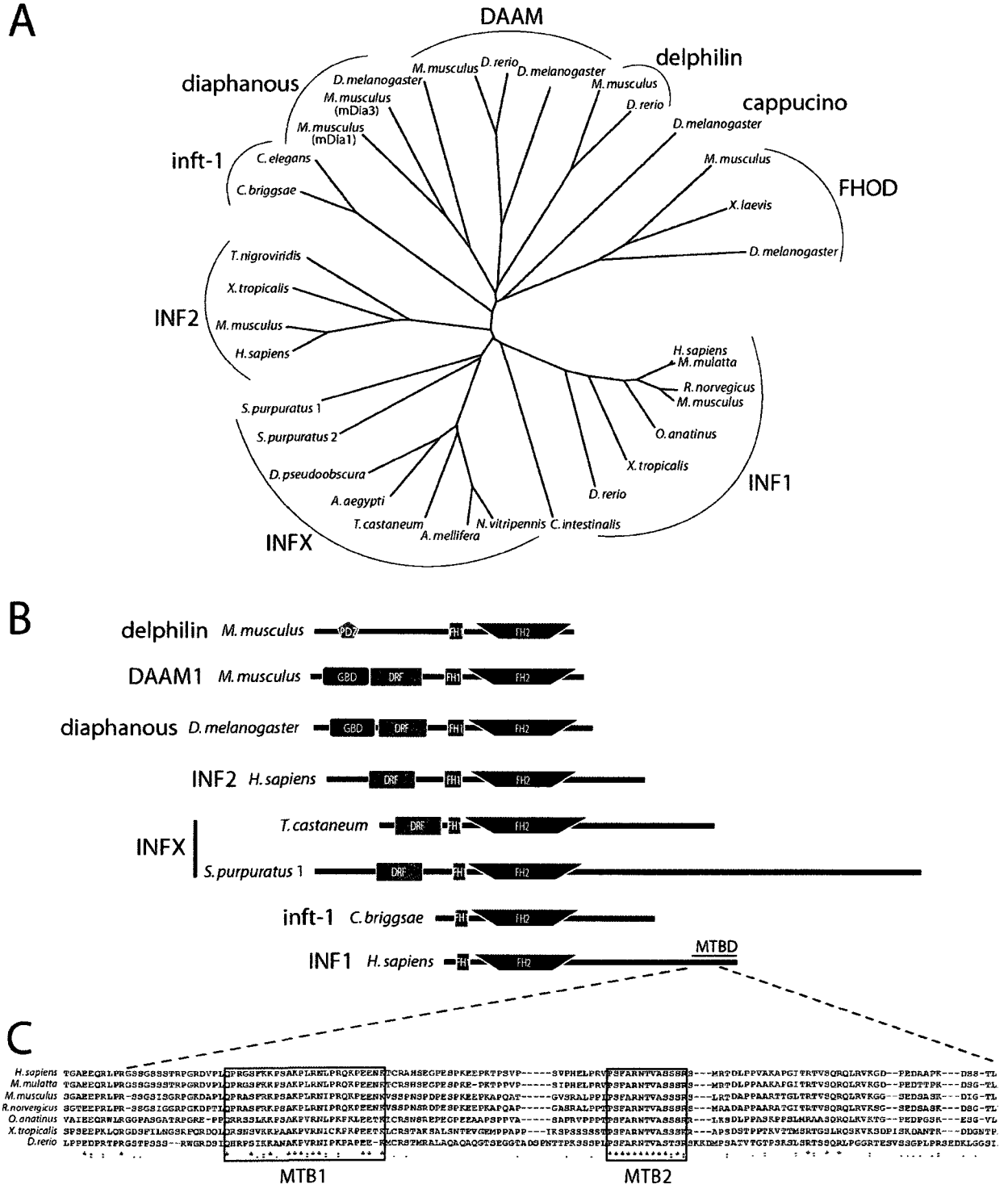
A
DAAM
delphilin
diaphanous
cappucino
inft-1
FHOD
INF2
INF1
INFX
M. musculus
D. rerio
D. melanogaster
M. musculus (mDia3)
M. musculus (mDia1)
C. elegans
C. briggsae
T. nigroviridis
X. tropicalis
H. sapiens
M. mulatta
R. norvegicus
S. purpuratus 1
S. purpuratus 2
O. anatinus
D. pseudoobscura
A. aegypti
T. castaneum
N. vitripennis
C. intestinalis
A. mellifera
X. laevis
B
delphilin M. musculus
DAAM1 M. musculus
diaphanous D. melanogaster
INF2 H. sapiens
INFX
T. castaneum
S. purpuratus 1
inft-1 C. briggsae
INF1 H. sapiens
GBD
DRF
FH1
FH2
PDZ
MTBD
C
MTB1
MTB2

**Figure 2.1. INF proteins in animals.**

(A) An unrooted phylogenetic tree based on a comparison of the FH2 domains of INF1, INF2 and other animal formins. Sequences used for this analysis (with GenBank accession numbers in brackets) came from human (H. sapiens) INF1 (NP_203751.2) and INF2 (NP_071934.3); monkey (M. mulatta) INF1 (XP_001085372.1); mouse (M. musculus) INF1 (NP_001028473.1), INF2 (ABI20145.1), mDia1 (O08808.1), mDia3 (AAH86779.1), DAAM1 (AAH76585.1), delphilin (NP_579933.1), and FHOD1 (NP_808367.1); rat (R. norvegicus) INF1 (NP_001099907.1); platypus (O. anatinus) INF1 (XP_001511976.1); toad (X. tropicalis or X. laevis) INF1 (CR942785.2), INF2 (NP_001072591.1), and FHOD1 (AAH84291.1); zebrafish (D. rerio) INF1 (predicted from BAC clone CH211-62K15), DAAM1 (XP_707353.2), and delphilin (XP_689509.2); pufferfish (T. nigroviridis) INF2 (CAG10691.1); sea squirt (C. intestinalis) INF1 (translated from AK173884.1); fruit fly (D. melanogaster or D. pseudoobscura) INFX (XP_001353341.1), diaphanous (NP_476981.1), DAAM (AAF45601.2), cappuccino (NP_722951.1), and FHOD (NP_729410.1); sea urchin (S. purpuratus) INFX (XP_793426.2 and XP_785094.2); wasp (N. vitripennis) INFX (XP_001600053.1); honey bee (A. mellifera) INFX (translated from XR_015075.1); flour beetle (T. castaneum) INFX (XP_970252.1); mosquito (A. aegypti) INFX (XP_001660600.1), and nematode worm (C. elegans and C. Briggsae) inft-1 (NP_497334.1 and XP_001666551.1, respectively). The novel INFX group contains FH2 domains most similar to both INF1 and INF2, as determined by both BLAST and ClustalW2 analysis. Branch lengths correspond to evolutionary distances. (B) Domain structures of representative animal formins. Delphilin, DAAM1 and diaphanous, as with most known formins, contain C-terminal FH1/FH2 regions. These formins also contain regulatory domains in the N-terminal half. Shown are the PDZ domain of delphilin, and the GTPase binding domain (GBD) and diaphanous related formin domain (DRF; diaphanous inhibitory domain region) of DAAM1 and diaphanous. INF2 and INFX proteins share the DRF domain in the N-terminal part of the protein. Each of the INF proteins has a C-terminal region downstream from the FH2 domain that is more extensive than in other formins. In INF1, and in the nematode worm inft-1 sequences, the region upstream from the FH1 domains is considerably shorter relative to other formins, thus placing the FH1/FH2 region in the N-terminal half. There are no obvious regulatory regions upstream of the INF1 FH1 region in the N-terminus. At the C-terminal end of INF1, we have mapped a novel microtubule binding domain (MTBD), in this study. (C) A ClustalW2 alignment of part of the novel C-terminal MTBD of INF1 showing two well conserved regions, which we have labeled as MTB1 and MTB2. Asterisks denote identical amino acid residues in each sequence, two dots denote conserved amino acids, and one dot denotes semi-conserved amino acids.

(Figure 2.1C). INF1 is therefore likely to be regulated in a manner fundamentally different than the better-characterized diaphanous-related formins, and may contain novel functions conferred on it by its unique C-terminal end.

To examine if INF1 exhibited functions characteristic of other formins, we assessed whether expression of INF1 fusion proteins could induce the formation of stress fibers and induce SRF activation in serum-starved NIH 3T3 fibroblasts. Transfection of cells with plasmids encoding full-length and N-terminal INF1 fusion proteins could induce the formation of stress fibers in the 3T3 cells following one day of expression (Figure 2.2 and Supplemental Figure 2.1.3). Induction of stress fiber formation by full-length INF1 was similar to that of the isolated FH2 domain from mDia1 (Fig. 2.1E). The N-terminal fusion proteins of INF1 were, however, less efficient at inducing thick stress fiber formation, producing mainly an increase in thin filaments. Interestingly, the full-length INF1 localized discretely with microtubules (insets in Figure 2.2A, C).

Full-length and N-terminal INF1 fusion proteins also induced SRF activation in serum-starved NIH 3T3 cells (Figure 2.2F). Expression of the FH2 domain alone (myc-FH2) was sufficient to induce activation of the SRF reporter gene, consistent with our previous results obtained with mDia1 (Copeland et al., 2002). Also similar to mDia1, expression of protein with both the FH1 and FH2 domains (myc-Nterm and myc-INF1FL) induced an increased response in the SRF activation assay. Expression of the C-terminal end of INF1 had no effect on SRF activation. Of note is that the full-length INF1 fusion protein was constitutively active in the SRF and stress fiber formation assays. This is consistent with INF1 activity being regulated differently than the diaphanous-related formins.

*Endogenous INF1 is predominantly microtubule-associated*

To examine expression of the INF1 protein, we produced affinity-purified polyclonal antibody against the human INF1 FH2 domain. This antibody recognized both mouse and human INF1 fusion proteins (Figure 2.3). By immunofluorescence, the INF1 antibody specifically recognized full-length INF1FL-YFP fusion protein expressed in Cos-1 cells (Figure 2.3A). Untransfected Cos-1 cells did not display any staining. By immunoblot analysis of NIH 3T3 lysates, we observed a prominent band of ~125 kD which could be knocked-down by transfecting cells with an siRNA duplex targeted to the INF1 transcript (Figure 2.3B). Unexpectedly, full-length INF1 fusion proteins ran appreciably higher than the 125 kD mark on standard SDS-PAGE gels (Figure 2.3C). We were able to observe a band corresponding to the size of full-length INF1 fusion protein, present in several cell lines analyzed, though only with the use of cell lysis buffer containing protease inhibitors with a high salt concentration (see Materials and Methods), and longer exposures of the blots. Detection of this second band, as well as the other bands recognized by the antibody, was greatly reduced by pre-incubating the INF1 antibody with purified GST-INF1 (data not shown). These data suggest that the predominant lower molecular weight band may be due to protein modification of the endogenous INF1. Alternatively, rapid protein degradation or modification upon cell lysis may occur. No evidence of alternative splicing for mouse INF1 was found by RT-PCR analysis (Supplemental Figure 2.1.1).

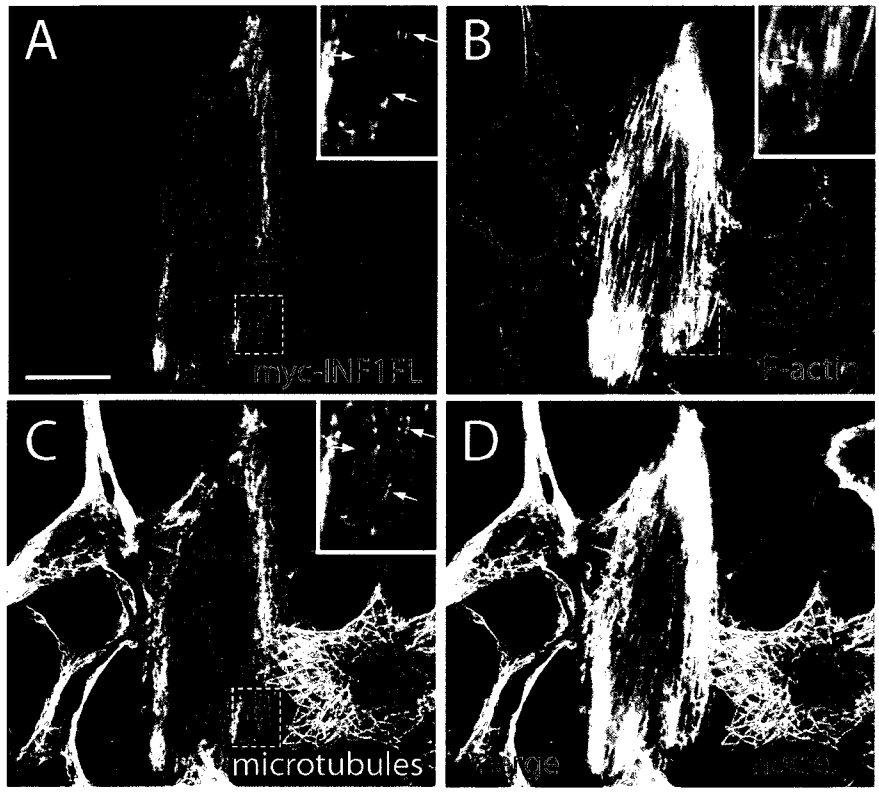


E

| | ↑thick filaments | ↑thin filaments | no diff. |
|---|---|---|---|
| INF1FL | 41 | 48 | 11 |
| Nterm | 9 | 71 | 20 |
| FH2 | 4 | 58 | 38 |
| Cterm | 2 | 19 | 79 |
| mDia1FL | 0 | 4 | 96 |
| mDia1 FH2 | 42 | 40 | 18 |

F

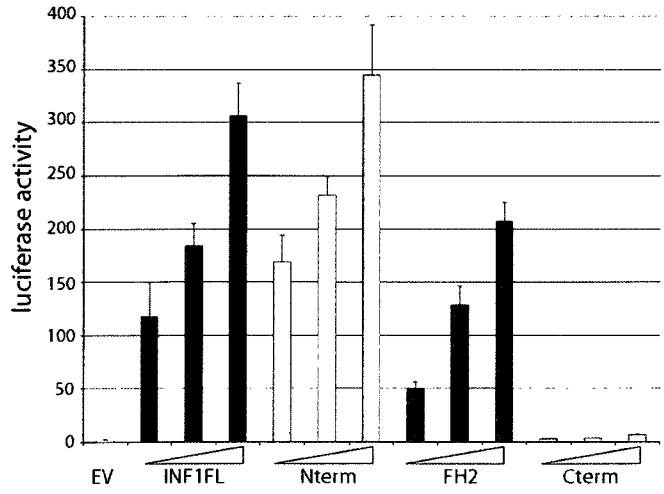

**Figure 2.2. INF1 induces stress fiber formation and SRF activation in NIH 3T3s.**

(A – D) Full length myc-INF1FL fusion protein induced the formation of actin filaments (B) in serum-starved 3T3 cells after one day of expression. (C) Microtubule staining in the transfected cells co-aligned with the INF1 fusion protein. Co-aligning INF1 and microtubules are indicated by arrows in the insets, which are enlarged from the boxed area of the transfected cell shown. Actin filaments also co-aligned to a more limited extent (indicated by the arrow in the inset in B). The merged image is shown in D. (E) Schematics of the myc-INF1FL fusion protein, myc-INF1 truncation mutants, and myc-mDia1 full-length (FL) and FH2 domain fusion proteins used to examine stress fiber formation, along with quantifications of starved 3T3 cells expressing these proteins that displayed increased actin filament formation. Cells were scored as having an increase in thick filaments if the filaments displayed markedly brighter phalloidin labeling compared to untransfected cells (as in panel B), and as having an increase in thin filaments if there were more actin filaments compared to the untransfected cells, but with a similar intensity of phalloidin labeling. (F) Full-length (myc-INF1FL) and N-terminal (myc-Nterm and myc-FH2) INF1 fusion proteins induced SRF activation after one day of expression in serum-starved 3T3 cells. 0.1, 0.3, and 1 μg of plasmid were transfected for each INF1 plasmid. Empty vector (EV) served as a negative control. Expression of a C-terminal INF1 fusion (myc-Cterm) did not induce SRF activation. Results are from three independent experiments, with standard error of the mean shown. Scale bar = 20 μm in A and also applies to the larger images in B – D.

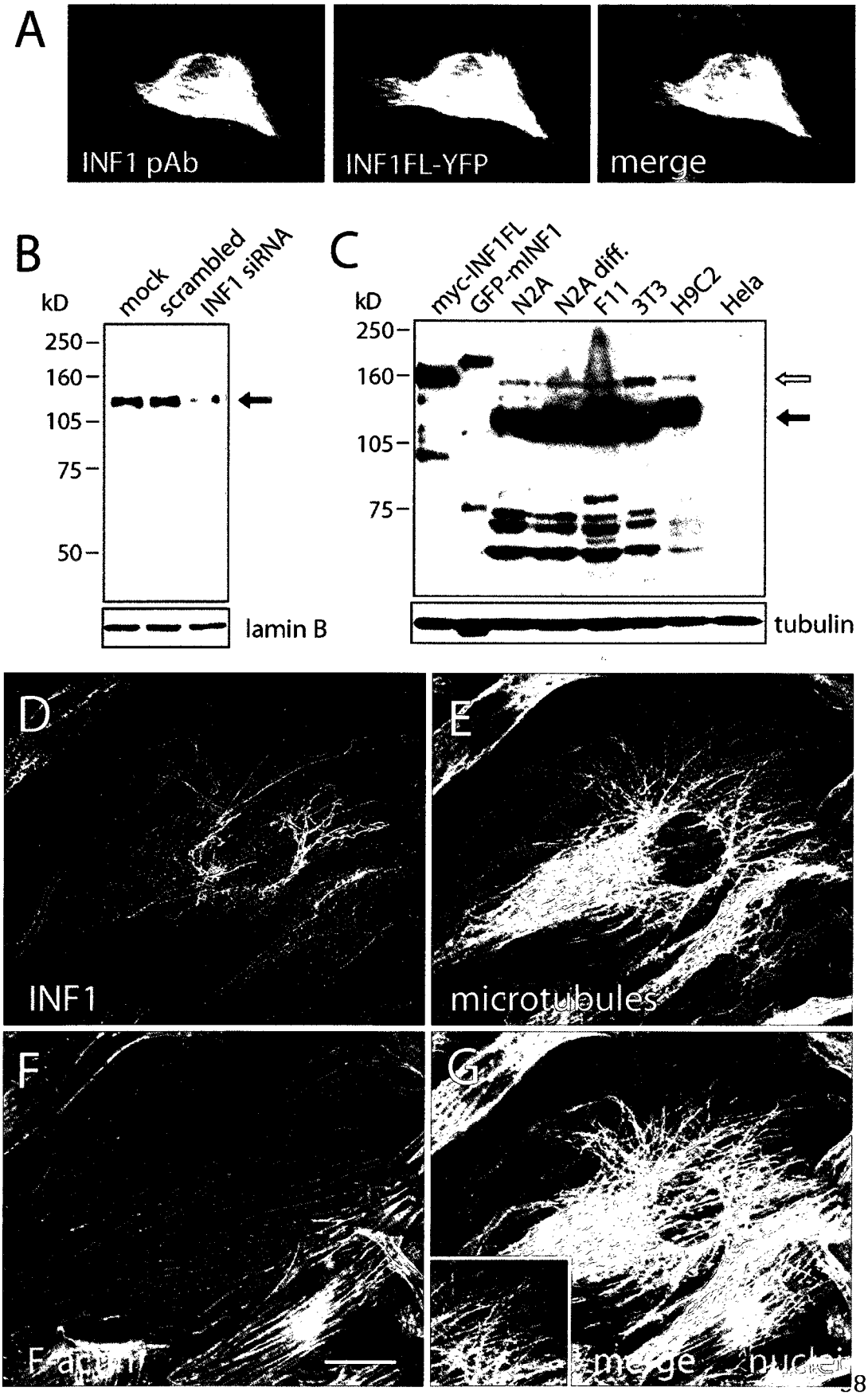
A
INF1 pAb
INF1FL-YFP
merge
B
kD
mock
scrambled
INF1 siRNA
250
160
105
75
50
lamin B
C
kD
myc-INF1FL
GFP-mINF1
N2A
N2A diff.
F11
3T3
H9C2
Hela
250
160
105
75
tubulin
D
INF1
E
microtubules
F
F-actin
G
merge
nuclei

**Figure 2.3. Endogenous INF1 protein is primarily associated with microtubules.**

(A) Full-length INF1FL-YFP expressed in Cos-1 cells was specifically detected using an affinity-purified INF1 pAb by immunofluorescence. Staining was not observed in untransfected cells. (B) Detection of endogenous INF1 by immunoblotting NIH 3T3 cell lysates. A band of ~125 kD was consistently the predominant band detected. Detection of this band was decreased by an average of 51% (three separate trials) using 1 nM INF1 siRNA duplex when compared to cells transfected with 1 nM control scrambled siRNA, in lysates collected seven days post-transfection. Mock transfected cells displayed similar levels of INF1 to the control transfected cells. Lamin B is shown as a loading control. Lysates were collected with lysis buffer containing a high salt concentration and protease inhibitors, as described in Materials and Methods, though similar results were obtained with a standard SDS buffer in this case (data not shown). (C) Immunoblotting with INF1 pAb using protein lysates from Cos-1 cells expressing myc-INF1FL or GFP-mINF1, two neuronal cell lines (N2A and F11), NIH 3T3 fibroblast cells, a cardiomyoblast cell line (H9C2), and HeLa cells. Endogenous protein running at a similar molecular weight to myc-INF1 (~ 160 kD; marked with an arrow) was detected in undifferentiated and differentiated N2A cells (N2A and N2A diff, respectively), undifferentiated F11 cells, NIH 3T3 cells, and H9C2 cells, but not in HeLa or Cos-1 cells (note no band of this size in the GFP-mINF1 lane, with this fusion protein running higher due to the additional size of the GFP). In the N2A, F11, NIH 3T3, and H9C2 lysates, the lower molecular weight band of ~125 kD was detected much more prominently, and was overexposed in order to detect the higher molecular weight band. (D) INF1 localized in a filamentous pattern in NIH 3T3 cells. This pattern co-aligned with a subset of microtubules (E). (F) F-actin staining was not consistently co-localized with the INF1 staining. (G) Merged image of D – G. The inset in G shows INF1 merged with microtubules alone from this cell, at a higher magnification. Scale bar = 20 μm in F.

By immunofluorescence analysis of endogenous INF1 in NIH 3T3 cells, the INF1 antibody detected protein discretely co-aligning with a subset of microtubules (Figure 2.3D – G). Filamentous INF1 staining was present in a majority of cells, with some punctate staining also being commonly observed. Both punctate and filamentous INF1 staining was primarily microtubule-associated in all cells. The same was true in a second cell line with a fibroblast-like morphology, H9C2 cardiomyoblasts (Supplemental Figure 2.1.4). Since the INF1 FH2 domain may be involved in actin filament association and polymerization, we also investigated whether INF1 co-localized with F-actin staining. There was, however, no consistent pattern of INF1 localization with F-actin in NIH 3T3 (Figure 2.3) or H9C2 cells. Correspondingly, disruption of microtubule polymerization with nocodazole in NIH 3T3 cells resulted in the diffuse localization of the endogenous INF1 (Figure 2.4E – H). The disruption of actin filament polymerization with latrunculin A had little effect on INF1 distribution (Figure 2.4I – L). Endogenous INF1 is therefore a predominantly microtubule-associated protein in these cells.

*INF1 expression in mouse*

To gain some insight into the types of structures INF1 might normally associate with in animal tissues, we screened several mouse tissues for INF1 expression. By immunoblot analysis, we observed INF1 to be readily detectable in brain, heart, and lung tissues (Figure 2.5A). Correspondingly, INF1 was easily detected by immunofluorescence staining in ventricular muscle sections of the heart, but not in kidney sections (Figure 2.5B, C). In the brain, we found INF1 to be most strongly expressed in Purkinje neurons of the cerebellum. In sections from five day-old animals,

INF1 was predominantly found in the cell bodies of the immature Purkinje neurons (Figure 2.5D), which do not fully mature until the second week after birth (Millen et al., 1994). In the adult animal, INF1 staining was primarily found in the white matter of the cerebellum, with weak staining in projections from the Purkinje cell layer (Figure 2.5E). This staining appeared to be axonal, and localized in proximity to neuronal β-tubulin staining (Figure 2.5F – H).

*The INF1 C-terminus contains a microtubule binding domain and is required for INF1 microtubule association*

To examine which domain of the INF1 protein might target INF1 to microtubules, we investigated whether the conserved regions in the C-terminal half may be necessary for proper localization. We initially examined the importance of the two conserved regions located towards the C-terminal end of the protein (labelled MTB1 and MTB2 in Figure 2.1). Full-length INF1FL-YFP fusion protein primarily co-aligned with microtubules in Cos-1 cells (Figure 2.6A – C). Transfection with a full-length mouse GFP-mINF1 construct additionally resulted in a noticeable bundling of the microtubules (Supplemental Figure 2.1.1). The INF1ΔC1-YFP fusion, which had sequence removed downstream of the MTB1 and MTB2 regions, also localized in a filamentous pattern along the length of the microtubules. This filamentous localization occurred in fewer than half of the cells compared to the full-length INF1 fusion protein, however, indicating a reduced ability to associate with microtubules (Figure 2.6D – F). More cells expressing INF1ΔC1-YFP displayed puncta or diffusely localized fusion protein.

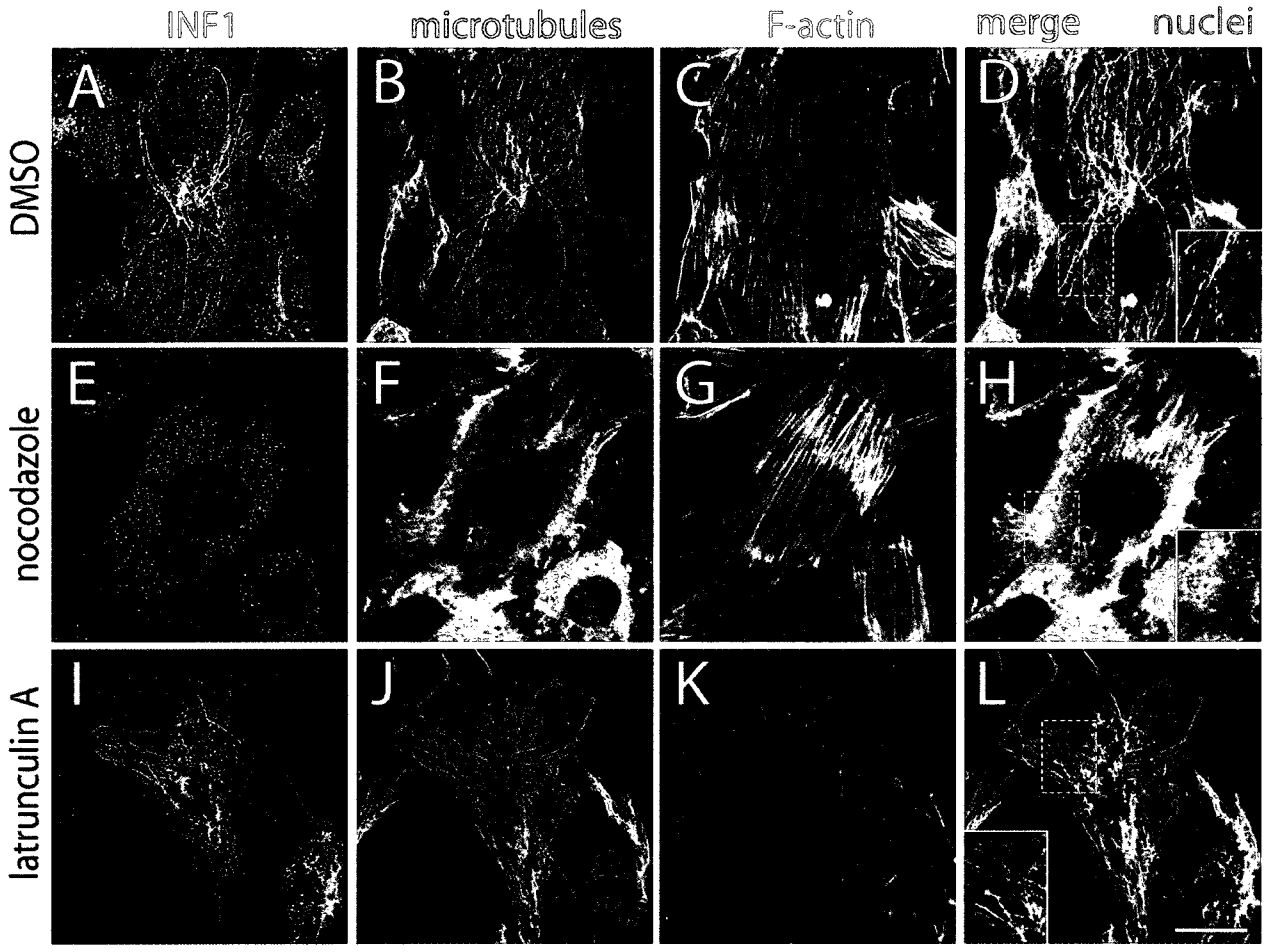
INF1
microtubules
F-actin
merge
nuclei
DMSO
nocodazole
latrunculin A
A
B
C
D
E
F
G
H
I
J
K
L

**Figure 2.4. INF1 localization is microtubule-dependent in NIH 3T3 cells.**

(A – D) Control cells treated with a 1:500 DMSO dilution, stained for INF1 (A), microtubules (B) and F-actin (C). INF1 localized in a filamentous pattern along microtubules in these cells. The merged image is shown in D, with enlargement from the boxed area in the inset. (E – H) Cells treated with the microtubule depolymerizing drug nocodazole (500 nM, 15 minutes) had dispersed microtubules (F) and dispersed INF1 staining (E). F-actin staining is shown in G, and the merged image in H, with enlargement from the boxed area in the inset. (I – L) Cells treated with the actin depolymerizing drug latrunculin A (1 μm, 15 minutes) had dispersed actin filaments (K) but INF1 (I) remained localized along the microtubules (J). The merged image is shown in L, with enlargement from the boxed area in the inset. Scale = 20 μm and applies to all images.

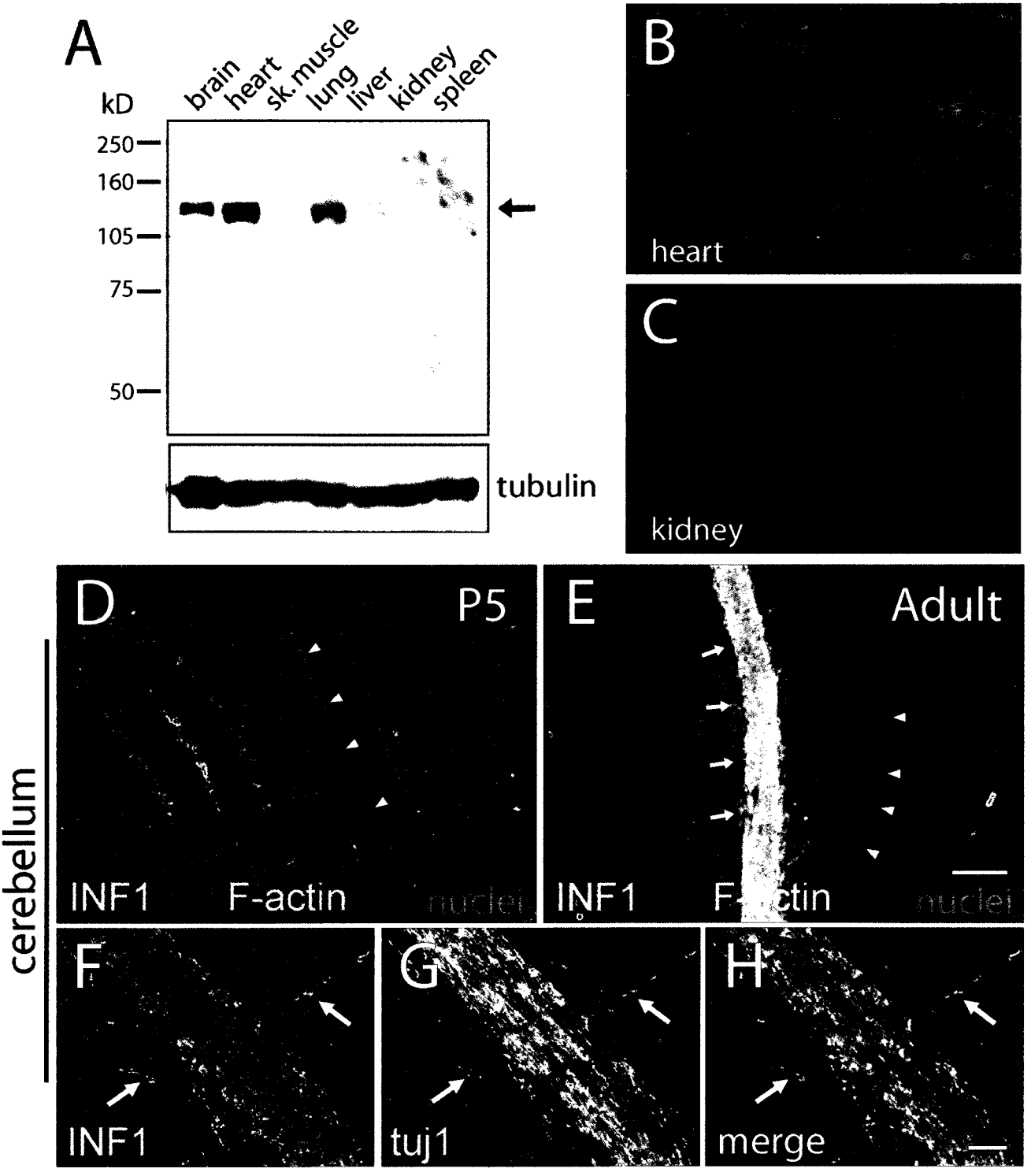
A
brain
heart
sk.muscle
lung
liver
kidney
spleen
kD
250
160
105
75
50
tubulin
B
heart
C
kidney
D
P5
INF1
F-actin
nuclei
E
Adult
INF1
nuclei
cerebellum
F
INF1
G
tuj1
H
merge

**Figure 2.5 Expression of INF1 in mouse tissues.**

(A) Immunoblot of mouse tissues showing expression of INF1 protein (arrow) in brain, heart and lung. (B) By immunofluorescence analysis, INF1 was readily detectable in ventricular muscle of the heart. (C) At an identical exposure as in B, an immunofluorescence signal was barely detectable in kidney, corresponding to immunoblotting results shown in A. (D) INF1 (green) staining in a 5 day-old (P5) mouse cerebellum coronal section. The section was counterstained for F-actin (red) and chromatin (blue). INF1 staining in Purkinje neuron cell bodies is indicated by the arrowheads. (E) Sagittal brain section showing INF1 (green) staining with F-actin (red) labeling in the cerebellum of a two month-old (adult) mouse. Arrows point to the white matter layer, and arrowheads to the Purkinje neuron cell bodies. (F – H) Higher magnification confocal images showing INF1 (F) with tuj1 (β tubulin) (G) in axons. The merged image is shown in E. While INF1 was consistently associated with tuj1 staining, they did not necessarily co-localize. Scale bar = 20 μm in E, and also applies to D, and 10 μm in H, and also applies to F, G.

The INF1ΔC2-YFP protein, which lacks the MTB1 and MTB2 regions, was primarily diffusely localized or localized in puncta (Figure 2.6G – I). A C-terminal fusion protein containing MTB1 and MTB2, GFP-INF1C, localized discretely with bundled microtubules in Cos-1 cells (Figure 2.6J – L). Prominent nuclear localization in most of the cells may have been an artifact of the high expression of this small fusion protein, and was not observed with the full-length fusion protein. The failure of INF1ΔC2-YFP to associate with microtubules, and the association of GFP-INF1C with bundled microtubules, demonstrates that the C-terminal end of INF1 is both necessary and sufficient for the microtubule association of INF1.

To further define the regions in the C-terminal end of INF1 that are necessary for microtubule association, we generated fusion proteins lacking the conserved MTB1 (GFP-ΔMTB1) or MTB2 (GFP-ΔMTB2) regions. In Cos-1 cells, these proteins were diffusely localized, with limited microtubule association (Figure 2.7C - F). Additionally, neither GFP-ΔMTB1 nor GFP-ΔMTB2 induced any microtubule bundling, whereas microtubule bundles were apparent in one third of the Cos-1 cells expressing GFP-INF1C (Figure 2.7A, B). Therefore, both the MTB1 and MTB2 regions play a role in the association of INF1 with microtubules.

To determine if the INF1 C-terminus is able to bind microtubules directly, we produced a GST-INF1C protein. The INF1 C-terminal end was purified by glutathione affinity chromatography and protease cleavage of the GST tag. The purified INF1C protein was then used in an *in vitro* microtubule spin-down assay and in a fluorescence-based microtubule bundling assay.

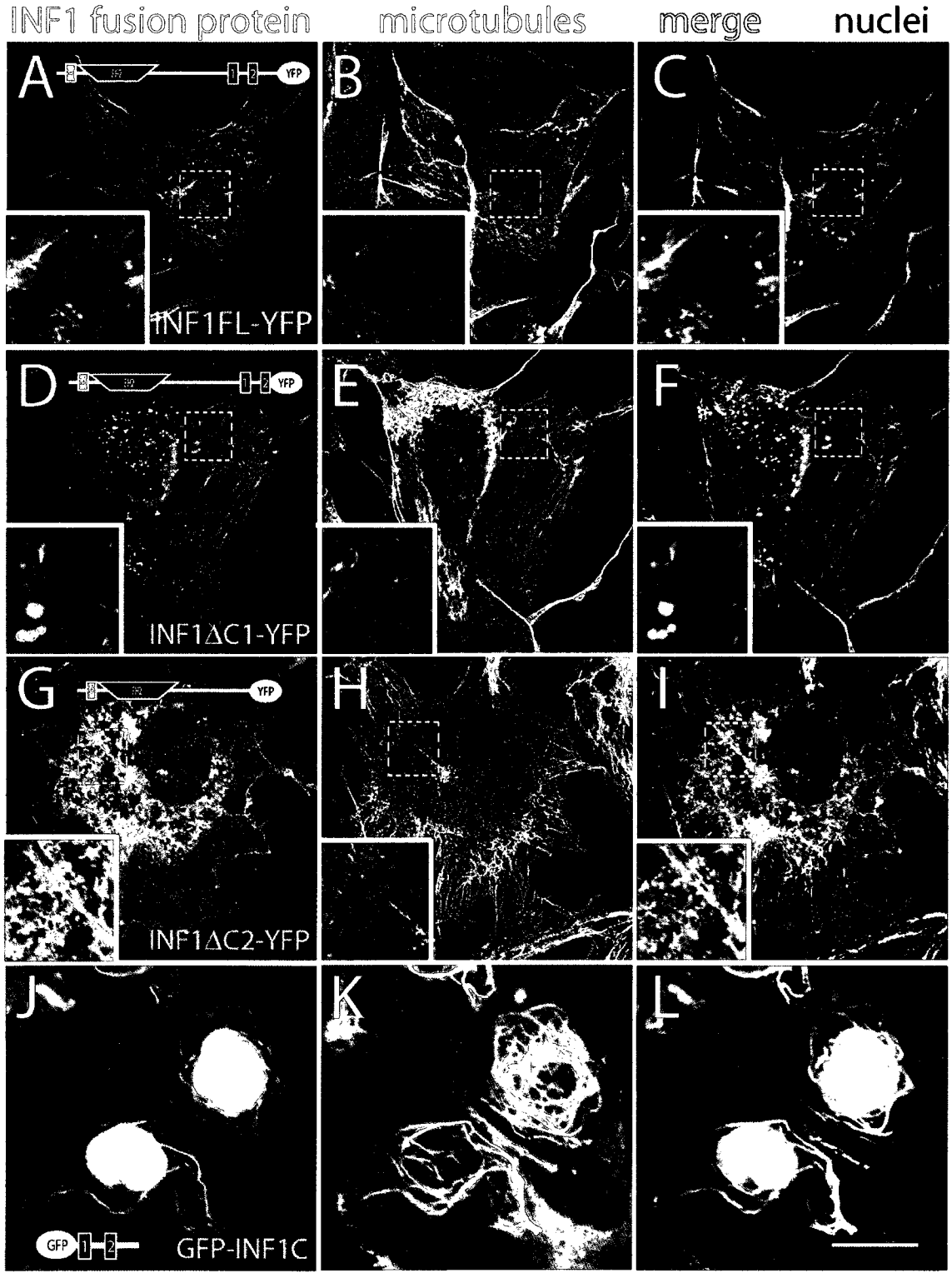
INF1 fusion protein
microtubules
merge
nuclei
A
B
C
YFP
INF1FL-YFP
D
E
F
YFP
INF1ΔC1-YFP
G
H
I
YFP
INF1ΔC2-YFP
J
K
L
GFP
GFP-INF1C

**Figure 2.6. The C-terminus of INF1 is required for INF1 microtubule association.**

(A – C) Full-length INF1FL-YFP fusion protein expressed in Cos-1 cells. The fusion protein (A) primarily co-aligned with microtubules (B) in 94% of the cells (n = 148 cells, two trials). The merged image is shown in C. Insets show an enlargement of the boxed region. (D – F) The truncated INF1ΔC1-YFP protein (D) was co-aligned with microtubules in 38% of the cells expressing this fusion (n = 138 cells, two trials) (E), though was more commonly diffusely localized, or localized to puncta. The INF1ΔC2-YFP protein (G) was almost completely diffusely localized or localized to puncta, and showed only a very limited association with microtubules (H). Microtubule co-alignment was observed in just 2% of the INF1ΔC2-YFP transfected cells (n = 169 cells, two trials). The merged image is shown in I. Insets show an enlarged image of the boxed region. (J – L) The C-terminal GFP-INF1C protein (J) localized with bundled microtubules (K) in the cytoplasm. This protein also localized to nuclei. The merged image is shown in L. Scale bar = 20 μm in L, and applies to all images.

Proteins that are normally soluble will co-sediment with the microtubules in the spin-down assay when centrifuged at 100,000 x *g* if they bind directly to the microtubules. In this assay, soluble INF1C incubated on its own remained in the supernatant following ultracentrifugation. In contrast, INF1C incubated with purified microtubules co-sedimented with the microtubules, and was found primarily in the pellet following the high speed spin (Figure 2.7G). To assess the effect of INF1C on microtubule bundling, we incubated INF1C with purified microtubules which were then fixed and stained on microscope slides. Incubation with INF1, but not control GST protein, induced microtubule bundling in this assay (Figure 2.7H, I). Thus, the INF1 C-terminus is able to bind and bundle microtubules directly.

*INF1 stabilizes microtubules*

The induction of bundled basket-like microtubules by INF1C is consistent with INF1 promoting microtubule stabilization. To test this, we treated Cos-1 cells with 1 μM or 10 μM nocodazole for one hour. Treatment with 1 μM was sufficient to depolymerize most microtubules outside of the centrosomes and midbodies, while 10 μM nocodazole additionally caused centrosome and midbody depolymerization. Cells expressing the full-length INF1FL-YFP were able to retain an extensive microtubule network at 1 μM nocodazole as well as at the 10 μM concentration, albeit to a lesser extent (Figure 2.8A, B, G). Cells expressing the C-terminal GFP-INF1C protein also retained extensive microtubule networks, with the microtubules commonly retaining a bundled appearance (Figure 2.8E, F). INF1ΔC2-YFP expressing cells contained primarily diffuse microtubule staining (Figure 2.8C, D).

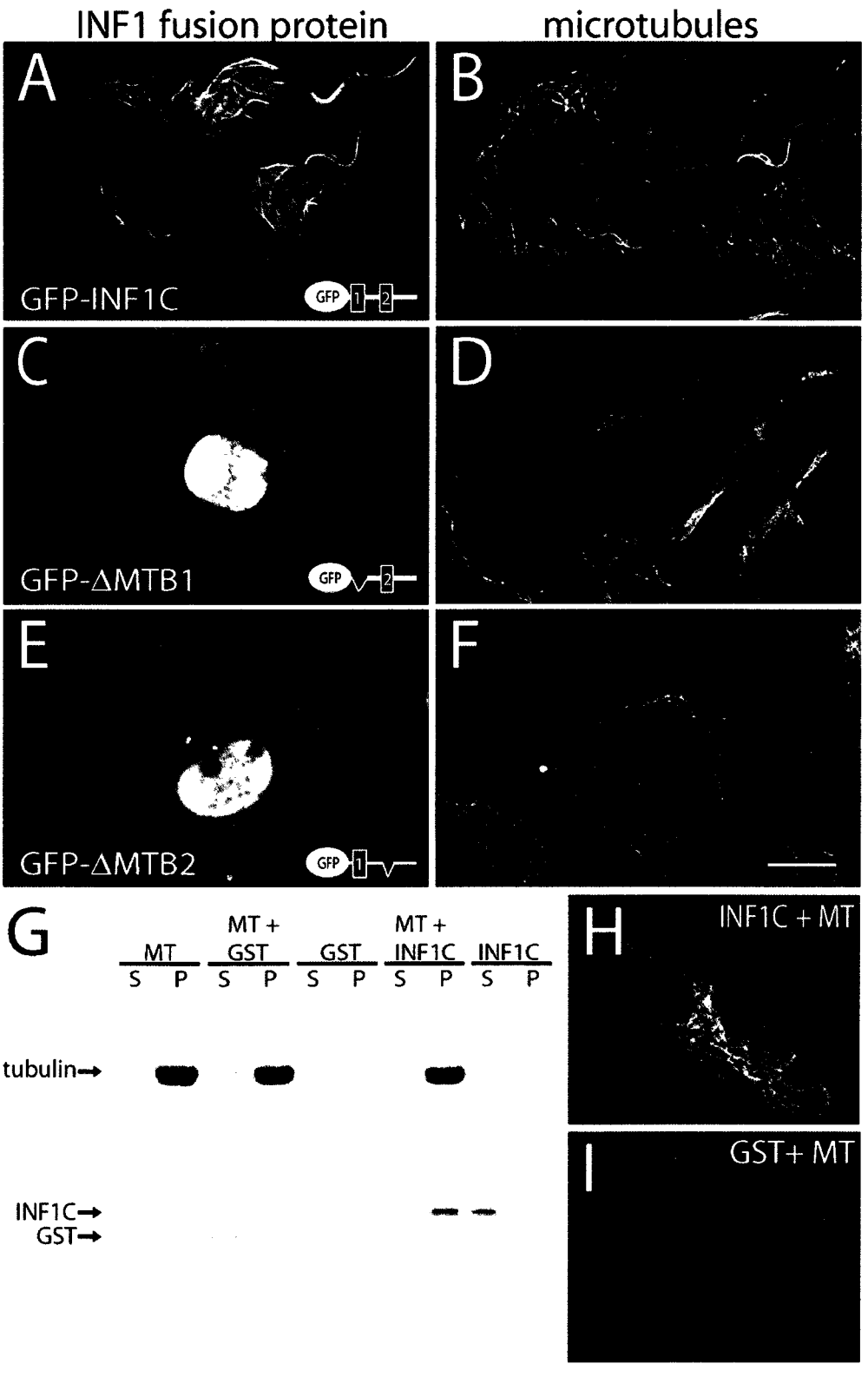
INF1 fusion protein
microtubules
A
B
GFP-INF1C
GFP
1
2
C
D
GFP-ΔMTB1
GFP
2
E
F
GFP-ΔMTB2
GFP
1
G
MT
MT + GST
GST
MT + INF1C
INF1C
S P S P S P S P S P
tubulin
INF1C
GST
H
INF1C + MT
I
GST+ MT

**Figure 2.7. The INF1 C-terminus interacts with and bundles microtubules directly.**

Cos-1 cells transfected with GFP-INF1C showed the fusion protein (A) associated with bundled microtubules (B). Microtubule co-alignment was observed in 62% of the transfected cells (n = 140 cells), with 33 % of the cells displaying thicker, bundled microtubules. When the MTB1 region was removed (GFP-ΔMTB1), the fusion protein was primarily diffusely localized (C). Limited microtubule co-alignment was observed in 15% of the GFP-ΔMTB1 transfected cells (n = 104 cells). Microtubules are shown in D. When the MTB2 region was removed (GFP-ΔMTB2), the fusion protein was again primarily diffusely localized (E). Limited microtubule co-alignment was observed in 26% of the GFP-ΔMTB2 transfected cells (n = 98 cells). Microtubules are shown in F. (G) Purified INF1C protein was incubated with microtubules and centrifuged at 100,000 X *g*. The INF1C protein was found mostly in the pellet (P) fraction when incubated with microtubules, but remained in the supernatant (S) when incubated alone. GST incubated with or without microtubules remained in the supernatant. (H) Purified INF1C protein incubated with microtubules, but not GST (I), induced microtubule bundling, as observed by immunofluorescence microscopy. Scale bar = 20 μm in F, and applies to all images of the cells.

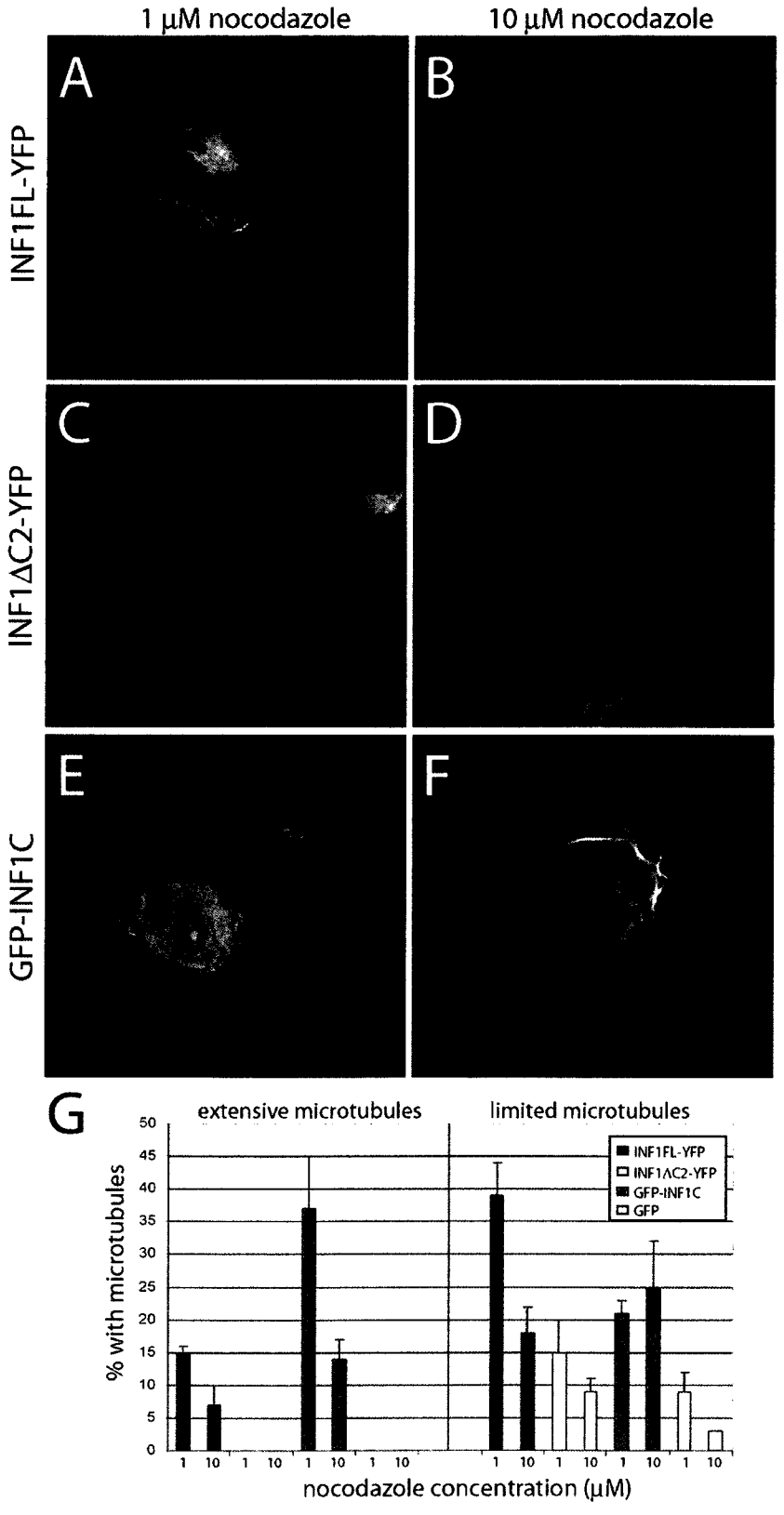
1 μM nocodazole
10 μM nocodazole
A
B
C
D
E
F
INF1FL-YFP
INF1ΔC2-YFP
GFP-INF1C
G
extensive microtubules
limited microtubules
INF1FL-YFP
INF1ΔC2-YFP
GFP-INF1C
GFP
% with microtubules
0
5
10
15
20
25
30
35
40
45
50
1 10 1 10 1 10 1 10 1 10 1 10 1 10 1 10
nocodazole concentration (μM)

**Figure 2.8. The INF1 C-terminus confers resistance against nocodazole-induced microtubule depolymerization.**

(A, B) Cos-1 cells expressing INF1FL-YFP were treated with 1 or 10 μM nocodazole for one hour, then fixed and labeled with α-tubulin antibody. Cells expressing the full-length INF1 fusion still retained intact microtubules, though they were very limited at the 10 uM nocodazole concentration. Microtubules were scored as being extensive if there was more filamentous labeling than diffuse labeling within a cell and limited if the labeling was more diffuse than filamentous. (C, D) In cells expressing the C-terminal truncated INF1ΔC2-YFP fusion protein, very few cells had any filamentous tubulin labeling at either nocodazole concentration. In cells expressing the C-terminal fusion protein, GFP-INF1C, many cells were observed to have filamentous labeling, with this being primarily extensive at the lower nocodazole concentration, and more limited at the higher concentration. (G) Quantification of the microtubule phenotypes from cells expressing INF1FL-YFP (n = 164 cells for 1 μM and 215 cells for 10 μM nocodazole), INF1ΔC2-YFP (n = 200 cells for 1 μM and 171 cells for 10 μM nocodazole), GFP-INF1C (n = 360 cells for 1 μM and 305 cells for 10 μM nocodazole), and GFP (n = 292 cells for 1 μM and 273 cells for 10 μM nocodazole) alone, observed from three separate trials. Error bars = standard error of the mean. The scale bar in F = 20 μm and applies to all images.

A few cells expressing INF1ΔC2-YFP displayed a very limited number of microtubule filaments (Figure 2.8G), though at the 1 μM nocodazole concentration this was not significantly different than GFP expressing control cells ($p = 0.34$, two-tailed t-test). There was, however, a marginally significant difference observed between INF1ΔC2-YFP and GFP expressing cells for the 10 μM concentration ($p = 0.04$).

*INF1 induces the formation of acetylated microtubules*

We next examined whether the expression of INF1 fusion proteins could be associated with the formation of acetylated microtubules, a marker for microtubule stabilization. We expressed INF1FL-YFP, INF1ΔC2-YFP, or GFP-INF1C in confluent NIH 3T3 cells. The confluent NIH 3T3 cells contained weak acetylated microtubule labeling, with strong labeling limited to the spindles of dividing cells and midbodies. As expected, expression of GFP-INF1C induced the robust formation of bundled, acetylated microtubules (Figure 2.9E, F). The INF1FL-YFP protein also induced acetylated microtubule formation, though to a lesser extent than the isolated C-terminus (Figure 2.9A, B). Surprisingly, expression of the INF1ΔC2-YFP protein, which did not obviously associate with microtubules, also induced the accumulation of acetylated microtubules in approximately one third of cells (Figure 2.9C, D). Unlike the full-length and C-terminal fusions, however, the INF1ΔC2-YFP did not necessarily co-localize with the acetylated microtubules. Transfection of a control GFP plasmid did not cause any increase in acetylated microtubule staining in the expressing cells. Thus the effect is specific to expression of INF1. The FH2 domain of other formins has been implicated in microtubule interactions (Ishizaki et al., 2001; Rosales-Nieves et al., 2006; Bartolini et

al., 2008). Therefore, we tested the ability of the INF1 FH2 domain to induce formation of acetylated microtubules. Expression of a Flag-tagged derivative of the INF1 FH2 domain failed to induce the accumulation of acetylated microtubules (Figure 2.7G, H).

Microtubule detyrosination is another marker of microtubule stability and therefore we examined whether INF1 overexpression could be associated with an increase in detyrosinated microtubules. In contrast to microtubule acetylation, we were unable to detect an INF1FL-YFP-induced increase in detyrosinated microtubules (Supplemental Figure 2.1.5).

Since INF1 appeared to promote the formation of acetylated microtubules in NIH 3T3 cells, we next examined if the knockdown of INF1 in these cells would result in decreased levels of acetylated microtubules. As assessed by immunoblot analysis, we observed a decrease in acetylated tubulin levels in cells with reduced INF1 levels (Figure 2.9J). Expression of α-tubulin, which is the acetylated monomer (Eddé et al., 1991), was not decreased, indicating that it is only tubulin acetylation that is reduced and not tubulin expression levels. Finally, to determine if endogenous INF1 was targeted to acetylated microtubules in NIH 3T3 cells, we immunostained cells for both and looked at their co-localization. INF1 was found to be associated with acetylated microtubules (Figure 2.9K, L). Together these data show that INF1 is able to bind to microtubules and induce microtubule stabilization and acetylation.

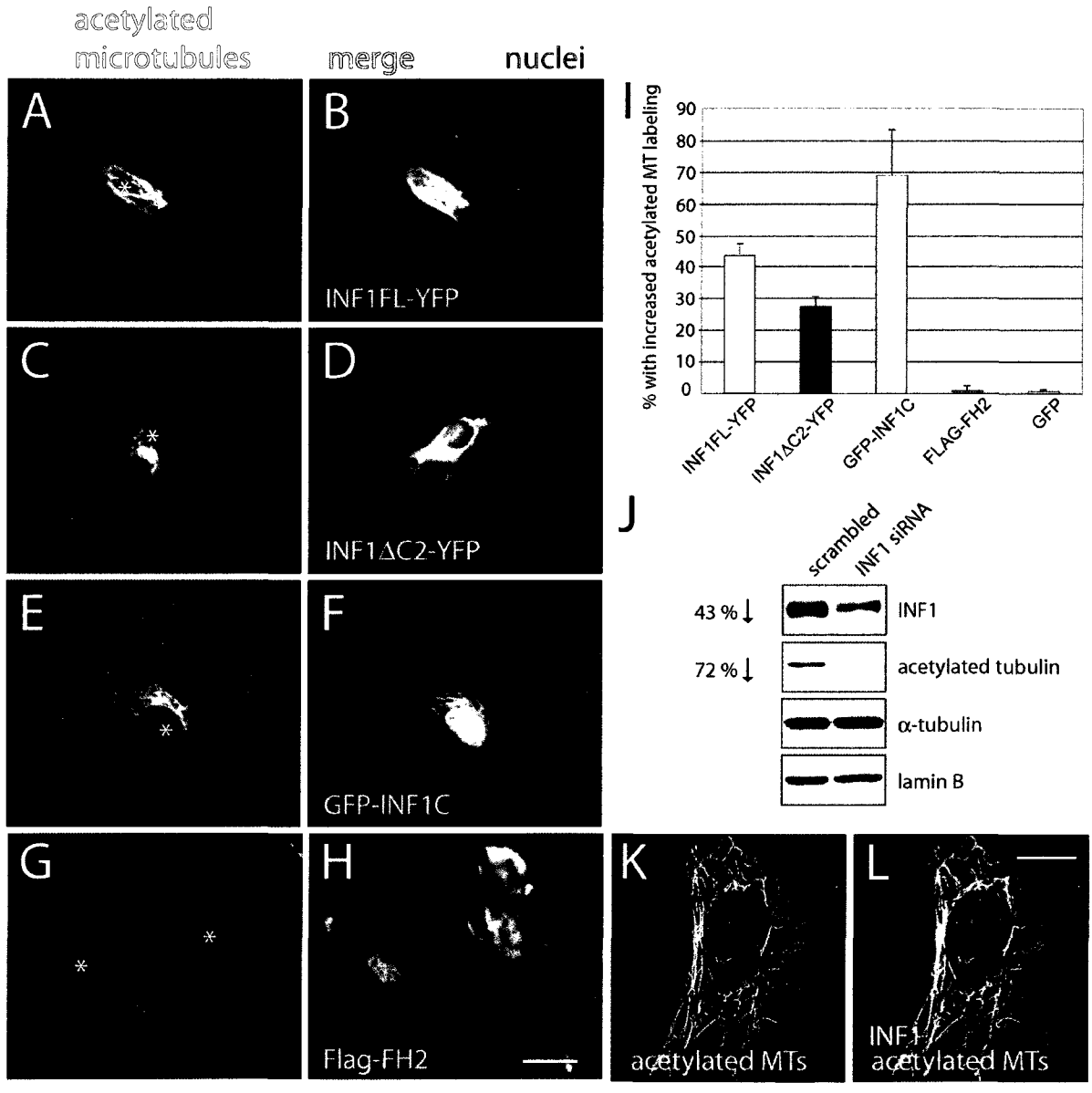
acetylated microtubules
merge
nuclei
A
B
INF1FL-YFP
C
D
INF1ΔC2-YFP
E
F
GFP-INF1C
G
H
Flag-FH2
I
% with increased acetylated MT labeling
90
80
70
60
50
40
30
20
10
0
INF1FL-YFP
INF1ΔC2-YFP
GFP-INF1C
FLAG-FH2
GFP
J
scrambled
INF1 siRNA
43 %
72 %
INF1
acetylated tubulin
α-tubulin
lamin B
K
acetylated MTs
L
INF1
acetylated MTs

**Figure 2.9 INF1 induces acetylated microtubule formation.**

Expression of INF1FL-YFP (B) in NIH 3T3 cells for one day induced an increase in labeling for acetylated microtubules (A) in 44% of the cells. Cells were counted as having increased labeling only when they showed a clearly stronger signal relative to all untransfected cells in the same field. (C) Acetylated microtubule formation was also induced in 28% of the cells expressing the INF1ΔC2-YFP fusion protein (D). Highly bundled acetylated microtubules (E) formed with the expression of the GFP-INF1C fusion protein (F) in 69% of the transfected cells. Expression of a Flag-FH2 protein (H) did not result in increased acetylated microtubule staining (G). Fusion protein expressing cells are marked with an asterisk in A, C, E, G. The numbers of cells expressing each of these fusion proteins which displayed increased acetylated microtubule staining relative to the surrounding untransfected cells is quantified in I, along with data from cells transfected with GFP alone. Data are from four separate trials for the INF1FL-YFP (n = 189 cells total), INF1ΔC2-YFP (n = 172 cells total) and GFP-INF1C (n = 207 cells total) groups, and two trials for the Flag-FH2 (n = 166 cells total) or GFP (n = 176 cells total) groups, with standard error of the mean shown. (J) The knockdown of INF1 using siRNA in NIH 3T3 cells resulted in a consistent reduction of acetylated tubulin levels. This did not involve a reduction in a-tubulin levels. Lamin B is also shown as a loading control. Scale bar = 20 μm in H, and also applies to A – G; bar in L = 20 μm and also applies to K.

## 2.5 Discussion

Great progress has been made over the last ten years in determining the function of the highly conserved domains found in the Diaphanous-Related Formins (DRFs). However, few studies have explored the function of more divergent members of the formin family. That formins can regulate the structure of both microfilaments and microtubules has been indicated by several studies (Ishizaki et al., 2001; Palazzo et al., 2001; Wen et al., 2004; Rosales-Nieves et al., 2006; Bartolini et al., 2008). How microtubule organization is coordinated by formins is still unclear, though the FH2 domain has been implicated as being important for mediating formin-microtubule interactions (Ishizaki et al., 2001; Rosales-Nieves et al., 2006; Bartolini et al., 2008). In this study, we show that the novel formin INF1 is unique in being discretely and primarily associated with microtubules. The binding of INF1 to microtubules occurs directly via a novel C-terminal MTBD. INF1 is therefore the only formin family member identified to date that is likely to act primarily through direct effects on the microtubule cytoskeleton.

The unique structure of INF1, and the novel C-terminal polypeptide sequence downstream of its FH2 domain, appears to have arisen in the early chordates (Figure 2.1). The most closely related formins in non-chordate animals, which we have termed INFX proteins, are distinct in structure from INF1. They appear to be intermediate in structure to INF1 and INF2. INF1 and INF2 likely diverged from a common INFX-like ancestor, with the INF1 lineage losing sequence at the N-terminal end. Though the MTBD at the C-terminal end of INF1 contains sequence conserved in the vertebrates, no similar

sequence was present in the INFX proteins. Our database searches have also found no similar MTBD in any other protein, indicating that this motif is unique to INF1.

The FH1/FH2 region of INF1 functions in a manner consistent with other formins in that it stimulates actin stress fiber formation and SRF activation (Figure 2.2). This activity is not autoregulated with INF1 overexpression, and INF1 does not possess any of the previously described formin autoregulatory domains. Within the INF1 C-terminal end, we have mapped a microtubule binding domain. This MTBD was necessary and sufficient for proper localization of INF1 with microtubules. It is possible that endogenous INF1 FH1/FH2 activity may be regulated by its association with microtubules. This would be similar to the case of another actin regulator, GEF H1, which becomes active in stimulating RhoA following its release from microtubules (Chang et al., 2008). Future experiments will be needed to determine the impact of microtubule binding on INF1 regulation of actin filaments.

INF1 overexpression promoted the formation of acetylated microtubules in NIH 3T3 cells (Figure 2.9). Both the MTBD and a second region in the INF1 C-terminal end likely play roles in stimulating acetylated microtubule formation as INF1 fusion protein lacking the MTBD also induced an increase in acetylated microtubules, though to a reduced extent. Consistent with these results we find that siRNA-mediated knockdown of INF1 expression caused a significant reduction in the accumulation of acetylated tubulin (Figure 2.9J). The FH2 domain of INF1 did not induce accumulation of acetylated microtubules (Figure 2.9G-H), nor did it associate discretely with microtubules or have any obvious affect on microtubule organization (data not shown). Thus, the N-terminal half of INF1 appears to primarily affect actin cytoskeleton structure and SRF activation,

while the C-terminal half associates with, and promotes the modification of, the microtubule cytoskeleton.

Microtubule driven alterations to cell morphology are prominent in many cells types. One notable example is the necessary role that stable, acetylated microtubules play in the development of the neuronal axon (Witte et al., 2008). Acetylated microtubules establish polarity in neurons, and are necessary for specifying axon formation. The association of INF1 with acetylated microtubules and its expression in neurons suggests that INF1 may play a modulatory role in the cytoskeletal organization of axons. It is of interest, then, that we observed INF1 to be an axonal protein in the cerebellum (Figure 2.5). INF1 was also prominently expressed in ventricular muscle of the heart. In cardiomyocytes microtubules play a role in resisting shear stress (Nishimura *et al.*, 2006) and are important in modulating the progression of cardiac hypertrophy (Cooper, 2006). Thus it is tempting to speculate that INF1 may also play a role in these processes.

With much of the formin protein family having been described only in recent years (Higgs and Peterson, 2005), the diversity of formin protein function remains to be demonstrated. INF1 is the first formin demonstrated to localize predominantly with microtubules and the first demonstrated to contain a MTBD that localizes discretely with microtubules. INF1 is involved in both F-actin and microtubule organization mediated through its N-terminal FH1/FH2 region and C-terminal MTBD and is unique among formins in being constitutively localized in a discrete manner along a cytoskeletal filament network. It will be of great interest to determine how the association of INF1 with microtubules is regulated and how microtubule binding may affect INF1-induced effects on actin dynamics.

## 2.6 Acknowledgements

We thank Dr. Henry Higgs for providing the protein preparation protocol used in this study. We also thank Dr. Rashmi Kothary for commentary on the manuscript, and for providing cell lines and mouse tissue samples. J.C. is supported by grant NA 5762 from the Heart and Stroke Foundation of Ontario and grant 68816 from the Canadian Institutes of Health Research.

## 2.7 Supplemental Figures

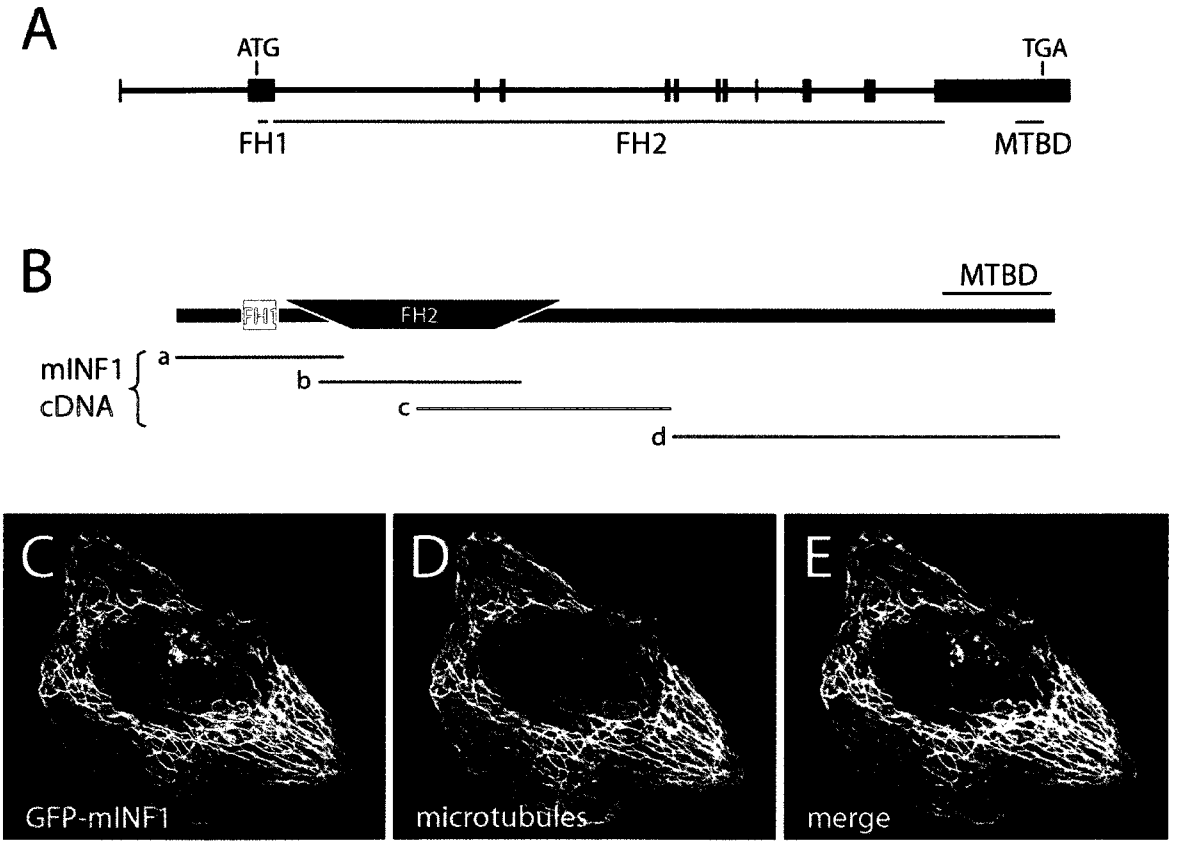

**Figure 2.7.1. Overview of the mouse INF1 (mINF1) gene, transcript, and protein.**

(A) The mINF1 gene is a ~37 kb, 12 exon gene. All of the exons encode regions of the FH2 domain, except the first exon which is non-coding. The final exon also encodes the entire unique C-terminal half of the protein downstream from the end of the FH2 domain. The translational start (ATG) and stop (TGA) sites are indicated. (B) Four overlapping cDNA (a – b) encoding the mINF1 open reading frame were generated by RT-PCR using NIH 3T3 total mRNA, and cloned into the pCR2.1 vector (Invitrogen). Primer sequences used were as follows: (a) 5'-AGATCTCAGTACTATGCATGTTAT-3' and 5'-CCTCTTCTGACTCCGGCAAAAGCT-3'; (b) 5'-GCTTTGAATTCATCCTTCAGAGATGCC-3' and 5'-CTGGATCCCCGGTCATGATTGTCCTT-3'; (c) 5'-GTTGGGATCCTTCCTCCAGGC-3' (d) 5'-AGCCTGGAGGAAGGATCCCAACTGACT and 5'-GTCGACTGTTTCTGCAGGGGACGGAGA-3'. Similar cDNA were obtained with N2A mRNA, and only single products were obtained with each amplification, providing no evidence of alternative splicing. The entire open reading frame is 3.45 kb. Following sequencing to ensure the accuracy of the amplifications, the cDNA were assembled into a full-length fusion construct in the pEGFP-C1 vector (GFP-mINF1). (C) Optical section of the GFP-mINF1 expressed in Cos-1 cells showing the fusion protein co-aligned with microtubules (D). Note that the microtubules have a more bundled appearance compared to the human INF1 protein expressed in Cos-1 cells (Figure 2.6). The merged image of the two is shown in E.

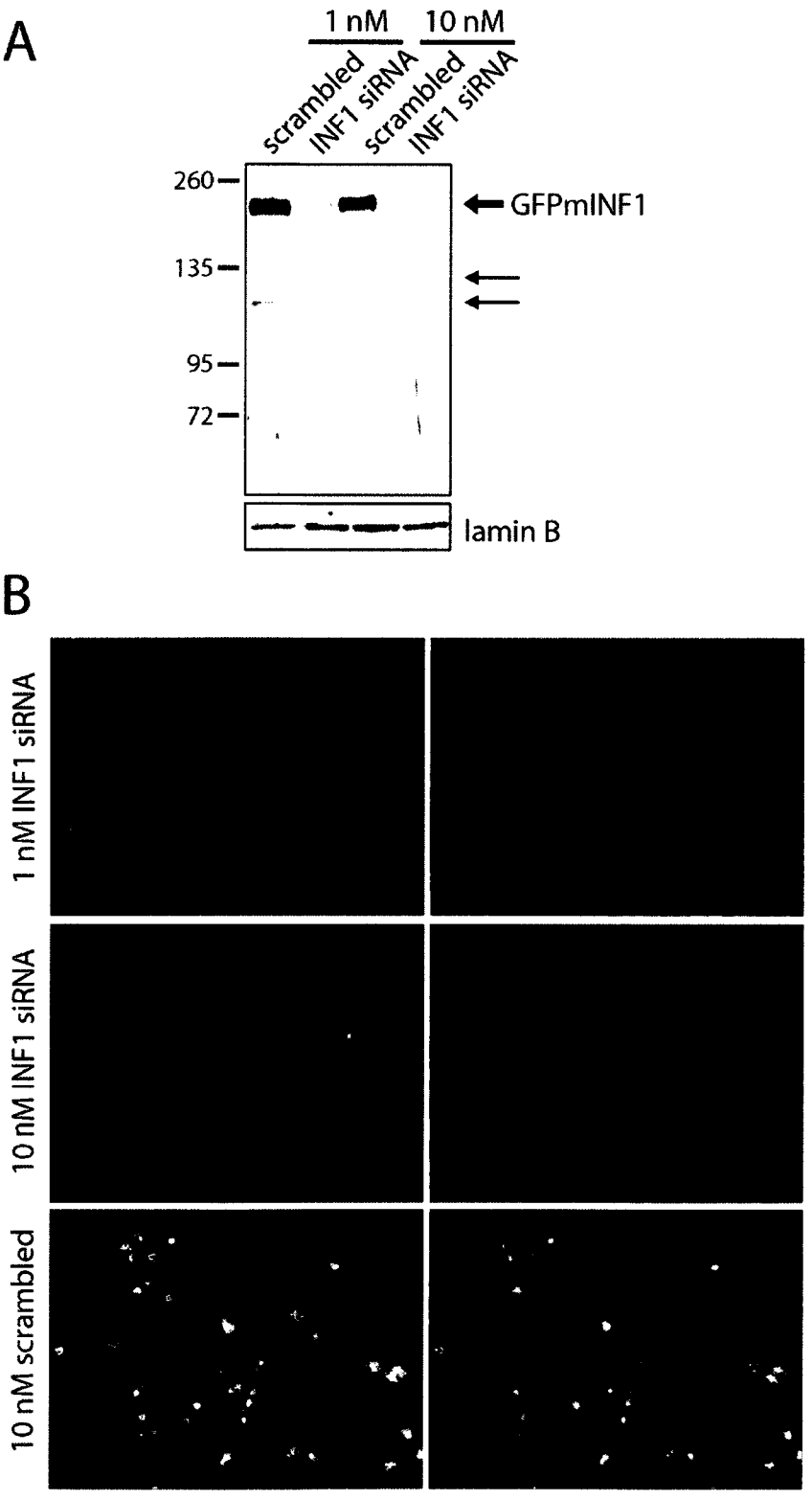
A
1 nM
10 nM
scrambled
INF1 siRNA
scrambled
INF1 siRNA
260
135
95
72
GFPmINF1
lamin B
B
1 nM INF1 siRNA
10 nM INF1 siRNA
10 nM scrambled

**Figure 2.7.2 siRNA knockdown of INF1 fusion protein.**

(A) Immunoblot analysis of lysates collected from GFP-mINF1-transfected Cos-1 cells co-transfected with either a control (scrambled) siRNA or INF1 siRNA. Lysates were collected three days following transfection. The blot was probed with a GFP antibody. Both 1 and 10 nM siRNA concentrations resulted in a dramatic inhibition of GFP-mINF1 expression. Both the major band corresponding to the full-length fusion protein (thick arrow) and lower molecular weight bands (thin arrows) were diminished by the siRNA. (B and C) Weak GFP fluorescence was observed in cells co-transfected with GFP-mINF1 and 1 nM INF1 siRNA. (D and E) In cells co-transfected with GFP-mINF1 and 10 nM INF1 siRNA, the GFP fluorescence was nearly absent. (F and G) Control cells co-transfected with GFP-mINF1 and 10 nM scrambled siRNA displayed strong GFP fluorescence. All images were taken at identical exposures, and processed identically.

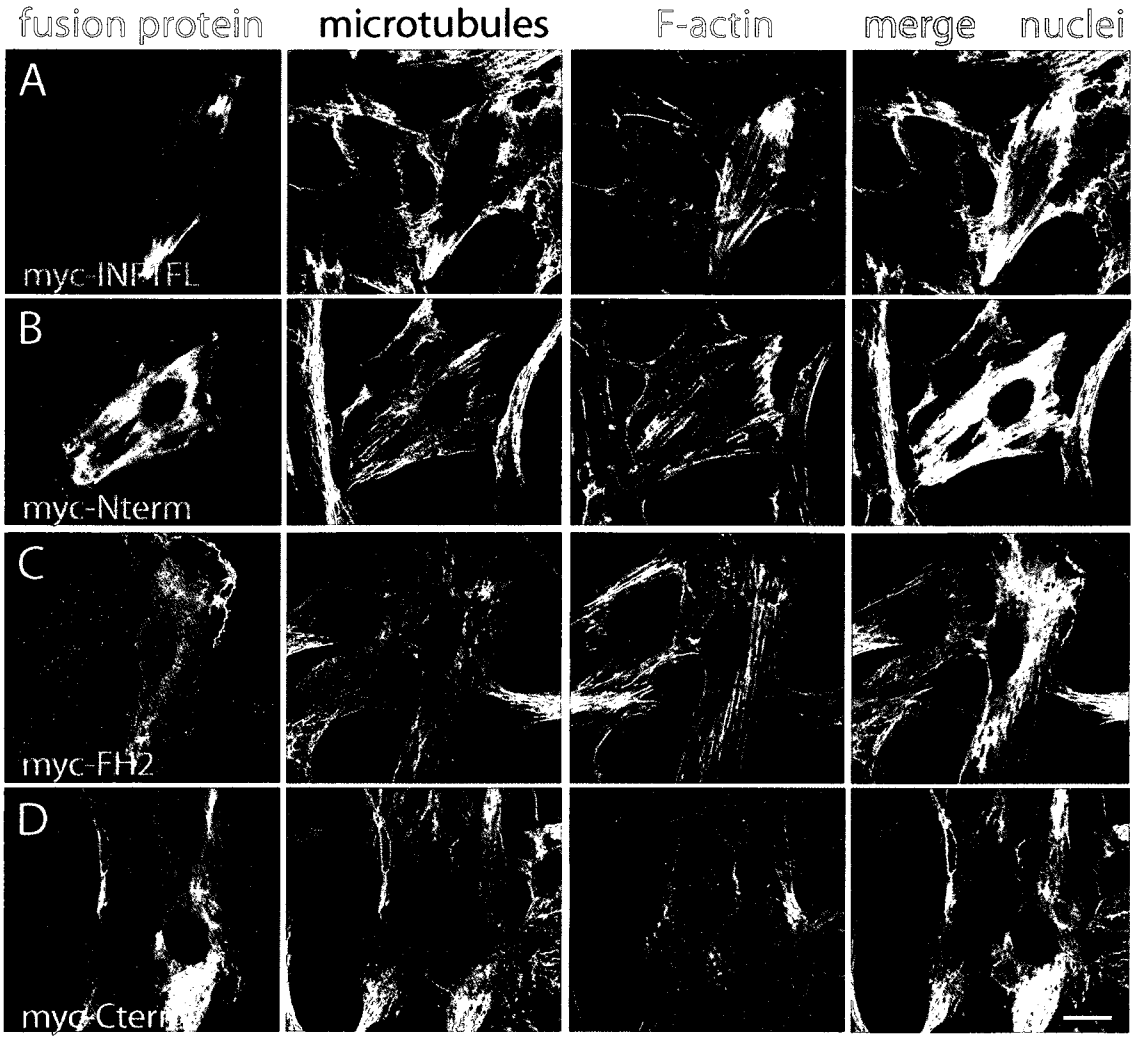
fusion protein
microtubules
F-actin
merge
nuclei
A
myc-INF1 FL
B
myc-Nterm
C
myc-FH2
D
myc-Cterm

**Figure 2.7.3. INF1 induction of stress fibre formation in NIH 3T3 cells.**

INF1 fusion constructs were transfected into NIH 3T3 cells, and cells were fixed and stained the following day. (A) Transiently transfected full length myc-INF1FL induced stress fibre formation, with increased F-actin labelling relative to the surrounding untransfected cells. In the pictured cell, myc-INF1FL and microtubules accumulated at cell tips. (B) Myc-Nterm was diffusely distributed in the cytoplasm and also lead to increased stress fiber formation (C) Myc-FH2 lead to a similar increase in stress fibers. As well as being diffusely localized, myc-FH2 also accumulated in lamellopodia-like structures at the periphery of the cell. (D) Myc-Cterm was primarily localized diffusely in the cytoplasm, but also displayed some filamentous patterning co-aligning with microtubules. Myc-Cterm did not induce any clear stress fibre formation. Scale bar = 20 μm, and applies to all images.

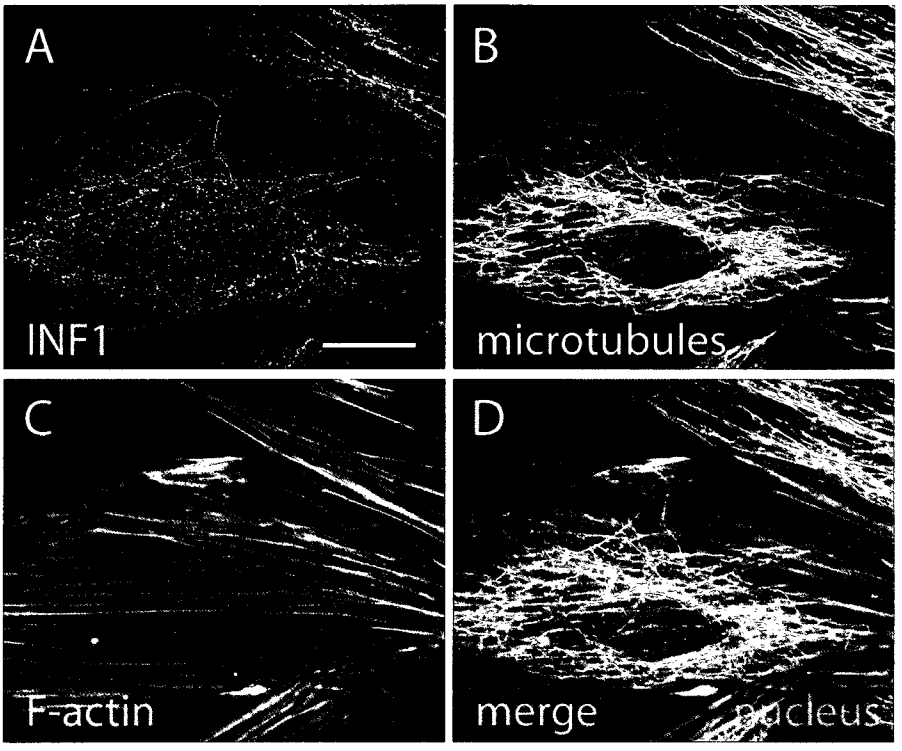


**Figure 2.7.4. Endogenous INF1 in H9C2 cells.**

(A) INF1 antibody labeled protein in a filamentous and punctate pattern. Most of this staining co-localized with microtubules (B). There was no clear co-localization with F-actin (C). The merged image is shown in D. Scale bar = 20 μm, and applies to all images.

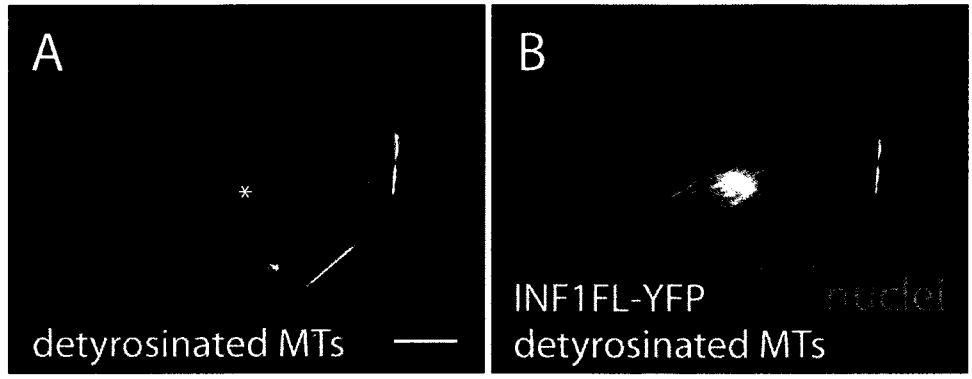


**Figure 2.7.5. Detyrosinated microtubule labeling is not increased by INF1 overexpression in NIH 3T3 cells.**

(A) NIH 3T3 cells grown to confluence display weak labeling with a detyrosinated microtubule antibody. In 94% of the cells expressing INF1FL-YFP (marked with an asterisk), the fusion protein did not cause an increase in detyrosinated microtubule labeling relative to the surrounding cells (n = 77). The merged image with the fusion protein is shown in B. Scale bar = 20 μm.

# Chapter 3:

# INF1 Cross-links Actin and Microtubules Through N- and C-terminal Domains

A similar report is to be submitted as part of a larger study:
Susan F. Thurston, Sarah J. Copeland, Kevin G. Young, Chelsea Smallwood and John W. Copeland

*Sarah Copeland purified FL INF1 used in Figures 3.6, 3.7 and 3.8 and generated the INF1 I180A mutant. I conducted all the experiments shown.

## 3.1 Abstract

Formins are best known for their ability to regulate actin dynamics via the direct action of the FH2 domain. It has been suggested FH2 might also mediate formin-induced MT stabilization and re-organization. We previously identified Inverted Formin 1 (INF1) as a novel MT-associated formin that binds MTs *in vivo* and *in vitro* via a C-terminal MTBD. Expression of the INF1 MTBD is sufficient to induce MT stabilization and acetylation. In contrast, expression of the INF1 FH2 domain has no effect on MT stability. Surprisingly, the MTBD is not essential for INF1-induced MT stabilization. We show here that INF1 induced MT stability is independently mediated by two distinct regions of the protein, the C-terminal MTBD and the N-terminal FH1/FH2 domains. Using *in vitro* binding assays we also show that full-length INF1 protein is able to cross-link actin and MTs directly. Finally, our results implicate a region in the INF1 C-terminus as a target for negative regulatory factors that control INF1 activity

## 3.2 Introduction

Formins are a group of highly conserved cytoskeletal remodelling proteins. Best known for their role in actin nucleation and polymerization, they contribute to cellular processes such as cell migration, filopodia formation, invasion and polarization (Faix and Gross, 2006, Goode and Eck, 2007). In mammals 15 formin genes have been identified, characterized by the formin homology domains, FH1 and FH2. The Diaphanous-related formins (DRFs) are the best characterized members of this protein family. DRFs include Dia (diaphanous), DAAM (disheveled-associated activators of morphogenesis) and FRL (formin-related proteins identified in leucocytes). All DRFs have additional conserved regulatory domains such as the diaphanous inhibitory domain (DID), diaphanous auto-regulatory domain (DAD) and GTPase binding domain (GBD) (Watanabe et al., 1999, Alberts, 2001, Li and Higgs, 2003, Copeland et al., 2007). The DID, DAD, and GBD regulatory domains are responsible for the characteristic autoinhibition displayed by DRFs. In the inhibited conformation DID associates with DAD and masks the functional domains FH1 and FH2. Binding of GTP-bound Rho GTPase to GBD disrupts the DID/DAD interaction and unmasks FH1 and FH2, thereby activating the formin. FH1 consists of proline-rich repeats that serve as a ligand for the small actin-binding protein profilin. FH2 nucleates directly *de novo* actin polymerization *in vitro* and induces F-actin accumulation *in vivo*. (Li and Higgs, 2003, Moseley et al., 2004, Romero et al., 2004). In addition, FH2-induced actin polymerization activates MRTF-dependent transcription of SRF target genes (Sotiropolos et al., 1999, Copeland and Treisman, 2002, Miralles et al., 2003, Copeland et al., 2004).

Intriguingly, formins have also been implicated in the direct regulation of microtubule dynamics and microtubule-dependent processes such as meiotic spindle alignment and chromosome gathering during mitosis (Palazzo et al., 2001, Leader et al., 2002, Yasuda et al., 2004, Wen et al., 2004, Gasteier et al., 2005, Rosales-Nieves et al., 2006, Bartolini et al., 2008). In migrating fibroblasts mDia1 regulates and stabilizes microtubules (MTs) downstream of lysophosphatidic acid (LPA)-induced Rho-signaling (Palazzo et al., 2001, Wen et al., 2004, Goulimari et al., 2005, Eng et al., 2006). mDia is thought to generate stabilized microtubules by forming a complex with EB1 and APC at the plus-tip of microtubules (Wen et al., 2004, Eng et al., 2006). In addition Rho-mDia regulates GSK3β inhibition of stable microtubule formation through novel PKCs (Eng et al., 2006). mDia induced stable microtubules are detyrosinated meaning that the C-terminal tyrosine residue is removed to expose the penultimate glutamate residue of α-tubulin (Gunderson et al., 1984, 1987). To date it has been unclear if detyrosination is a cause or result of microtubule stabilization. However, recent work suggests that detyrosination in fibroblasts inhibits MT disassembly by suppressing the activity of MT depolymerising motors (Peris et al., 2009).

Like mDia, FHOD1 expression in HeLa cells induces thick stress fibers aligned in parallel with microtubules (Gasteier et al., 2005). Although both FHOD1 and mDia have been shown to regulate the organization of microtubules, neither is recruited to microtubules *in vivo*. In *Drosophila melanogaster*, Cappuccino FH1 and FH2 domains directly regulate Rho-dependent actin-MT cross talk during ooplasmic streaming (Rosales-Nieves et al., 2006).

Recently our laboratory identified INF1 as a novel microtubule-associated formin (Young et al., 2008). INF1 is a uniquely structured formin with FH1 and FH2 at the N-terminus rather than the C-terminus, as is the case with other family members. Full-length INF1 is constitutively active when overexpressed and induces the formation of stress fiber and stable acetylated-MTs in NIH 3T3s. We show here that INF1 possesses two microtubule stabilization activities. One activity is dependent on the MTBD and the other independent of MTBD but requiring FH1 and FH2. In the absence of the MTBD, the FH1 domain is required for inducing MT acetylation and is dependent on FH2 activity. The C-terminus of INF1 lacks any previously described regulatory domains, however, it does contain five unique conserved regions unrelated to anything in the protein database. In this study we show overexpression of the INF1 C-terminus is sufficient to induce stress fiber formation through activation of the endogenous INF1 protein. In addition, we show *in vitro* that full-length INF1 is capable of simultaneously binding both microtubules and F-actin. INF1 is the only formin that has been shown to associate directly with F-actin and microtubules both *in vitro* and *in vivo*. Our results suggest INF1 likely acts as a bridging factor linking actin and microtubule dynamics.

## 3.3 Materials and Methods

*Plasmid constructs*

The constructs FL INF1 (codons 1-1143), INF1 N-terminus (1-485), INF1 C-terminus (486-1143), INF1 FH2 (85-485), INF1 F1F2 (25-485), N-terminal series (1-644, 1-751, 1-846, 1-891, 1-958, 1-968) and C-terminal series (644-1143, 751-1143, 846-1143, 891-

1143, 958-1143, 968-1143) were all generated using PCR from full-length INF1 sequence and inserted into pEF-Cherry Tag, pEF-FLAG, and pEF.link tag vectors (Vaillant et al., 2008) using standard cloning techniques. Codon numbering is given for the human INF1 protein in GenBank accession number NP_203751. All subclones generated by PCR were confirmed by sequencing; molecular weights of the expressed fusion proteins were confirmed by immunoblotting. Constructs used for SRF reporter gene activation assays, 3DA.Luc and MLV-LacZ, have been described previously (Sotiropoulos et al., 1999, Geneste et al., 2002)

*Cell culture and animals*

Cos-1 cells were maintained in Dulbecco's Modified Eagle Medium (DMEM, Invitrogen) containing 10% FBS (Wisent) and 1% pen/strep with 5% $CO_2$ and passaged using standard protocols. Mouse NIH 3T3 fibroblasts were maintained in DMEM containing 10% FBS and 1% pen/strep in 10% $CO_2$. For microscopy, cells were plated at a density of 125,000 cells per well on sterile acid etched glass coverslips.

Cells were transfected with PEI (Polyethyleneimine; Polysciences Inc., Warrington, PA Cat #23966); 5 µl of 1 µg/µL PEI solution was mixed with 1.5 µg of plasmid DNA in 50 µl of OptiMEM (Invitrogen) for 15–30 minutes. Empty vector was used to yield a total of 1.5µg of DNA per well in 6 well plates. DNA/PEI mix was added to cells in 1ml of OptiMEM in 6 well plates. After 5 hours DNA was removed and replaced with normal growth medium with either 0.5% FBS or 10% FBS in DMEM with 1% pen/strep.

*Immunofluorescence*

Immunofluorescence was performed as previously described (Young et al., 2008). Briefly, cells were washed in PBS then fixed in fresh 4% paraformaldehyde in PBS for 10 minutes. Cells were then washed 3 X in PBS, permeabilized and blocked with 0.3% Triton X-100 in PBS and 10% Donor Bovine Serum (DBS, Wisent). Coverslips were incubated with antibodies diluted in PBS containing 0.03% Triton X-100 and 5% DBS for 1 hour at room temperature or overnight at 4°C. Primary antibodies used were affinity purified rabbit anti-INF1 polyclonal at 1:50 (Young et al., 2008), mouse anti-α-tubulin monoclonal at 1:500 (Sigma), mouse anti-acetylated tubulin monoclonal at 1:1000 (Sigma), goat anti-actin at 1:100 (sc-1616, Santa Cruz) and anti-flag at 1:500 (Sigma Cat # F7425), anti-myc at 1:500, Fluorescein phalloidin at 1:100 (Invitrogen) or phalloidin-Alexa Fluor 488 at 1:100 (Invitrogen). Following a final wash in PBS, the samples were mounted using Vectashield with DAPI (Vector Laboratories) or Fluoromount G (Electron Microscopy Sciences). Cells were imaged with a Zeiss AxioImager equipped with an apotome. Apotome optical sections were taken with a 63X Plan Apochromat objective producing sections of 0.7 μm.

*Serum response factor activation assay*

SRF activation assays were performed as previously described (Copeland et al., 2002). Briefly, NIH 3T3 cells were transfected with 50ng of the reporter construct 3DA.Luc, 250ng of the reference plasmid MLV-LacZ, and the indicated expression plasmids. Following the transfection, cells were maintained in 0.5% FBS in DMEM with 1% penicillin/streptomycin. After 24 hours, cells were harvested for luciferase assay

using standard protocols. Transfection efficiency was standardized by a β-galactosidase assay. Activator is expressed relative to reporter activation by the constitutively active SRF derivative, SRFVP16 (50 ng).

*Protein Purification*

Full-length INF1 was expressed as a his-tagged fusion protein in pET-30a+ in BL21 Rosetta DE3. Protein expression was induced with 0.2mM IPTG at 18°C for 16-20hrs. Cell lysates were incubated on $Ni^{2+}$ resin (GE Healthcare) in a Phosphate Binding Buffer (50mM $NaH_2PO_4$, 500mM NaCl, 10mM Imidazole pH 8.0, 0.05% Tween-20, 10% Glycerol, 100μM PMSF, 5mM β-mecaptoethanol and protease inhibitors). Purified protein was eluted in 1mL of Elution Buffer (50mM $NaH_2PO_4$, 500mM NaCl, 100μM PMSF, 5mM β-mecaptoethanol) with increasing concentrations of Imidazole pH 8.0 (100mM, 250mM, 500mM and 750mM). The purified protein was dialyzed in High Salt Buffer (20mM HEPES pH 7.5, 300mM NaCl, 10% Glycerol and 5mM β-mecaptoethanol).

In vitro *microtubule binding and bundling assays*

Microtubule binding assays were performed using a microtubule binding protein spin-down assay kit (Cat# BK029, Cytoskeleton Inc.) according to manufacture's protocol. Briefly, microtubules were assembled for 20 minutes at 35°C in a general tubulin buffer (80mM PIPES pH 7.0, 2mM $MgCl_2$, 0.5mM EGTA, 100μM GTP) then stabilized with 20μM taxol. Purified full-length INF1 protein or a control protein was incubated with MTs for 30 minutes at room temperature. Microtubules and associated

proteins were then layered on a 50% glycerol cushion buffer and centrifuged at 100,000 x *g* (49,000 RPM) using a Beckman Ultracentrifuge in a TLA 100.3 fixed-angle rotor. Supernatants and pellets were diluted in Laemmli loading buffer and equivalent samples were run on a 10% SDS-PAGE gel for analysis by Coomasie blue staining.

To examine microtubule bundling *in vitro* immunofluorescence was performed as previously described (Young et al., 2008). Briefly, FL INF1 and control samples were incubated with taxol stabilized microtubules and/or polymerized F-actin at room temperature for 30 minutes. Samples were then mounted on gelatin-coated Superfrost Plus slides (Fisher) and incubated for 10 minutes before fixing with 4% paraformaldehyde. Microtubules were visualized with mouse anti-α-tubulin antibody, F-actin with goat anti-actin and INF1 antibody (Young et al, 2008). The samples were visualized on an AxioImager microscope (Zeiss) with a 63X Plan Apochromat objective.

*Actin Bundling Assay*

F-actin bundling assays were performed as previously described (Vaillant et al., 2008). F-actin was prepared from pyrene-actin according to manufacturer's instructions (Cat# BK003, Cytoskeleton Inc.). Purified INF1 at 0.375μM, 0.75μM and 1.5μM was incubated with a final concentration of 2μM F-actin for 10 minutes at room temperature. Samples were then centrifuged at 16,000 x g for 10 minutes at 4°C. The top 80% of the supernatant was transferred to a new tube, and total protein was precipitated with 5 volumes of cold acetone (at -20°C). The precipitated protein was pelleted at 16,000 x g for 10 minutes @ 4°C then resuspended in 20μl of 1X SDS gel loading buffer. The remaining supernatant was removed and pellets were washed in 1X Actin Polymerization

Buffer (APB) and resuspended in 25μl of 1X SDS gel loading buffer. Equal volumes of each sample were subjected to SDS-PAGE and visualized by Coomassie Blue staining.

*Immunoprecipitations*

Co-immunoprecipitations of FLAG- and Myc- tagged proteins expressed by transient transfection in NIH 3T3 cells and Co-IPs were performed as previously described (Copeland et al., 2004, Copeland et al., 2007). Briefly, cells were washed in ice-cold phosphate-buffered saline, scraped in lysis buffer (50mM Tris, pH 7.0, 150mM NaCl, 1mM EDTA, 1mM dithiothreitol, 0.5% Triton X-100, 5mM NaF, and protease inhibitors), and kept on ice for 10 min. The lysate was cleared by centrifugation and supernatant incubated with 10ul anti-FLAG beads (Sigma) for 1-2 hours with tumbling at 4°C. The beads were washed 4X with 1mL of cold lysis buffer, and the immunoprecipitated proteins were eluted with 50μl of SDS-PAGE loading buffer. Equal volumes of the lysate and precipitated samples were analyzed by immunoblotting.

## 3.4 Results

*INF1 has Multiple Domains Which Regulate Microtubule Acetylation*

We previously showed that INF1 is a microtubule binding protein that induces microtubule stabilization and acetylation (Young et al., 2008). Surprisingly expression of an INF1 derivative lacking the microtubule binding domain (MTBD) (a.a. 1-958) is sufficient to induce MT stabilization and acetylation. To gain further insight into the mechanism by which INF1 regulates MT dynamics, we wanted to identify which domains are essential for the induction of MT acetylation. To do so, we generated a series of deletion derivatives that progressively removed each of the conserved C-terminal domains (Figure 3.1E). These derivatives were expressed in NIH 3T3 cells and the effects on MT acetylation visualized by immunofluorescence. As previously observed, expression of amino acids 1-958 induced acetylation at levels only slightly lower than full-length INF1 (42% of transfected cells, Figure 3.1A, D). However, further removal of C-terminal sequence did not greatly decrease MT acetylation levels (30% of transfected cells, Figure 3.1B, D). Thus, FH1 and FH2 alone are sufficient to induce MT stabilization in the absence of the MTBD. In earlier studies expression of the mDia FH2 is shown to be sufficient to induce microtubule stabilization (Palazzo et al., 2001, Wen et al., 2004). In contrast, expression of the isolated INF1 FH2 has no effect on MTs stabilization (Figure 3.1C, D). Thus, unlike Dia1, the INF1 FH2 domain alone is not sufficient for MT acetylation.

Our results suggest that sequence N-terminal to the FH2 is required for acetylation. Consequently, we wanted to determine whether FH1 or another N-terminal

sequence is responsible for the formation of stable MTs. We created a deletion derivative that removed the conserved region N-terminal to FH1 to determine if this domain, or FH1, is responsible for MT stabilization (Figure 3.2D). Removal of the first 25 amino acids has no effect and thus FH1/FH2 alone is sufficient to induce acetylated MT formation (Figure 3.2A). However, the FH1 domain is not required for acetylation in the presence of the MTBD (Figure 3.2C).

We next wanted to test whether a functional FH2 is required for MT stabilization by the N-terminus. To test requirements for FH2 activity, we mutated a conserved isoleucine at codon 180 to alanine (Figure 3.3F). Corresponding mutants in mDia are unable to polymerize actin filament growth (Xu et al., 2004, Bartolini et al., 2008). To confirm that the full-length and 1-485 I180A mutants are unable to polymerize F-actin we tested their ability to activate an SRF reporter gene that responds to changes in actin dynamics (Sotiropoulos et al, 1999). As expected, FL I180A and 1-485 I180A induced activation of the reporter gene is approximately 200-fold lower than the corresponding wild-type constructs (Figure 3.4A) showing that these mutants are indeed deficient in regulating actin dynamics. We then examined the ability of both constructs to induce MT acetylation. We found FL I180A is still able to induce microtubule acetylation similar to wild-type INF1 (Figure 3.3E). Surprisingly, 1-485 I180A, as well as the longer derivative 1-958 I180A, did not induce microtubule acetylation above background levels (Figure 3C-E). This suggests that MT acetylation by the N-terminus is dependent on the presence of a functional FH2 domain. Together our results suggest that in the presence of the MTBD, FH1/FH2 function is dispensable for INF1 induced MT acetylation. However, in the absence of the MTBD, functional FH1 and FH2 domains are required.

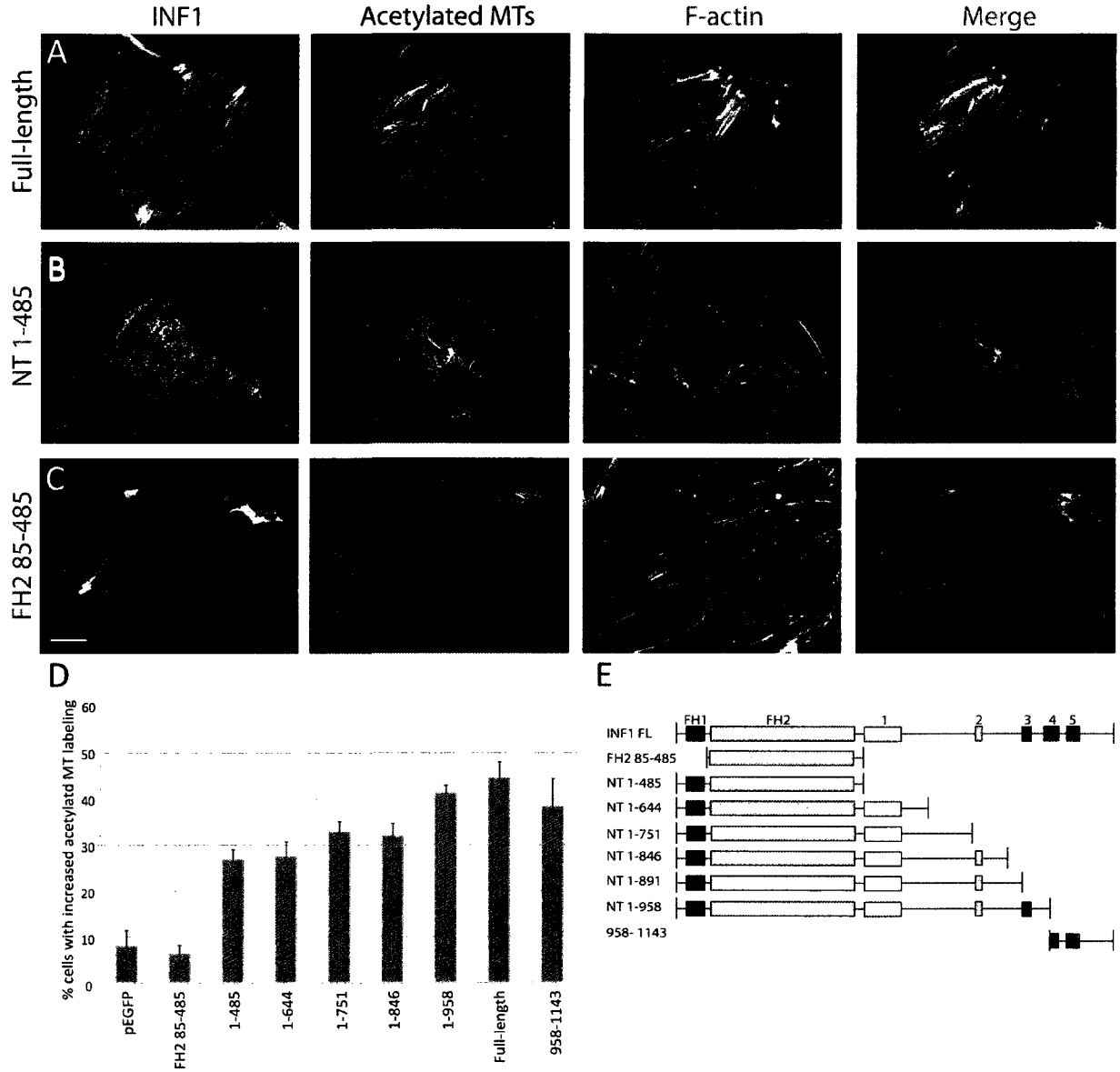
INF1
Acetylated MTs
F-actin
Merge
A
Full-length
B
NT 1-485
C
FH2 85-485
D
% cells with increased acetylatd MT labeling
60
50
40
30
20
10
0
pEGFP
FH2 85-485
1-485
1-644
1-751
1-846
1-958
Full-length
958-1143
E
FH1
FH2
1
2
3
4
5
INF1 FL
FH2 85-485
NT 1-485
NT 1-644
NT 1-751
NT 1-846
NT 1-891
NT 1-958
958- 1143

**Figure 3.1. INF1 uses multiple domains to induce microtubule stabilization.**

Various INF1-Flag tagged constructs were expressed in NIH 3T3 cells and grown 2 days until a confluent monolayer was formed. (A) Full-length INF1 induced microtubule acetylation in 44.6% of cells. (B) The N-terminal protein (a.a. 1-485) induced acetylation in 26.8% of cells. (C) Cells expressing FH2 (a.a. 85-485) did not increase acetylated MT labeling compared to empty GFP control. (D) N-terminal series from a.a. 1-485 to a.a. 1-846 induced MT acetylation averaging around 30% of transfected cells. Cells expressing 1-958, full-length and the C-terminus alone (a.a. 958-1143) were capable of inducing MT acetylation in approximately 40-45% of cells. Data for cell counts were obtained from five separate trials with approximately n=100 cells counted for each construct. The standard error of the mean is shown as error bars for five separate trials. (E) Schematic representation of flag fusion proteins. FH = formin homology domains. FHDC 1, 2, 3, 4, and 5 are conserved regions in the C-terminus of INF1. FHDC 4 and 5 are also known as microtubule-binding domain (MTBD) 1 and 2. Scale bar = 20μm, applies to all images.

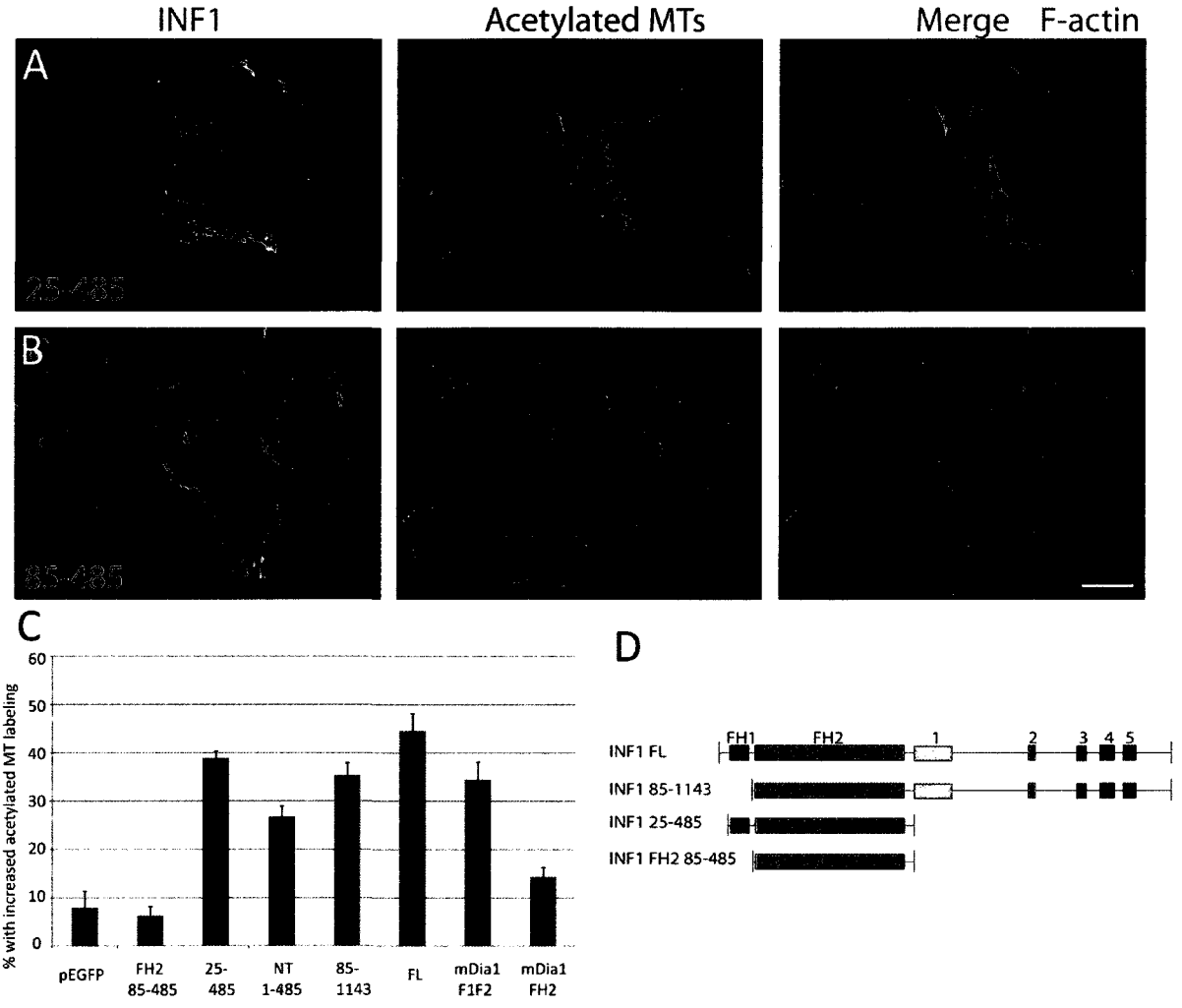
INF1
Acetylated MTs
Merge F-actin
A
25-485
B
85-485
C
% with increased acetylated MT labeling
60
50
40
30
20
10
0
pEGFP
FH2 85-485
25-485
NT 1-485
85-1143
FL
mDia1 F1F2
mDia1 FH2
D
FH1
FH2
1
2
3
4
5
INF1 FL
INF1 85-1143
INF1 25-485
INF1 FH2 85-485

**Figure 3.2. The FH1 domain of INF1 contributes to microtubules acetylation.**

NIH3T3 cells were transfected with various INF1 fusion proteins truncated at the N-terminus. (A) Expression 25-485 induced microtubule acetylation in 38.9% of cells. (B) The FH2 domain alone cannot induce acetylation (6.2% of transfected cells) (C) Cells expressing constructs with FH1 stabilized microtubules at a higher percentage than constructs without FH1. Values were taken from four separate experiments with N=100 cells counted per experiment. The standard error of the mean is shown as error bars for the 4 trials. (D) A schematic representation of constructs transfected into cells. Scale bar = 20μm, applies to all images.

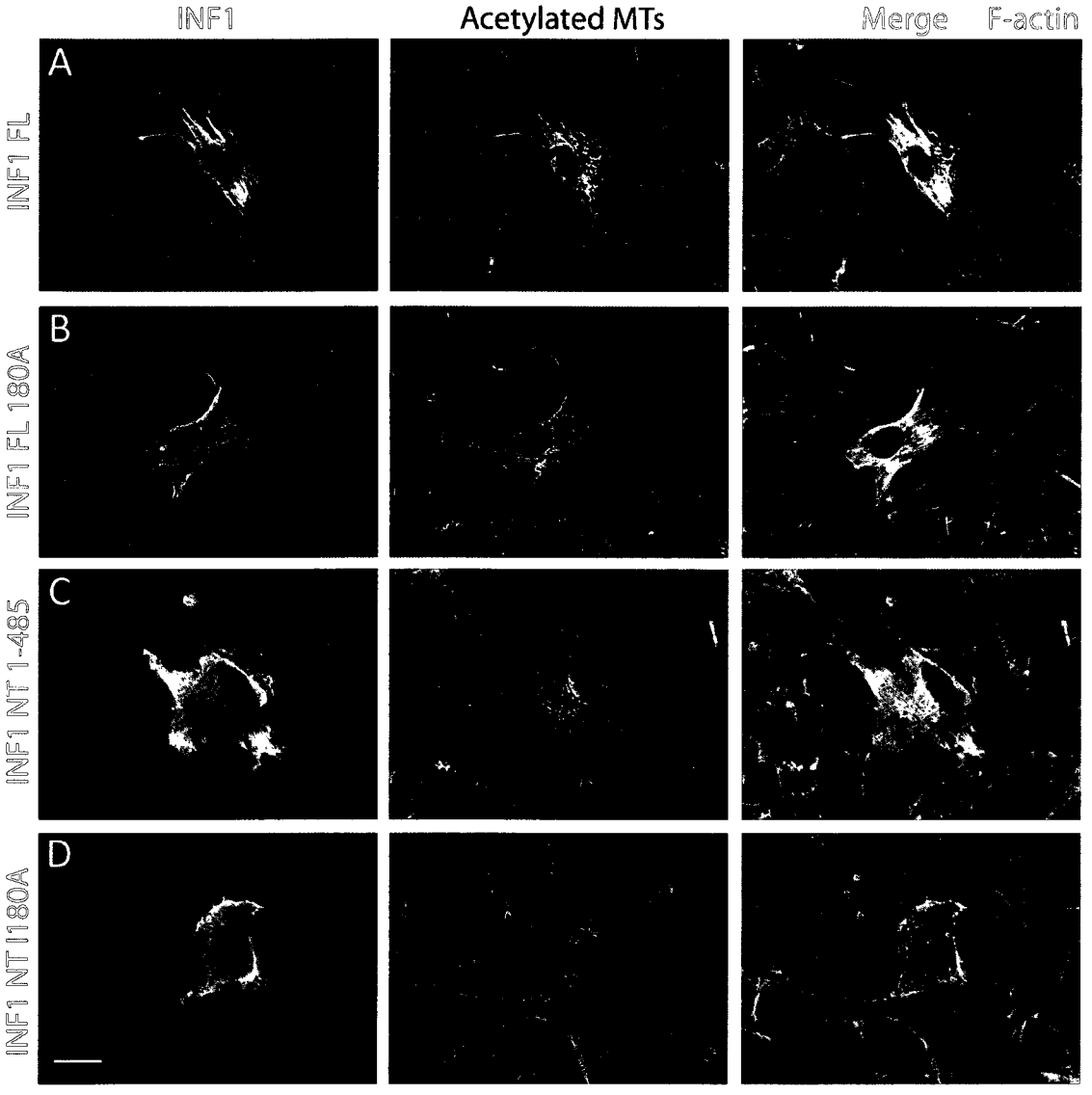
INF1
Acetylated MTs
Merge
F-actin
A
INF1 FL
B
INF1 FL I80A
C
INF1 NT 1-485
D
INF1 NT I80A

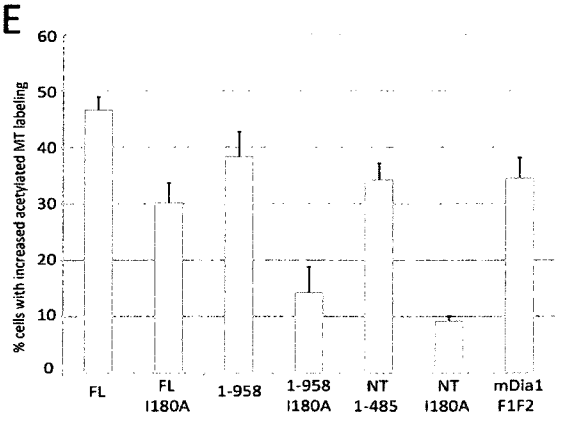
E
% cells with increased acetylated MT labeling
60
50
40
30
20
10
0
FL
FL I180A
1-958
1-958 I180A
NT 1-485
NT I180A
mDia1 F1F2

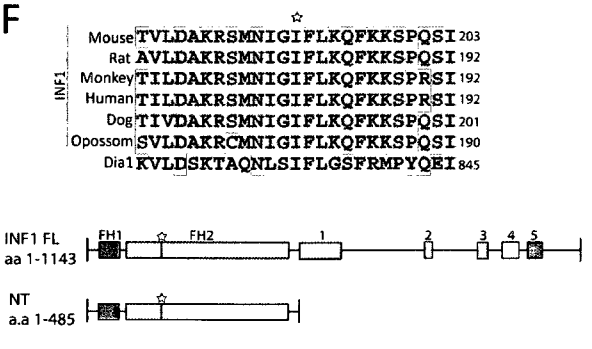
F
INF1
Mouse TVLDAKRSMNIGIFLKQFKKSPQSI 203
Rat AVLDAKRSMNIGIFLKQFKKSPQSI 192
Monkey TILDAKRSMNIGIFLKQFKKSPRSI 192
Human TILDAKRSMNIGIFLKQFKKSPRSI 192
Dog TIVDAKRSMNIGIFLKQFKKSPQSI 201
Opossom SVLDAKRCMNIGIFLKQFKKSPQSI 190
Dia1 KVLDSKTAQNLSIFLGSFRMPYQEI 845
INF1 FL
aa 1-1143
FH1
FH2
1
2
3
4
5
NT
a.a 1-485

**Figure 3.3. A functional FH2 is required for acetylation in the absence of MTBD.**

A point mutation in the FH2 domain were made in full-length (FL), 1-958 and the 1-485 constructs and transfected in NIH 3T3 cells. Cells were fixed after 2 days when a confluent mono-layer was formed. (A,B) Wild-type full-length INF1 induced MT acetylation in 46.7% of cells, while the full-length I180A mutants was only 30.1% in cells. (C) The N-terminus induced acetylation in 34.4% of cells. (D) Cells transfected with a mutant version of 1-485 I180A induced acetylation in 9.2%. (E) Data for cell counts were obtained from four separate trials with n=100 cells counted for each construct. Fusion mDia1 F1F2 is given as a comparison because of its previous reported stabilization activity (Bartolini et al., 2008). mDia1 F1F2 induced acetylation at similar levels to the N-terminus of INF1. The standard error of the mean is shown as error bars for the 4 trails. (F) A clustal alignment of the FH2 domain of INF1 from various species compared to mDia1. Amino acid numbers are shown at end of sequence. The highly conserved Ile 180 was mutated to Ala to create the actin mutant previously described. The bottom portion of (F) is a schematic representation of fusion proteins. Star points out amino acid mutation. Scale bar = 20μm, applies to all images.

*INF1 I180A Induces Stress Fiber Formation Through Endogenous Proteins*

We noted by immunofluorescence that FL I180A induces formation of stress fiber in a larger proportion of cells compared to the N-terminal I180A mutant. Stress fibers induced by FL I180A are thick unlike wild-type induced stress fibers, which are thin and wispy. A closer examination of the SRF reporter gene results showed that, although significantly lower than wild type, the FL I180A mutant still induced activation to a level above background and somewhat higher than 1-485 I180A (Figure 3.4B).

The enhanced ability of FL I180A to induce stress fibers over 1-485 I180A suggests that the C-terminus might be contributing to stress fiber formation. Therefore, we examined the ability of the isolated INF1 C-terminus to induce the formation of stress fibers in NIH 3T3 cells. Cells expressing CT @ 751 (a.a. 751-1143) has a noticeable accumulation of F-actin in 50% of transfected cells, similar to the levels seen with full-length I180A (Figure 3.5A, E). We then wanted to determine if expression of the C-terminus is activating the endogenous protein, similar to what is observed with the DRFs DAD over-expression. We transiently expressed INF1 constructs in Cos-1 cells that do not express endogenous INF1. Full-length INF1 expressed in Cos-1 induces thick stress fibers that appear to co-localize with MT associated INF1 filaments (Figure 3.5B, E). However, full-length I180A has no effect on the organization or accumulation of F-actin in Cos-1 cells (Figure 3.5C, E). Similarly, CT @ 751 expression in Cos-1 cells also has no effect on F-actin accumulation. These results suggest that F-actin accumulation by I180A or the C-terminus is likely mediated by activation of endogenous INF1.

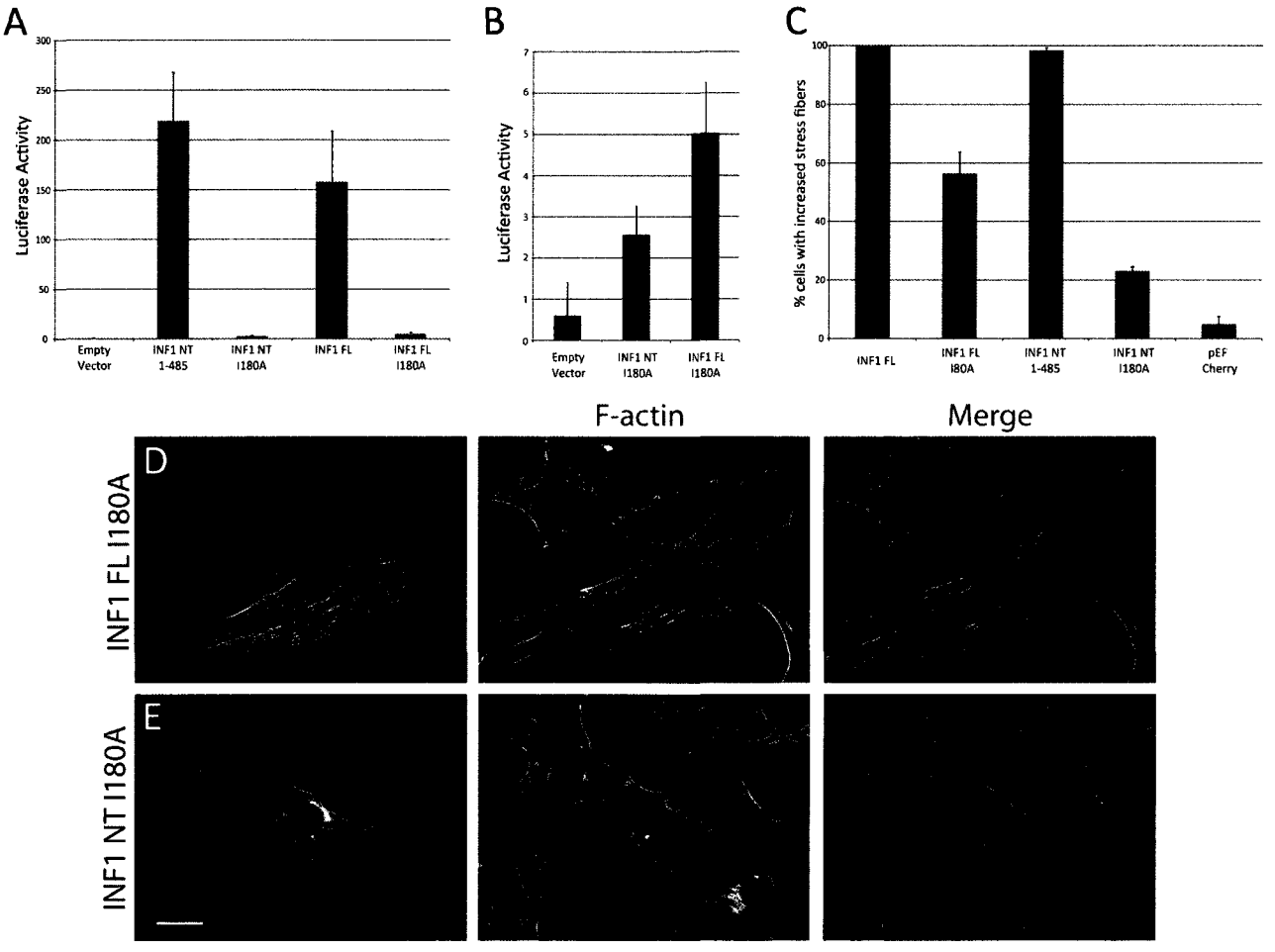
A
Luciferase Activity
300
250
200
150
100
50
0
Empty Vector
INF1 NT 1-485
INF1 NT I180A
INF1 FL
INF1 FL I180A
B
Luciferase Activity
7
6
5
4
3
2
1
0
Empty Vector
INF1 NT I180A
INF1 FL I180A
C
% cells with increased stress fibers
100
80
60
40
20
0
INF1 FL
INF1 FL I80A
INF1 NT 1-485
INF1 NT I180A
pEF Cherry
F-actin
Merge
D
INF1 FL I180A
E
INF1 NT I180A

**Figure 3.4. I180A mutants induce stress fiber formation in NIH 3T3 cells.**

Full-length, NT 1-485 and corresponding I180A mutants were transfected into NIH 3T3 cells. After 1 day of expression cells were either fix for immunofluorescence or harvested for a luciferase assay. Cell counts were completed from three separate experiments with n>60. (A) Averages of three separate luciferase experiments are shown with error bars representing the standard error of the mean. The wild-type N-terminus and the full-length protein have strong luciferase activity. I180A mutants show low levels of activation. (B) Expanded graph from (A) of luciferase activation by full-length and N-terminal I180A mutants. (C) Cell counts show that the actin mutants were capable of inducing stress fiber formation. Full-length mutants induce stress fiber formation in 56.5% of cells and the N-terminal mutant in 23.1% of cells. (D) Full-length mutants induce the formation of thin F-actin. (E) N-terminal mutants increase levels of F-actin staining in transfected cells, but did not show filament formation. Scale bar = 20μm, applies to all images. The standard error of the mean is shown as error bars for the 3 separate trails.

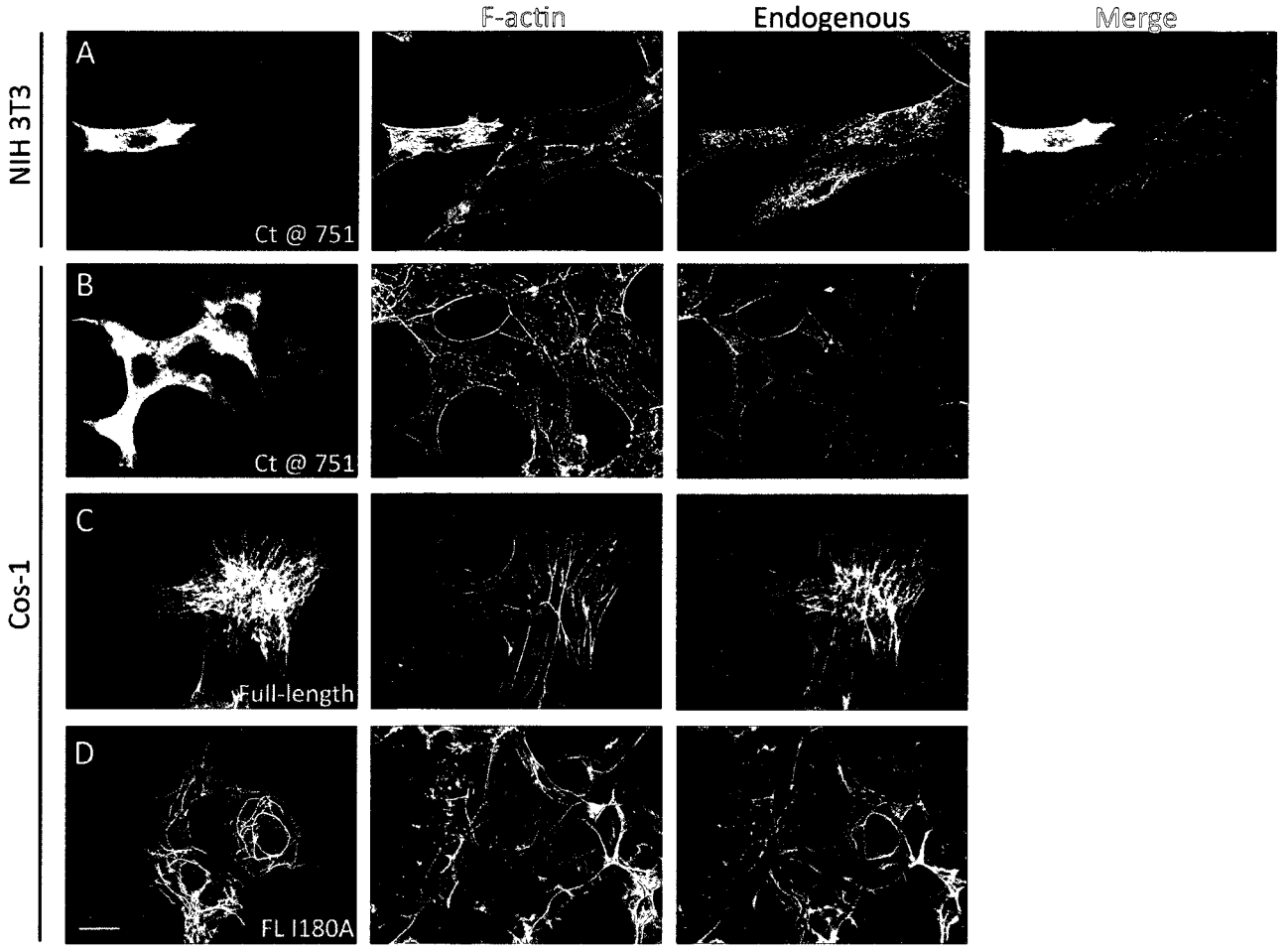
F-actin
Endogenous
Merge
NIH 3T3
Cos-1
A
Ct @ 751
B
Ct @ 751
C
Full-length
D
FL I180A

E

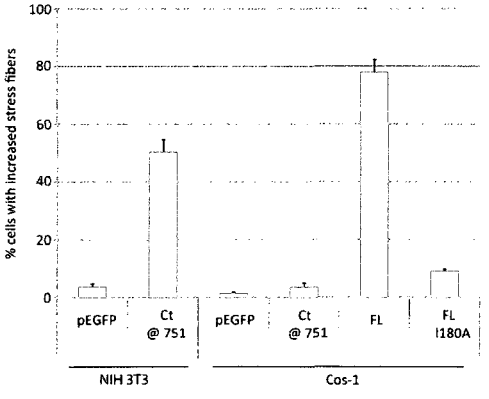
% cells with increased stress fibers
100
80
60
40
20
0
pEGFP
Ct @ 751
pEGFP
Ct @ 751
FL
FL I180A
NIH 3T3
Cos-1

**Figure 3.5. INF1 I180A mutants induce stress fiber formation through endogenous INF1.**

(A) NIH 3T3 fibroblasts transfected with INF1 CT @ 751 (751-1143) induced stress fibers in 50% of cells. (B) The same construct was transfected into Cos-1 cells and there is no induction of stress fibers beyond background levels. (C) Cos-1 cells were the transfected with full-length protein, which induced stress fiber formation. Stress fibers also co-aligned with filamentous INF1/MTs. (D) Cells transfected with mutant full-length protein did not change stress fibers. For immunofluorescence cells were fixed then stained with anti-INF1 for endogenous protein, anti-myc for fusion proteins and fluorescein phalloidin was used to visualize stress fibers. (E) Cell counts were taken from three separate experiments and n=100 cells were counted for each set. The standard error of the mean is shown as error bars for the 3 separate trails. Scale bar = 20μm, applies to all images.

*INF1 Binds Both Microtubules and F-actin in vitro*

FL INF1 overexpression in Cos-1 cells induced a striking re-organization of F-actin that was extensively co-aligned with MTs (Figure 3.5C). To investigate if INF1 plays a direct role in the re-organization of F-actin and MTs we tested INF1 for the ability to bind both MTs and F-actin *in vitro*. Our group has already demonstrated that the MTBD is sufficient to bind MTs *in vitro* and we wanted to verify that FL also binds MTs. Full-length His-tagged INF1 protein purified from bacteria was used in an *in vitro* microtubule spin-down assay and a fluorescent-based microtubule bundling assay. The MT spin-down assay is based on the ability of MTs to co-sediment associated proteins when centrifuged at 100,000 x g. In the absence of MTs, full-length INF1 remains in the supernatant. However, when incubated with microtubules, INF1 is depleted from the supernatant and co-sediments with microtubules (Figure 3.6G). To visualize microtubule binding and bundling directly we use an *in vitro* immunofluorescence (IF) based assay as previously described (Young et al., 2008). Full-length INF1 was incubated with taxol-stabilized microtubules then fixed and stained on microscope slides. MTs incubated with FL INF1, but not BSA, are bundled in a dense network and co-align with INF1 protein (Figure 3.6A-F). Thus, full-length INF1 is capable of binding and bundling microtubules directly.

To determine if full-length INF1 is able to bind and/or bundle actin, purified INF1 protein is incubated with F-actin and spun for 10 minutes at 16,000 x g. Using this assay we find that FL INF1 bundles F-actin in a concentration dependent manner (Figure 3.7D). We also used immunofluorescence to visualize INF1 induced F-actin bundles, as we did above for MTs.

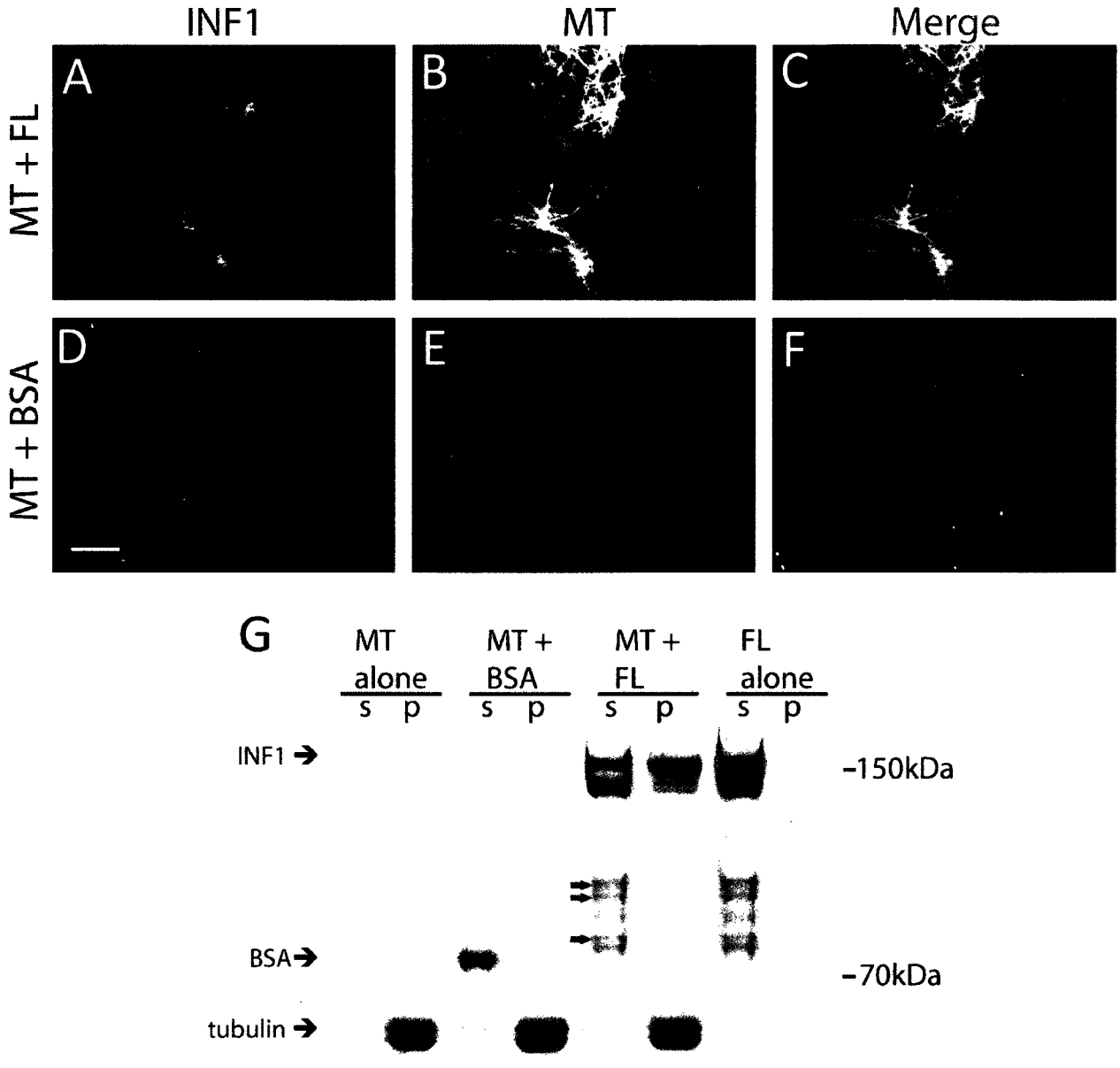
INF1
MT
Merge
A
B
C
MT + FL
D
E
F
MT + BSA
G
MT alone
MT + BSA
MT + FL
FL alone
s p
s p
s p
s p
INF1 →
-150kDa
BSA →
-70kDa
tubulin →

**Figure 3.6. Full-length INF1 binds and bundles microtubules *in vitro.***

(A-C) Purified His-FL INF1 protein was incubated with microtubules and visualized by immunofluorescence. Full-length INF1 bundles microtubules. (D-F) Without INF1 microtubules are small filaments without any bundles formed. (G) Purified protein was incubated with microtubules and centrifuged at 100,000 x *g*. The INF1 FL protein was found mostly in the pellet (P) fraction when incubated with microtubules, but remained in the supernatant (S) when incubated alone. Smaller degradation bands (arrows) of INF1 did not co-sediment with MTs. BSA incubated with microtubules remained in the supernatant. Scale bar = 20μm, applies to all images.

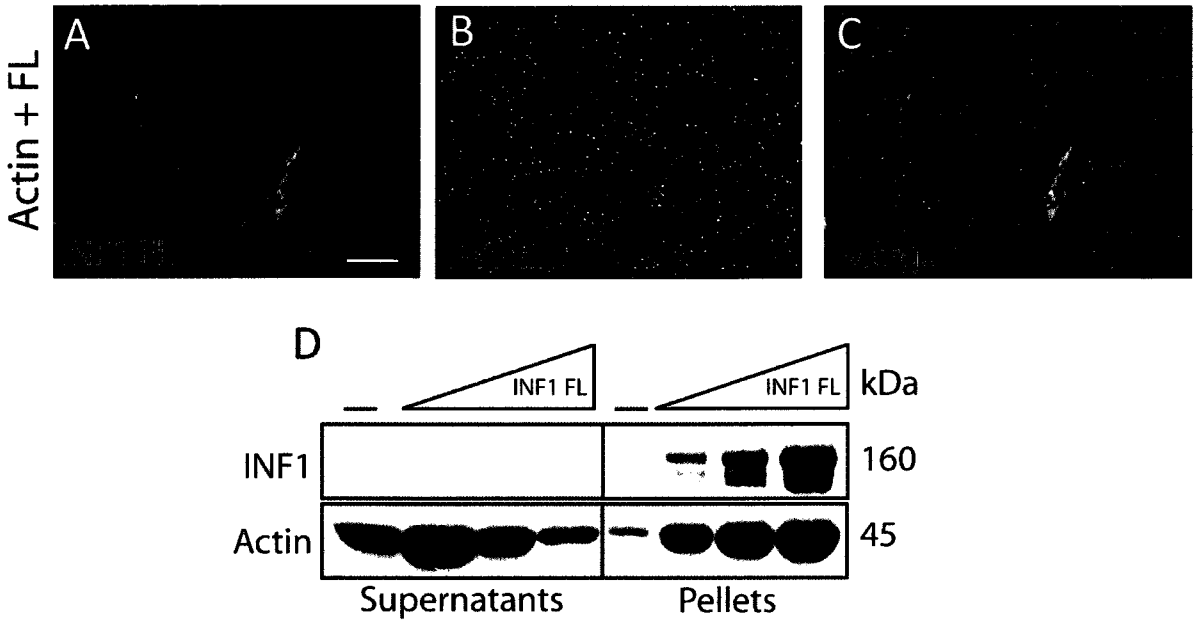


**Figure 3.7. INF1 binds and bundles filamentous actin.**

(A-C) Immunofluorescence was used to image purified full-length incubated with F-actin. Full-length protein bundles and co-aligns with actin filaments. (D) Increasing concentrations of full-length protein was incubate with F-actin (2μM) and then centrifuged at 16,000 x g for ten minutes to pellet F-actin bundles. Equivalent samples of the supernatant and pellet were subjected to SDS-PAGE, and the proteins were visualized with Coomasie blue. INF1 pellets and bundles F-actin. Scale bar = 20μm, applies to all images.

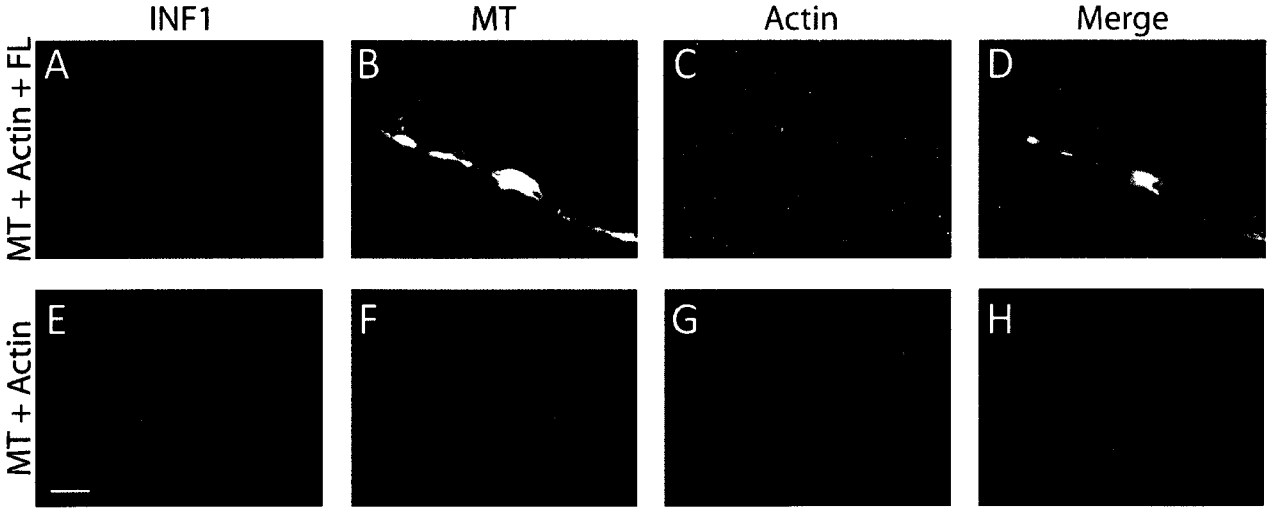


**Figure 3.8. INF1 bundles F-actin and microtubules.**

(A-D) Purified full-length protein was incubated with microtubules and F-actin and visualized by immunofluorescence. INF1 bundles microtubules and F-actin, simultaneously. (E-H) Without INF1, microtubules and actin filaments do not bundle or co-align. Scale bar = 20μm, applies to all images.

In the absence of INF1, F-actin filaments are not detectable by IF in this assay (Figure 3.8G). However, in the presence of INF1 F-actin bundles are seen as thick filaments that co-align with INF1 protein (Figure 3.7A-C).

Having shown that FL INF1 binds and bundles MTs and F-actin individually, we were interested to see if it is able to bind microtubules and F-actin simultaneously. This cannot be addressed in the spin-down assay, therefore we used the immunofluorescence binding assay to determine if INF1 cross-links F-actin and MTs. Full-length INF1 was incubated with F-actin and taxol-stabilized microtubules and the reaction products mounted onto microscope slides. Without INF1, there is no visible co-alignment of MTs with F-actin (Figure 3.8E-H). However pre-incubation of MTs and F-actin with INF1 induces formation of thick bundles of both MT and F-actin that co-align with INF1 (Figure 3.8A-D). Thus, INF1 is able to simultaneously bind and bundle both microtubules and actin filaments *in vitro*.

## 3.5 Discussion

To date a handful of formins have been shown to organize and stabilize microtubules, but it still remains unclear as to whether or not they cross-link actin and microtubules directly (Ishizaki et al., 2001, Gasteier et al., 2005). INF1 is the only formin that is primarily localized to MTs and a MT binding domain has been identified in the INF1 C-terminus (Young et al., 2008). We present here a structure/function analysis of

the novel formin INF1 in an attempt to further our understanding of the mechanisms by which it regulates actin and microtubule dynamics.

*The INF1 is not autoinhibited*

Full-length INF1 appears to be constitutively active and not subject to autoregulation. There are no previously described regulatory domains found in the INF1 sequence, however, our data supports a role for the C-terminus in INF1 regulation. Expression of the INF1 C-terminus in NIH 3T3 fibroblasts induced stress fiber formation, while expression of the same derivative in Cos-1 cells had no effect on F-actin accumulation or organization. Cos-1 cells do not express INF1 endogenously and this likely accounts for the difference in the results obtained in these different cell-types i.e. the INF1 C-terminus induces stress fiber formation through activation of endogenous INF1. The C-terminus contains five conserved regions that may participate in the regulation of INF1 activity. We do not feel that these results reflect a "DAD"-like role for the INF1 C-terminus as there is no evidence that INF1 is auto-regulated *in vivo* or *in vitro*. Rather we favour a model where the INF1 C-terminus activates the endogenous protein by titrating out a negative regulatory factor that normally suppresses INF1 effects on F-actin. The identification of this factor will be an important goal of our future studies.

*INF1 Induces MT Acetylation Through Multiple Mechanisms*

INF1 contains at least three domains contributing to the formation of stable acetylated microtubules. Our previous report showed the C-terminus of INF1 (a.a. 958-1143) contains a bipartite microtubule-binding domain (MTBD) that is sufficient to induce

microtubule stabilization and acetylation. Surprisingly, this domain is not essential for INF1 induced MT acetylation (Young et al., 2008, Figure 2.9). Our deletional analysis shows that, in the absence of the MTBD, the activity of both FH1 and FH2 (a.a 25-485) are required for the induction of MT acetylation. In the absence of FH1, the FH2 does not induce acetylation. Conversely, the I180A mutation in FH2 also inhibits FH1-dependent MT acetylation. Interestingly, we found that purified INF1 FH2 protein has a weak affinity for MTs in the spin-down assay (Supplemental Figure 3.1.1). Thus, in the absence of the MTBD, the FH2 is likely required to deliver the MT-stabilizing activity of the FH1 domain to MTs. However, in the presence of the MTBD, neither FH1 nor FH2 function are essential for the induction of MT acetylation; full-length I180A and 85-1143 both induce the formation of acetylated MTs. We propose a model where INF1 induces MT stabilization by two distinct mechanisms. The first is through the direct association of the MTBD with MTs. The second is through the FH2-dependent delivery to the MTs of FH1. Recent studies have shown that cytoskeleton-associated protein-glycine-rich (CAP-Gly) domains interact with proline-rich sequences such as those found in FH1 (Steinmetz and Akhmanova, 2008). Therefore FH1 may stabilize MTs as part of a complex with CAP-Gly proteins at the +Tip.

Our data also suggests that INF1-induced MT stabilization must be through a mechanism distinct from that of the formin mDia. Unlike INF1, the FH2 domain of mDia is both necessary and sufficient to induce MT stabilization. Also unlike INF1, mDia-induced MT stability is not affected by mutations that abolish FH2 dimerization or the ability to regulate actin dynamics. Thus, INF1 must induce MT stabilization via a different mechanism, as INF1 requires a FH1 and a functional FH2 domain.

We found that overexpression of full-length INF1 in Cos-1 cells induced a dramatic and extensive co-alignment of F-actin with MT-bound INF1, highlighting its potential to serve as a "bridging factor" between F-actin and MTs. These results were confirmed *in vitro* using purified full-length INF1 protein. We showed for the first time that INF1 is able to bind and bundle F-actin directly and is able to do the same with MTs. More importantly, we provide direct evidence that INF1 is able to bind to both F-actin and MTs simultaneously. Together our data suggest INF1 acts directly to mediate cross-talk between actin filaments and microtubules.

In summary, our results further describe a novel MT associated formin, that has the ability to stabilize MTs and polymerize actin. In future work we would like to determine the physiological role of INF1. It has been found that the re-orientation of the Golgi is essential for directed cell migration and requires the coordinated regulation of actin and MT dynamics. Preliminary work shows that overexpression of INF1 induces Golgi dispersion (S.J. Copeland, unpublished data). We favour a model where INF1 plays a central role in cell polarity through the coordinated regulation of actin and MT dynamics

### 3.6 Acknowledgements

We thank Karine Gauthier and Thea Worthylake for their help in generating some of the INF1 derivatives described in this study.

## 3.7 Supplemental Figures

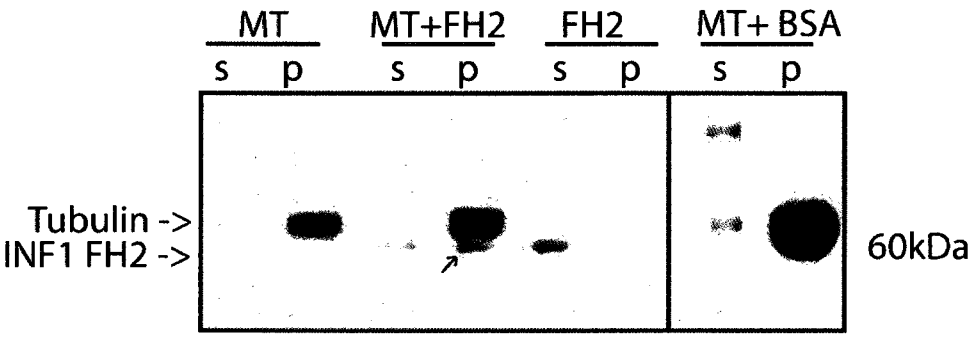


**Figure 3.7.1. INF1 FH2 associates with microtubules.**

Purified His-tagged FH2 protein (a.a. 85-485) was incubated with stabilized microtubules and then spun at 100,000 x g for 40 minutes. Equal volumes of supernatant(s) and pellet (p) were subjected to SDS-PAGE and analyzed by Coomasie blue staining. FH2 was co-sedimented with MTs (arrow), but remains in the supernatant when centrifuged alone. BSA control does not co-sediment with microtubules.

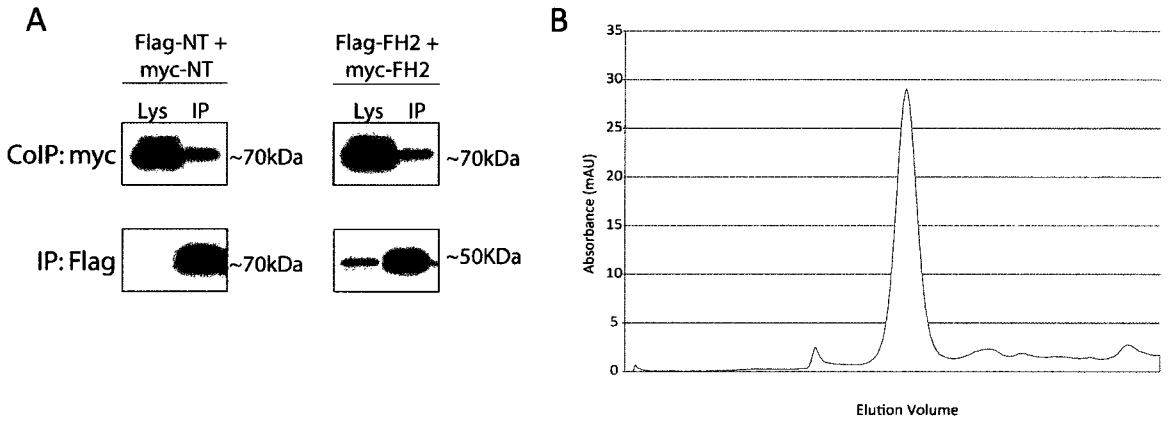


**Figure 3.7.2. INF1 forms FH2 dimers.**

(A) Flag and myc N-terminal (a.a. 1-485) and FH2 (85-485) constructs were co-expressed in NIH 3T3 cells. Flag co-immunoprecipitated myc-INF1 constructs suggesting FH2 dimerization. (B) Purified His-tagged INF1 FH2 protein (46.6kDA) was run through a Superdex 200 analytical gel filtration column. One large peak eluted before standard Chicken uvalbumin (44kDa), suggesting FH2 is larger than uvalbumin and most likely forms an extended dimer.

# Chapter 4: Discussion, Preliminary studies and Future Work

## 4.1 Discussion

### 4.1.1 INF1 Regulation

There are no previously defined autoregulatory domains found within the INF1 sequence (Young et al., 2008). Full-length INF1 is constitutively active when overexpressed and induces the formation of stress fibers in NIH 3T3 fibroblast and monkey kidney Cos-1 cells. In addition, full-length INF1 protein expressed in bacteria is able to bind and bundle both F-actin and MTs *in vitro* suggesting the protein is active in the absence of any activating factors. Together these results suggest INF1 is not subject to auto-inhibition, unlike other formins.

Some insight into how INF1 is regulated can be obtained from our studies of the INF1 I180A mutant. Surprisingly, INF1 I180A overexpression in NIH 3T3 cells is able to induce the formation of stress fibers, however, the same effect is not observed in Cos-1 cells which do not have endogenous INF1 suggesting that I180A is activating endogenous INF1 to induce stress fiber formation. We found that similar results could be obtained with an isolated segment of the INF1 C-terminus (CT @ 751). If INF1 is not subject to auto-inhibition, then the ability of the C-terminus to activate the endogenous protein suggests it may be titrating out an inhibitory factor. Based on our data we favor a model where INF1 regulation is mediated by a negative regulatory factor that targets the INF1 C-terminus.

The nature of the putative INF1 inhibitor is unknown, but it is likely that INF1 regulation is mediated in part by post-translational modifications. Using our INF1 antibody, we tested various cells and tissues by Western Blotting, to evaluate INF1 expression. We found that endogenous INF1 runs at approximately 125kDa, while the overexpressed fusion protein runs closer to 160kDa. There is no data to suggest this difference is due to the presence of alternative INF1 splice forms, therefore, it is therefore likely to arise from post-translational modifications of the protein. Protein phosphorylation can induce faster mobility depending on the location of the modification. We have preliminary data suggesting that INF1 is regulated by the kinase MARK2, a regulator of MT stability (JC personal communication). It is also possible that the mature INF1 protein is proteolytically processed. If so, then cleavage must be at the C-terminus as our antibody recognizes an N-terminal epitope. A proteolytic processing model would also have to incorporate the observation that the majority of INF1 protein is bound to MTs and therefore leaves the C-terminal MTBD intact. Clearly there is still much to learn about the mechanism of INF1 regulation and the nature of any putative INF1 post-translational modifications.

### 4.1.2 INF1 Associates Directly with MTs

Endogenous INF1 protein has both a punctate and filamentous subcellular localization. The dispersion of MTs with nocodazole disperses INF1 throughout the cell demonstrating that the filamentous distribution of INF1 is dependent on MT integrity. Like mDia and FHOD1, INF1 expression induces the alignment of MTs parallel to actin stress fibers (Ishizaki et al., 2001, Gasteier et al., 2005, Young et al., 2008). However,

INF1 is the only formin shown to co-align along the length of MTs in vivo. We show that both the full-length protein and the isolated MTBD are able to bind directly to MTs *in vitro*.

The INF1 MTBD consists of two conserved regions in the C-terminus, MTB1 and MTB2, which correspond to FHDC4 and FHDC5 in the original description of the INF1 gene (Katoh and Katoh, 2004). We found that without these two regions, INF1 no longer co-localizes to MTs. In addition, neither domain alone is sufficient for co-localization to MTs. While MTB1 and MTB2 have been designated as two separate domains, it is likely that they make up a single diffuse MTBD. Expression of this domain induced a MT "basket" phenotype, with thick bundles of MTs wrapped around the cell. This basket effect is commonly seen with the overexpression of many microtubule-binding proteins (Ligon et al., 2003). The isolated MTBD as well as FL INF1 are sufficient for MT binding and bundling *in vitro*. This is consistent with the idea that bundling is a product of the diffuse nature of most MT binding domains and overall MT affinity. Thus, at high concentrations the full-length protein has the same effect as the isolated MTBD.

Interestingly, we show that INF1 FH2 protein co-sediments and thus binds MTs in a MT-spin down assay. However, overexpressed INF1 FH2 does not co-localize with MTs in NIH 3T3 or Cos-1 cells. Other formins, such as mDia FH2, are also reported to bind MTs with low affinity (Palazzo et al., 2001, Bartolini et al., 2008). This raises the intriguing possibility that all FH2 domains may have a low affinity for MTs. The function of MT-binding by FH2 is not fully understood. It has been suggested that actin/MT bridging factors facilitate MT stabilization *in vivo* by guiding dynamic MTs to cortical receptors that capture and stabilize the MT plus tip.

### 4.1.3 INF1 Induces MT stabilization and Acetylation Via Three Domains

A 50% knockdown of INF1 resulted in a 70% knockdown of acetylated MTs in NIH 3T3 cells, suggesting that INF1 is essential for MT stabilization in NIH 3T3 cells. We also found that overexpression of FL INF1 induced the formation of stable acetylated MTs. mDia has been shown to induce the formation of both detyrosinated (Glu-MTs) and acetylated MTs (Palazzo et al., 2001, Bartolini et al., 2008) and it has been suggested that these two modifications identify the same pool of stable MTs (Palazzo et al., 2003). However, we found INF1 expression had no effect on levels of Glu-MTs suggesting that these two MT populations are distinct. MT acetylation promotes the binding of specific kinesin motor proteins and is reported to be an essential component of pathways that regulate neuronal polarity. This suggests INF1 may have a role in generating a distinct sub-population of stable MTs whose specific function may depend on the cellular context (e.g. fibroblasts vs neurons).

Multiple domains of INF1 participate in the regulation of MT stabilization. Full-length INF1 and the C-terminal MTBD are sufficient to induce the formation of stable MTs. Surprisingly, without the MTBD, the N-terminus of INF1 (a.a. 1-958), or the isolated FH1FH2 domains, are sufficient to induce stabilization. Similar results were obtained with mDia where it has been suggested that an isolated functional FH2 domain is both necessary and sufficient for the induction of MT stabilization (Bartolini et al., 2008). This is not the case with INF1 where the FH2 is necessary, but not sufficient for MT stabilization. These results suggest that INF1-induced MT stabilization must be mediated by a mechanism distinct from mDia.

### 4.1.4 INF1 Cross-links the Actin and Microtubule Cytoskeletal Networks

We then wished to test FL INF1 to see if it is capable of associating to both MTs and F-actin, simultaneously. By immunofluorescence we found that INF1 bundles both F-actin and MTs separately. We then pre-incubated assembled MTs and actin with FL INF1 and found that INF1 bundles both filaments at the same time. However, when looking at MT and actin alone, there were no discernable filaments. We also noted that when looking at overexpressed INF1 in Cos-1 cells, F-actin co-aligns with INF1/MT filaments. Thus, INF1 is the only formin shown capable of regulating both actin and MT activity *in vitro*.

### 4.1.5 Biological function of INF1

As noted above, both endogenous and overexpressed INF1 also have a punctate distribution in NIH 3T3 fibroblasts. The puncta did occasionally co-align with microtubules, but not always. These puncta do not co-localize with the Rab 4, 5, 7 or 11 markers for endocytic vesicles, nor do they co-localize with ER, peroxisome or mitochondrial organelle markers. We did note that the endogenous INF1 protein is concentrated in a perinuclear in a region that coincides with the Golgi (Figure 4.1). This may reflect the increased abundance of MTs originating from the MTOC that is usually in association with the Golgi, or a role for INF1 in Golgi dynamics or Golgi dependent MT assembly. Golgi morphology and proper subcellular localization is dependent on the coordinated regulation of actin and MT dynamics. In preliminary experiments we find INF1 expression induces Golgi dispersion (JC unpublished observations) supporting a role for the endogenous protein in the regulation of Golgi dynamics.

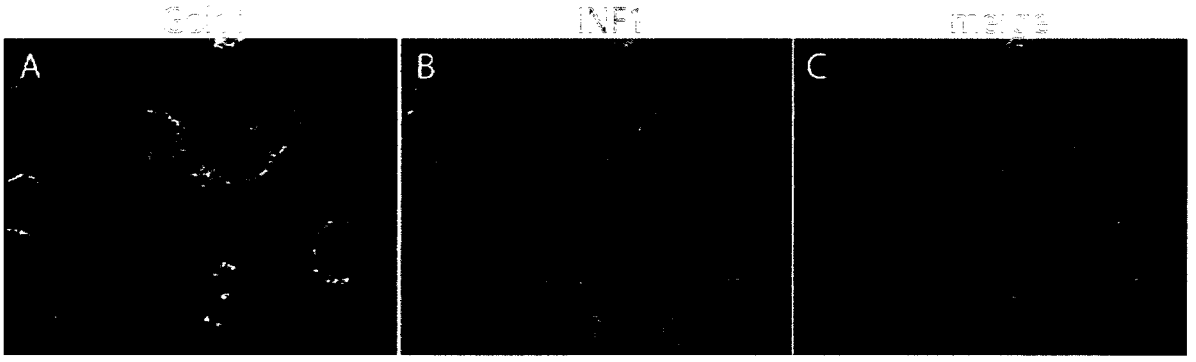


**Figure 4.1. Perinuclear INF1 co-localizes with the Golgi in NIH 3T3 fibroblasts.**

(A) Golgi staining in green co-localizes with concentrated perinuclear filamentous endogenous INF1 shown in red.

### 4.1.6 Cardiac Hypertrophy

INF1 is highly expressed in the brain, heart and lung of adult mice. The ability of INF1 to induce MT acetylation suggests it may play a role in neuronal polarity. It is not clear as to what function INF1 might have in the lung. In preliminary immunohistochemistry studies of cardiac muscle, INF1 displays a striated pattern and is concentrated at the intercalated discs joining adjacent muscle cells (Figure 4.2). A number of physiological and pathophysiological roles can envisioned for INF1 in cardiac muscle. Gap junction assembly requires the MT-dependent transport of connexins to the intercalated discs (Gutstein et al., 2003, Nishimura et al., 2006, Noorman et al., 2009). The assembly of the cardiomyocyte acto-myosin contractile apparatus is MT-dependent and is likely facilitated by the activity of an actin/MT bridging factor to facilitate this process. Alternatively, INF1 may play a role in the pathophysiology of cardiac hypertrophy. Cardiac cells undergoing pressure overload often hypertrophy and over-proliferation of microtubules in hypertrophic cardiomyocytes is thought to cause the observed contractile dysfunction (Cooper, 2006).

I have initiated preliminary experiments to test the involvement of INF1 in cardiac hypertrophy. We have examined INF1 expression in several heart muscle cell lines as well as in primary rat neonatal cardiomyocytes (Figure 4.2). Precursor P19 and H9C2 cells lines differentiated into cardiomyocytes did not have the required morphologies required to study INF1 expression (Figure 4.2). I did find that INF1 is expressed in these cells, however, it is difficult to distinguish any discernable structures.

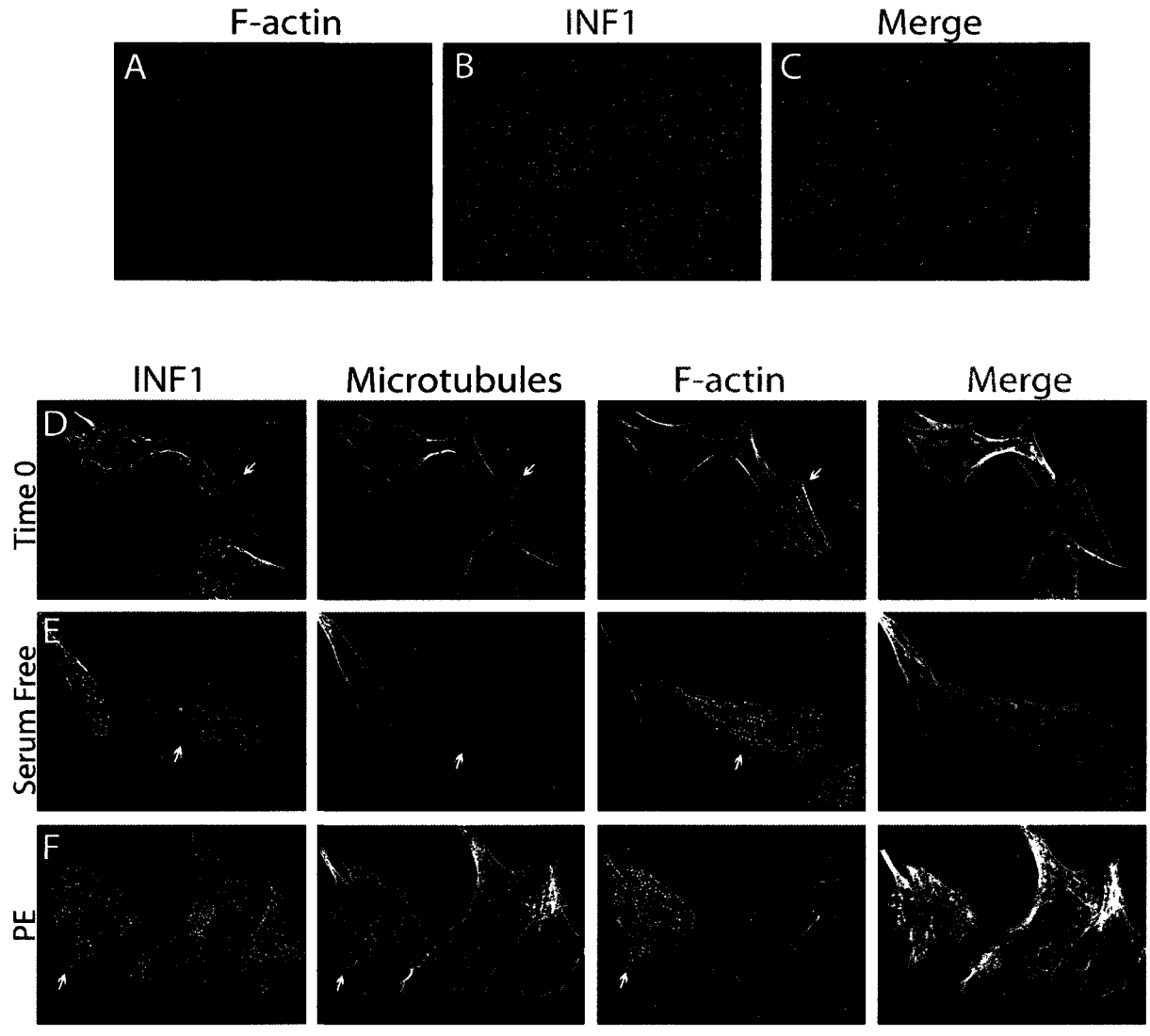


**Figure 4.2. INF1 in Cardiomyocytes.**

(A-C) Immunofluorescence of endogenous INF1 in adult mouse heart tissue. INF1 (green) shows a striated pattern. INF1 also accumulates at intercalated discs. (D-F ) Primary rat cardiomyocytes were treated with Phenylephrine (PE) for 12 hrs and then stained for INF1. INF1 protein looses its filamentous pattern in striated cardiomyocytes (arrows). Induction of hypertrophy with PE increases punctate INF1 signal in cardiomyocytes compared to control serum free and time 0.

Primary rat cardiomyocytes were treated with phenylephrine to simulate cardiac hypertrophy and then stained to look at INF1 expression. I found that INF1 puncta expression increased compared to untreated cells (Figure 4.2). We believe that this cell model provides the best model of hypertrophy, allowing the assessment of the function of INF1 in cardiomyocytes. Furthermore, I would like to develop INF1 knock out mice to determine its function and physiological role in the heart.

## 4.2 Conclusion

INF1 is a novel microtubule-associated formin. INF1 is constitutively active and does not contain any previously recognized formin regulatory domains. Overexpression of the C-terminus, however, does induce activation of the endogenous protein suggesting that it is capable of titrating an unknown inhibitory factor and therefore must encode some form of a regulatory sequence. INF1 associates with MTs through a unique bipartite MT-binding domain. Endogenous and overexpressed INF1 bind along the length of MTs both *in vivo* and *in vitro* and this is apparently sufficient to induce the stabilization and acetylation of MTs. INF1-induced MT stabilization is mediated by three domains. The MTBD is sufficient, on its own, to induce MT acetylation. In the absence of the MTBD, the INF1 N-terminus induces MT-stabilization in an FH1 and FH2 dependent manner. INF1 was also shown to bind F-actin directly suggesting the potential for INF1 to act as a cytoskeletal cross-linking protein. Through these activities INF1 may participate in a diverse array of biological functions such as neuronal polarity and cardiomyocyte development.

## References

**Akhmanova, A. and M. O. Steinmetz.** 2008. Tracking the ends: a dynamic protein network controls the fate of microtubule tips. Nat. Rev. Mol. Cell Biol. **9:**309-322.

**Alberts, A. S.** 2001. Identification of a carboxyl-terminal diaphanous-related formin homology protein autoregulatory domain. J. Biol. Chem. **276:**2824-2830.

**Alberts, B.** 2002. Molecular biology of the cell.

**Barry, S. P., S. M. Davidson, and P. A. Townsend.** 2008. Molecular regulation of cardiac hypertrophy. Int. J. Biochem. Cell Biol. **40:**2023-2039.

**Bartolini, F. and G. G. Gundersen.** 2009. Formins and microtubules. Biochem. Biophys. Acta

**Bartolini, F., J. B. Moseley, J. Schmoranzer, L. Cassimeris, B. L. Goode, and G. G. Gundersen.** 2008. The formin mDia2 stabilizes microtubules independently of its actin nucleation activity. J. Cell Biol. **181:**523-536.

**Basu, R. and F. Chang.** 2007. Shaping the actin cytoskeleton using microtubule tips. Curr. Opin. Cell Biol. **19:**88-94.

**Bloom, K.** 2004. Microtubule composition: cryptography of dynamic polymers. Proc. Natl. Acad. Sci. U. S. A. **101:**6839-6840.

**Bulinski, J. C.** 2007. Microtubule modification: acetylation speeds anterograde traffic flow. Curr. Biol. **17:**R18-20.

**Castrillon, D. H. and S. A. Wasserman.** 1994. Diaphanous is required for cytokinesis in Drosophila and shares domains of similarity with the products of the limb deformity gene. Development **120:**3367-3377.

**Chang, F., D. Drubin, and P. Nurse.** 1997. Cdc12p, a Protein Required for Cytokinesis in Fission Yeast, is a Component of the Cell Division Ring and Interacts with Profilin. J. Cell Biol. **137:**169-182.

**Chang, Y. C., P. Nalbant, J. Birkenfeld, Z. F. Chang, and G. M. Bokoch.** 2008. GEF-H1 couples nocodazole-induced microtubule disassembly to cell contractility via RhoA. Mol. Biol. Cell **19:**2147-2153.

**Chhabra, E. S. and H. N. Higgs.** 2006. INF2 Is a WASP homology 2 motif-containing formin that severs actin filaments and accelerates both polymerization and depolymerization. J. Biol. Chem. **281:**26754-26767.

**Chhabra, E. S. and H. N. Higgs.** 2007. The many faces of actin: matching assembly factors with cellular structures. Nat. Cell Biol. **9:**1110-1121.

**Chhabra, E. S., V. Ramabhadran, S. A. Gerber, and H. N. Higgs.** 2009. INF2 is an endoplasmic reticulum-associated formin protein. J. Cell. Sci. **122:**1430-1440.

**Cooper, G.,4th.** 2006. Cytoskeletal networks and the regulation of cardiac contractility: microtubules, hypertrophy, and cardiac dysfunction. Am. J. Physiol. Heart Circ. Physiol. **291:**H1003-14.

**Copeland, J. W., S. J. Copeland, and R. Treisman.** 2004. Homo-oligomerization is essential for F-actin assembly by the formin family FH2 domain. J. Biol. Chem. **279:**50250-50256.

**Copeland, J. W., A. Nasiadka, B. H. Dietrich, and H. M. Krause.** 1996. Patterning of the Drosophila embryo by a homeodomain-deleted Ftz polypeptide. Nature **379:**162-165.

**Copeland, J. W. and R. Treisman.** 2002. The diaphanous-related formin mDia1 controls serum response factor activity through its effects on actin polymerization. Mol. Biol. Cell **13:**4088-4099.

**Copeland, S. J., B. J. Green, S. Burchat, G. A. Papalia, D. Banner, and J. W. Copeland.** 2007. The diaphanous inhibitory domain/diaphanous autoregulatory domain interaction is able to mediate heterodimerization between mDia1 and mDia2. J. Biol. Chem. **282:**30120-30130.

**DeWard, A. D. and A. S. Alberts.** 2008. Microtubule stabilization: formins assert their independence. Curr. Biol. **18:**R605-8.

**Di Vizio, D., J. Kim, M. H. Hager, M. Morello, W. Yang, C. J. Lafargue, L. D. True, M. A. Rubin, R. M. Adam, R. Beroukhim, F. Demichelis, and M. R. Freeman.** 2009. Oncosome formation in prostate cancer: association with a region of frequent chromosomal deletion in metastatic disease. Cancer Res. **69:**5601-5609.

**Downing, K. H. and E. Nogales.** 1999. Crystallographic structure of tubulin: implications for dynamics and drug binding. Cell Struct. Funct. **24:**269-275.

**Downing, K. H. and E. Nogales.** 1998. Tubulin structure: insights into microtubule properties and functions. Curr. Opin. Struct. Biol. **8:**785-791.

**Edde, B., J. Rossier, J. P. Le Caer, Y. Berwald-Netter, A. Koulakoff, F. Gros, and P. Denoulet.** 1991. A combination of posttranslational modifications is responsible for the production of neuronal alpha-tubulin heterogeneity. J. Cell. Biochem. **46:**134-142.

**Eng, C. H., T. M. Huckaba, and G. G. Gundersen.** 2006. The formin mDia regulates GSK3beta through novel PKCs to promote microtubule stabilization but not MTOC reorientation in migrating fibroblasts. Mol. Biol. Cell **17:**5004-5016.

**Etienne-Manneville, S. and A. Hall.** 2003. Cdc42 regulates GSK-3beta and adenomatous polyposis coli to control cell polarity. Nature **421:**753-756.

**Etienne-Manneville, S. and A. Hall.** 2003. Cell polarity: Par6, aPKC and cytoskeletal crosstalk. Curr. Opin. Cell Biol. **15:**67-72.

**Evangelista, M., K. Blundell, M. S. Longtine, C. J. Chow, N. Adames, J. R. Pringle, M. Peter, and C. Boone.** 1997. Bni1p, a yeast formin linking cdc42p and the actin cytoskeleton during polarized morphogenesis. Science **276:**118-122.

**Evangelista, M., D. Pruyne, D. C. Amberg, C. Boone, and A. Bretscher.** 2002. Formins direct Arp2/3-independent actin filament assembly to polarize cell growth in yeast. Nat. Cell Biol. **4:**260-269.

**Evangelista, M., S. Zigmond, and C. Boone.** 2003. Formins: signaling effectors for assembly and polarization of actin filaments. J. Cell. Sci. **116:**2603-2611.

**Ezezika, O. C., N. S. Younger, J. Lu, D. A. Kaiser, Z. A. Corbin, B. J. Nolen, D. R. Kovar, and T. D. Pollard.** 2009. Incompatibility with formin Cdc12p prevents human profilin from substituting for fission yeast profilin: insights from crystal structures of fission yeast profilin. J. Biol. Chem. **284:**2088-2097.

**Faix, J. and R. Grosse.** 2006. Staying in shape with formins. Dev. Cell. **10:**693-706.

**Frey, N., H. A. Katus, E. N. Olson, and J. A. Hill.** 2004. Hypertrophy of the heart: a new therapeutic target? Circulation **109:**1580-1589.

**Frey, N. and E. N. Olson.** 2003. Cardiac hypertrophy: the good, the bad, and the ugly. Annu. Rev. Physiol. **65:**45-79.

**Gaertig, J., M. A. Cruz, J. Bowen, L. Gu, D. G. Pennock, and M. A. Gorovsky.** 1995. Acetylation of lysine 40 in alpha-tubulin is not essential in Tetrahymena thermophila. J. Cell Biol. **129:**1301-1310.

**Gartner, A., X. Huang, and A. Hall.** 2006. Neuronal polarity is regulated by glycogen synthase kinase-3 (GSK-3beta) independently of Akt/PKB serine phosphorylation. J. Cell. Sci. **119:**3927-3934.

**Gasteier, J. E., S. Schroeder, W. Muranyi, R. Madrid, S. Benichou, and O. T. Fackler.** 2005. FHOD1 coordinates actin filament and microtubule alignment to mediate cell elongation. Exp. Cell Res. **306:**192-202.

**Geneste, O., J. W. Copeland, and R. Treisman.** 2002. LIM kinase and Diaphanous cooperate to regulate serum response factor and actin dynamics. J. Cell Biol. **157:**831-838.

**Geuens, G., A. M. Hill, N. Levilliers, A. Adoutte, and M. DeBrabander.** 1989. Microtubule dynamics investigated by microinjection of Paramecium axonemal tubulin:

lack of nucleation but proximal assembly of microtubules at the kinetochore during prometaphase. J. Cell Biol. **108:**939-953.

**Goode, B. L. and M. J. Eck.** 2007. Mechanism and Function of Formins in Control of Actin Assembly. Annu. Rev. Biochem.

**Goulimari, P., T. M. Kitzing, H. Knieling, D. T. Brandt, S. Offermanns, and R. Grosse.** 2005. Galpha12/13 is essential for directed cell migration and localized Rho-Dia1 function. J. Biol. Chem. **280:**42242-42251.

**Grosse, R., J. W. Copeland, T. P. Newsome, M. Way, and R. Treisman.** 2003. A role for VASP in RhoA-Diaphanous signalling to actin dynamics and SRF activity. EMBO J. **22:**3050-3061.

**Guichet, A., J. W. Copeland, M. Erdelyi, D. Hlousek, P. Zavorszky, J. Ho, S. Brown, A. Percival-Smith, H. M. Krause, and A. Ephrussi.** 1997. The nuclear receptor homologue Ftz-F1 and the homeodomain protein Ftz are mutually dependent cofactors. Nature **385:**548-552.

**Gundersen, G. G. and J. C. Bulinski.** 1986. Distribution of tyrosinated and nontyrosinated alpha-tubulin during mitosis. J. Cell Biol. **102:**1118-1126.

**Gundersen, G. G., M. H. Kalnoski, and J. C. Bulinski.** 1984. Distinct populations of microtubules: tyrosinated and nontyrosinated alpha tubulin are distributed differently in vivo. Cell **38:**779-789.

**Gundersen, G. G., S. Khawaja, and J. C. Bulinski.** 1987. Postpolymerization detyrosination of alpha-tubulin: a mechanism for subcellular differentiation of microtubules. J. Cell Biol. **105:**251-264.

**Gundersen, G. G., Y. Wen, C. H. Eng, J. Schmoranzer, N. Cabrera-Poch, E. J. Morris, M. Chen, and E. R. Gomes.** 2005. Regulation of microtubules by Rho GTPases in migrating cells. Novartis Found. Symp. **269:**106-16; discussion 116-26, 223-30.

**Gutstein, D. E., F. Y. Liu, M. B. Meyers, A. Choo, and G. I. Fishman.** 2003. The organization of adherens junctions and desmosomes at the cardiac intercalated disc is independent of gap junctions. J. Cell. Sci. **116:**875-885.

**Hall, A.** 1998. Rho GTPases and the actin cytoskeleton. Science **279:**509-514.

**Hammond, J. W., D. Cai, and K. J. Verhey.** 2008. Tubulin modifications and their cellular functions. Curr. Opin. Cell Biol. **20:**71-76.

**Harris, E. S. and H. N. Higgs.** 2006. Biochemical analysis of mammalian formin effects on actin dynamics. Methods Enzymol. **406:**190-214.

**Harris, E. S., F. Li, and H. N. Higgs.** 2004. The mouse formin, FRLalpha, slows actin filament barbed end elongation, competes with capping protein, accelerates

polymerization from monomers, and severs filaments. J. Biol. Chem. **279:**20076-20087.

**Harwood, A. and V. M. Braga.** 2003. Cdc42 & GSK-3: signals at the crossroads. Nat. Cell Biol. **5:**275-277.

**Higgs, H. N.** 2005. Formin proteins: a domain-based approach. Trends Biochem. Sci. **30:**342-353.

**Higgs, H. N. and K. J. Peterson.** 2005. Phylogenetic analysis of the formin homology 2 domain. Mol. Biol. Cell **16:**1-13.

**Hori, M., H. Sato, K. Iwai, S. Takashima, H. Sato, M. Inoue, A. Kitabatake, and T. Kamada.** 1992. Disruption of microtubules in cultured neonatal rat cardiomyocytes during rapid contractions: protective effects of beta-adrenoceptor antagonist. Jpn. Circ. J. **56:**62-68.

**Hubbert, C., A. Guardiola, R. Shao, Y. Kawaguchi, A. Ito, A. Nixon, M. Yoshida, X. F. Wang, and T. P. Yao.** 2002. HDAC6 is a microtubule-associated deacetylase. Nature **417:**455-458.

**Ishizaki, T., Y. Morishima, M. Okamoto, T. Furuyashiki, T. Kato, and S. Narumiya.** 2001. Coordination of microtubules and the actin cytoskeleton by the Rho effector mDia1. Nat. Cell Biol. **3:**8-14.

**Ji, P., S. R. Jayapal, and H. F. Lodish.** 2008. Enucleation of cultured mouse fetal erythroblasts requires Rac GTPases and mDia2. Nat. Cell Biol. **10:**314-321.

**Johnston, R. J.,Jr, J. W. Copeland, M. Fasnacht, J. F. Etchberger, J. Liu, B. Honig, and O. Hobert.** 2006. An unusual Zn-finger/FH2 domain protein controls a left/right asymmetric neuronal fate decision in C. elegans. Development **133:**3317-3328.

**Jope, R. S. and G. V. Johnson.** 2004. The glamour and gloom of glycogen synthase kinase-3. Trends Biochem. Sci. **29:**95-102.

**Katoh, M. and M. Katoh.** 2004. Identification and characterization of human FHDC1, mouse Fhdc1 and zebrafish fhdc1 genes in silico. Int. J. Mol. Med. **13:**929-934.

**Kirschner, M. and T. Mitchison.** 1986. Beyond self-assembly: from microtubules to morphogenesis. Cell **45:**329-342.

**Kirschner, M. W. and T. Mitchison.** 1986. Microtubule dynamics. Nature **324:**621.

**Kovar, D. R.** 2006. Molecular details of formin-mediated actin assembly. Curr. Opin. Cell Biol. **18:**11-17.

**Kovar, D. R., J. R. Kuhn, A. L. Tichy, and T. D. Pollard.** 2003. The fission yeast cytokinesis formin Cdc12p is a barbed end actin filament capping protein gated by profilin. J. Cell Biol. **161:**875-887.

**Krebs, A., M. Rothkegel, M. Klar, and B. M. Jockusch.** 2001. Characterization of functional domains of mDia1, a link between the small GTPase Rho and the actin cytoskeleton. J. Cell. Sci. **114:**3663-3672.

**Leader, B., H. Lim, M. J. Carabatsos, A. Harrington, J. Ecsedy, D. Pellman, R. Maas, and P. Leder.** 2002. Formin-2, polyploidy, hypofertility and positioning of the meiotic spindle in mouse oocytes. Nat. Cell Biol. **4:**921-928.

**Li, F. and H. N. Higgs.** 2005. Dissecting requirements for auto-inhibition of actin nucleation by the formin, mDia1. J. Biol. Chem. **280:**6986-6992.

**Li, F. and H. N. Higgs.** 2003. The mouse Formin mDia1 is a potent actin nucleation factor regulated by autoinhibition. Curr. Biol. **13:**1335-1340.

**Li, H., D. J. DeRosier, W. V. Nicholson, E. Nogales, and K. H. Downing.** 2002. Microtubule structure at 8 A resolution. Structure **10:**1317-1328.

**Ligon, L. A., S. S. Shelly, M. Tokito, and E. L. Holzbaur.** 2003. The microtubule plus-end proteins EB1 and dynactin have differential effects on microtubule polymerization. Mol. Biol. Cell **14:**1405-1417.

**Liu, R., E. V. Linardopoulou, G. E. Osborn, and S. M. Parkhurst.** 2008. Formins in development: Orchestrating body plan origami. Biochim. Biophys. Acta

**Lu, J., W. Meng, F. Poy, S. Maiti, B. L. Goode, and M. J. Eck.** 2007. Structure of the FH2 domain of Daam1: implications for formin regulation of actin assembly. J. Mol. Biol. **369:**1258-1269.

**Mass, R. L., R. Zeller, R. P. Woychik, T. F. Vogt, and P. Leder.** 1990. Disruption of formin-encoding transcripts in two mutant limb deformity alleles. Nature **346:**853-855.

**Millen, K. J., W. Wurst, K. Herrup, and A. L. Joyner.** 1994. Abnormal embryonic cerebellar development and patterning of postnatal foliation in two mouse Engrailed-2 mutants. Development **120:**695-706.

**Miralles, F., G. Posern, A. I. Zaromytidou, and R. Treisman.** 2003. Actin dynamics control SRF activity by regulation of its coactivator MAL. Cell **113:**329-342.

**Mitchison, T., L. Evans, E. Schulze, and M. Kirschner.** 1986. Sites of microtubule assembly and disassembly in the mitotic spindle. Cell **45:**515-527.

**Mitchison, T. J. and M. W. Kirschner.** 1987. Some thoughts on the partitioning of tubulin between monomer and polymer under conditions of dynamic instability. Cell Biophys. **11:**35-55.

**Miyagi, Y., T. Yamashita, M. Fukaya, T. Sonoda, T. Okuno, K. Yamada, M. Watanabe, Y. Nagashima, I. Aoki, K. Okuda, M. Mishina, and S. Kawamoto.** 2002. Delphilin: a novel PDZ and formin homology domain-containing protein that

synaptically colocalizes and interacts with glutamate receptor delta 2 subunit. J. Neurosci. **22:**803-814.

**Morita, T., T. Mayanagi, and K. Sobue.** 2007. Reorganization of the actin cytoskeleton via transcriptional regulation of cytoskeletal/focal adhesion genes by myocardin-related transcription factors (MRTFs/MAL/MKLs). Exp. Cell Res. **313:**3432-3445.

**Morrison, E. E.** 2007. Action and interactions at microtubule ends. Cell Mol. Life Sci. **64:**307-317.

**Moseley, J. B., F. Bartolini, K. Okada, Y. Wen, G. G. Gundersen, and B. L. Goode.** 2007. Regulated binding of adenomatous polyposis coli protein to actin. J. Biol. Chem. **282:**12661-12668.

**Moseley, J. B., I. Sagot, A. L. Manning, Y. Xu, M. J. Eck, D. Pellman, and B. L. Goode.** 2004. A conserved mechanism for Bni1- and mDia1-induced actin assembly and dual regulation of Bni1 by Bud6 and profilin. Mol. Biol. Cell **15:**896-907.

**Nagase, T., R. Kikuno, A. Hattori, Y. Kondo, K. Okumura, and O. Ohara.** 2000. Prediction of the coding sequences of unidentified human genes. XIX. The complete sequences of 100 new cDNA clones from brain which code for large proteins in vitro. DNA Res. **7:**347-355.

**Nishimura, S., S. Nagai, M. Katoh, H. Yamashita, Y. Saeki, J. Okada, T. Hisada, R. Nagai, and S. Sugiura.** 2006. Microtubules modulate the stiffness of cardiomyocytes against shear stress. Circ. Res. **98:**81-87.

**Nogales, E., M. Whittaker, R. A. Milligan, and K. H. Downing.** 1999. High-resolution model of the microtubule. Cell **96:**79-88.

**Otomo, T., D. R. Tomchick, C. Otomo, S. C. Panchal, M. Machius, and M. K. Rosen.** 2005. Structural basis of actin filament nucleation and processive capping by a formin homology 2 domain. Nature **433:**488-494.

**Palazzo, A., B. Ackerman, and G. G. Gundersen.** 2003. Cell biology: Tubulin acetylation and cell motility. Nature **421:**230.

**Palazzo, A. F., T. A. Cook, A. S. Alberts, and G. G. Gundersen.** 2001. mDia mediates Rho-regulated formation and orientation of stable microtubules. Nat. Cell Biol. **3:**723-729.

**Palazzo, A. F., H. L. Joseph, Y. J. Chen, D. L. Dujardin, A. S. Alberts, K. K. Pfister, R. B. Vallee, and G. G. Gundersen.** 2001. Cdc42, dynein, and dynactin regulate MTOC reorientation independent of Rho-regulated microtubule stabilization. Curr. Biol. **11:**1536-1541.

**Peng, J., S. M. Kitchen, R. A. West, R. Sigler, K. M. Eisenmann, and A. S. Alberts.** 2007. Myeloproliferative defects following targeting of the Drf1 gene encoding the

mammalian diaphanous related formin mDia1. Cancer Res. **67:**7565-7571.

**Peris, L., M. Wagenbach, L. Lafanechere, J. Brocard, A. T. Moore, F. Kozielski, D. Job, L. Wordeman, and A. Andrieux.** 2009. Motor-dependent microtubule disassembly driven by tubulin tyrosination. J. Cell Biol. **185:**1159-1166.

**Pollard, T. D., L. Blanchoin, and R. D. Mullins.** 2001. Actin dynamics. J. Cell. Sci. **114:**3-4.

**Pollard, T. D., L. Blanchoin, and R. D. Mullins.** 2000. Molecular mechanisms controlling actin filament dynamics in nonmuscle cells. Annu. Rev. Biophys. Biomol. Struct. **29:**545-576.

**Pollard, T. D. and W. C. Earnshaw.** 2004. Cell biology.

**Posern, G., F. Miralles, S. Guettler, and R. Treisman.** 2004. Mutant actins that stabilise F-actin use distinct mechanisms to activate the SRF coactivator MAL. EMBO J. **23:**3973-3983.

**Pring, M., M. Evangelista, C. Boone, C. Yang, and S. H. Zigmond.** 2003. Mechanism of formin-induced nucleation of actin filaments. Biochemistry **42:**486-496.

**Pruyne, D., M. Evangelista, C. Yang, E. Bi, S. Zigmond, A. Bretscher, and C. Boone.** 2002. Role of formins in actin assembly: nucleation and barbed-end association. Science **297:**612-615.

**Reed, N. A., D. Cai, T. L. Blasius, G. T. Jih, E. Meyhofer, J. Gaertig, and K. J. Verhey.** 2006. Microtubule acetylation promotes kinesin-1 binding and transport. Curr. Biol. **16:**2166-2172.

**Romero, S., C. Le Clainche, D. Didry, C. Egile, D. Pantaloni, and M. F. Carlier.** 2004. Formin is a processive motor that requires profilin to accelerate actin assembly and associated ATP hydrolysis. Cell **119:**419-429.

**Rosales-Nieves, A. E., J. E. Johndrow, L. C. Keller, C. R. Magie, D. M. Pinto-Santini, and S. M. Parkhurst.** 2006. Coordination of microtubule and microfilament dynamics by Drosophila Rho1, Spire and Cappuccino. Nat. Cell Biol. **8:**367-376.

**Russell, R. J., S. L. Xia, R. B. Dickinson, and T. P. Lele.** 2009. Sarcomere mechanics in capillary endothelial cells. Biophys. J. **97:**1578-1585.

**Ryley, D. A., H. H. Wu, B. Leader, A. Zimon, R. H. Reindollar, and M. R. Gray.** 2005. Characterization and mutation analysis of the human formin-2 (FMN2) gene in women with unexplained infertility. Fertil. Steril. **83:**1363-1371.

**Sagot, I., A. A. Rodal, J. Moseley, B. L. Goode, and D. Pellman.** 2002. An actin nucleation mechanism mediated by Bni1 and profilin. Nat. Cell Biol. **4:**626-631.

**Sarmiento, C., W. Wang, A. Dovas, H. Yamaguchi, M. Sidani, M. El-Sibai, V. Desmarais, H. A. Holman, S. Kitchen, J. M. Backer, A. Alberts, and J. Condeelis.** 2008. WASP family members and formin proteins coordinate regulation of cell protrusions in carcinoma cells. J. Cell Biol. **180:**1245-1260.

**Schratt, G., U. Philippar, J. Berger, H. Schwarz, O. Heidenreich, and A. Nordheim.** 2002. Serum response factor is crucial for actin cytoskeletal organization and focal adhesion assembly in embryonic stem cells. J. Cell Biol. **156:**737-750.

**Schwartz, C. J., H. M. Sampson, D. Hlousek, A. Percival-Smith, J. W. Copeland, A. J. Simmonds, and H. M. Krause.** 2001. FTZ-Factor1 and Fushi tarazu interact via conserved nuclear receptor and coactivator motifs. EMBO J. **20:**510-519.

**Seth, A., C. Otomo, and M. K. Rosen.** 2006. Autoinhibition regulates cellular localization and actin assembly activity of the diaphanous-related formins FRLalpha and mDia1. J. Cell Biol. **174:**701-713.

**Shimada, A., M. Nyitrai, I. R. Vetter, D. Kuhlmann, B. Bugyi, S. Narumiya, M. A. Geeves, and A. Wittinghofer.** 2004. The core FH2 domain of diaphanous-related formins is an elongated actin binding protein that inhibits polymerization. Mol. Cell **13:**511-522.

**Soderling, S. H.** 2009. Grab your partner with both hands: cytoskeletal remodeling by Arp2/3 signaling. Sci. Signal. **2:**pe5.

**Sotiropoulos, A., D. Gineitis, J. Copeland, and R. Treisman.** 1999. Signal-regulated activation of serum response factor is mediated by changes in actin dynamics. Cell **98:**159-169.

**Steinmetz, M. O. and A. Akhmanova.** 2008. Capturing protein tails by CAP-Gly domains. Trends Biochem. Sci. **33:**535-545.

**Tanaka, K.** 2000. Formin family proteins in cytoskeletal control. Biochem. Biophys. Res. Commun. **267:**479-481.

**Vaillant, D. C., S. J. Copeland, C. Davis, S. F. Thurston, N. Abdennur, and J. W. Copeland.** 2008. Interaction of the N- and C-terminal autoregulatory domains of FRL2 does not inhibit FRL2 activity. J. Biol. Chem. **283:**33750-33762.

**Vinogradova, T., P. M. Miller, and I. Kaverina.** 2009. Microtubule network asymmetry in motile cells: role of Golgi-derived array. Cell. Cycle **8:**2168-2174.

**Wallar, B. J. and A. S. Alberts.** 2003. The formins: active scaffolds that remodel the cytoskeleton. Trends Cell Biol. **13:**435-446.

**Watanabe, N., T. Kato, A. Fujita, T. Ishizaki, and S. Narumiya.** 1999. Cooperation between mDia1 and ROCK in Rho-induced actin reorganization. Nat. Cell Biol. **1:**136-143.

**Watanabe, N., P. Madaule, T. Reid, T. Ishizaki, G. Watanabe, A. Kakizuka, Y. Saito, K. Nakao, B. M. Jockusch, and S. Narumiya.** 1997. p140mDia, a mammalian homolog of Drosophila diaphanous, is a target protein for Rho small GTPase and is a ligand for profilin. EMBO J. **16:**3044-3056.

**Wen, Y., C. H. Eng, J. Schmoranzer, N. Cabrera-Poch, E. J. Morris, M. Chen, B. J. Wallar, A. S. Alberts, and G. G. Gundersen.** 2004. EB1 and APC bind to mDia to stabilize microtubules downstream of Rho and promote cell migration. Nat. Cell Biol. **6:**820-830.

**Witke, W.** 2004. The role of profilin complexes in cell motility and other cellular processes. Trends Cell Biol. **14:**461-469.

**Witte, H., D. Neukirchen, and F. Bradke.** 2008. Microtubule stabilization specifies initial neuronal polarization. J. Cell Biol. **180:**619-632.

**Woychik, R. P., R. L. Maas, R. Zeller, T. F. Vogt, and P. Leder.** 1990. 'Formins': proteins deduced from the alternative transcripts of the limb deformity gene. Nature **346:**850-853.

**Wynshaw-Boris, A., G. Ryan, C. X. Deng, D. C. Chan, L. Jackson-Grusby, D. Larson, J. H. Dunmore, and P. Leder.** 1997. The role of a single formin isoform in the limb and renal phenotypes of limb deformity. Mol. Med. **3:**372-384.

**Xu, Y., J. B. Moseley, I. Sagot, F. Poy, D. Pellman, B. L. Goode, and M. J. Eck.** 2004. Crystal structures of a Formin Homology-2 domain reveal a tethered dimer architecture. Cell **116:**711-723.

**Yamana, N., Y. Arakawa, T. Nishino, K. Kurokawa, M. Tanji, R. E. Itoh, J. Monypenny, T. Ishizaki, H. Bito, K. Nozaki, N. Hashimoto, M. Matsuda, and S. Narumiya.** 2006. The Rho-mDia1 pathway regulates cell polarity and focal adhesion turnover in migrating cells through mobilizing Apc and c-Src. Mol. Cell. Biol. **26:**6844-6858.

**Yasuda, S., F. Oceguera-Yanez, T. Kato, M. Okamoto, S. Yonemura, Y. Terada, T. Ishizaki, and S. Narumiya.** 2004. Cdc42 and mDia3 regulate microtubule attachment to kinetochores. Nature **428:**767-771.

**Young, K. G. and J. W. Copeland.** 2008. Formins in cell signaling. Biochim. Biophys. Acta

**Young, K. G., S. F. Thurston, S. Copeland, C. Smallwood, and J. W. Copeland.** 2008. INF1 is a novel microtubule-associated formin. Mol. Biol. Cell **19:**5168-5180.

**Zhou, F., P. Leder, and S. S. Martin.** 2006. Formin-1 protein associates with microtubules through a peptide domain encoded by exon-2. Exp. Cell Res. **312:**1119-1126.

**Zhou, F., P. Leder, A. Zuniga, and M. Dettenhofer.** 2009. Formin1 disruption confers oligodactylism and alters Bmp signaling. Hum. Mol. Genet. **18:**2472-2482.

**Zhu, X. L., L. Liang, and Y. Q. Ding.** 2008. Overexpression of FMNL2 is closely related to metastasis of colorectal cancer. Int. J. Colorectal Dis. **23:**1041-1047.

**Zigmond, S. H.** 2004. Formin-induced nucleation of actin filaments. Curr. Opin. Cell Biol. **16:**99-105.

**Zigmond, S. H., M. Evangelista, C. Boone, C. Yang, A. C. Dar, F. Sicheri, J. Forkey, and M. Pring.** 2003. Formin leaky cap allows elongation in the presence of tight capping proteins. Curr. Biol. **13:**1820-1823.

**Zuniga, A., O. Michos, F. Spitz, A. P. Haramis, L. Panman, A. Galli, K. Vintersten, C. Klasen, W. Mansfield, S. Kuc, D. Duboule, R. Dono, and R. Zeller.** 2004. Mouse limb deformity mutations disrupt a global control region within the large regulatory landscape required for Gremlin expression. Genes Dev. **18:**1553-1564.